COATING OF BISMUTH AND CARBONATE DOPED HYDROXYAPATITE ON
ACID ETCHED TI6AL4V VIA BIOMIMETIC METHOD; INVESTIGATION OF
MECHANICAL, STRUCTURAL AND BIOLOGICAL PROPERTIES

A THESIS SUBMITTED TO
THE GRADUATE SCHOOL OF NATURAL AND APPLIED SCIENCES
OF
MIDDLE EAST TECHNICAL UNIVERSITY

BY

TUĞÇE HACIOĞLU

IN PARTIAL FULFILLMENT OF THE REQUIREMENTS
FOR
THE DEGREE OF DOCTOR OF PHILOSOPHY
IN
MICRO AND NANOTECHNOLOGY

JANUARY 2018

Approval of the thesis:

COATING OF BISMUTH AND CARBONATE DOPED HYDROXYAPATITE ON ACID ETCHED TI6AL4V VIA BIOMIMETIC METHOD; INVESTIGATION OF MECHANICAL, STRUCTURAL AND BIOLOGICAL PROPERTIES

Submitted by **TUĞÇE HACIOĞLU** in partial fulfillment of the requirements for the degree of **Doctor of Philosophy in Micro and Nanotechnology Department, Middle East Technical University** by,

Prof. Dr. Gülbin Dural Ünver
Dean, Graduate of **Natural and Applied Sciences**   _____

Assoc. Prof. Dr. Burcu Akata Kurç
Head of Department, **Micro and Nanotechnology, METU**   _____

Prof. Dr. Zafer Evis
Supervisor, **Engineering Sciences Dept., METU**   _____

Prof. Dr. Mehmet Kadri Aydınol
Co-Supervisor, **Metallurgical and Materials Eng. Dept., METU** _____

Examining Committee Members:

Prof. Dr. Ayşen Tezcaner
Engineering Sciences Dept., METU   _____

Prof. Dr. Zafer Evis
Engineering Sciences Dept., METU   _____

Prof. Dr. Dilek Keskin
Engineering Sciences Dept., METU   _____

Prof. Dr. Nuray Yıldız
Chemical Engineering Dept., Ankara University   _____

Prof. Dr. Volkan Şahin
Prosthodontics Dept., Kırıkkale University   _____

Date: 24.01.2018

I hereby declare that all information in this document has been obtained and presented in accordance with academic rules and ethical conduct. I also declare that, as required by these rules and conduct, I have fully cited and referenced all material and results that are not original to this work.

Name, Last name: Tuğçe Hacıoğlu

Signature:

ABSTRACT

COATING OF BISMUTH AND CARBONATE DOPED HYDROXYAPATITE ON ACID ETCHED TI6AL4V VIA BIOMIMETIC METHOD; INVESTIGATION OF MECHANICAL, STRUCTURAL AND BIOLOGICAL PROPERTIES

Hacıoğlu, Tuğçe

Ph.D., Department of Micro and Nano Technology

Supervisor: Prof. Dr. Zafer Evis

Co-Supervisor: Prof. Dr. M. Kadri Aydınol

January 2018, 135 Pages

Titanium and its alloys are used in both engineering and dental applications. Ti6Al4V alloy is one of the most commonly preferred titanium alloy used in medical industry. Ti6Al4V with hydroxyapatite (HAp) coating has been frequently used material combinations. Though coating Ti6Al4V with HAp does not provide the desired amount of biocompatibility, it is significant to coat doped HAp on titanium alloy with antibacterial properties.

In this thesis, first of all best experimental conditions for pre-treatment and coating process were determined. To prepare a new generation and high quality Ti6Al4V implant coating, bismuth + carbonate co-doped and pure HAps were coated on rough surfaces of Ti6Al4V plates by biomimetic method. After that, the coated plates were examined by SEM, EDS, AFM, FTIR, XRD, ICP and XPS. Furthermore, mechanical profilometer tests, scratch tests and in vitro cell studies were carried out. To investigate the antibacterial property of the coating, the survival of the *Staphylococcus epidermidis* on the surface of the implant was determined.

Optimum pretreatment procedure was found to be three steps (sandblasted + acid etched + preheated) pretreatment. AFM results proved that the surface roughness increased by sandblasting, acid etching and preheating, respectively. By applying three steps method, substrate's surface became much rougher which enabled advanced mechanical interlocking between the substrate surface and precipitated coating. Structural analysis performed for pure and co-doped coatings proved that HAp nucleation started 4 days after immersion, nucleation increased with the incubation time and co-dopants had great effect on surface characteristics. Furthermore the pretreatment procedure and dopants had significant influence on mechanical properties of the coatings. The resulting coatings had very high critical loads and surface adhesion. The critical load values obtained for coating failure were found to be above 100 mN for all type of coatings. Co-doped coatings, especially 0.3 mM co-doped coatings, had much higher critical loads than pure coatings.

The proliferation of fibroblast (L929) and cancerous bone cells (SaOS-2) on pure and co-doped HAp coatings were evaluated in terms of biological properties. For L929 cell line, low concentrations of bismuth ion slightly improved cell viability. In case of SaOS-2 cell line, 0.1-C7 and 0.3-C7 exhibited highest reduction percentage among all co-doped samples. The higher stability and coherence of 0.3 mM co-doped coatings were also verified by mechanical test results. Further increase in dopants concentrations up to 0.5 mM lead to increase in toxicity and decrease in cell proliferation. The adherences of SaOS-2 cells onto the coatings were also investigated by the SEM analysis. In order to study antibacterial property of coating *S.epidermidis* bacteria was used. Antibacterial test results showed the most antibacterial samples were 0.1-C7 and 0.3-C7, the results were consistent with cell culture study.

Keywords: Bismuth, Carbonate, Hydroxyapatite, Ti6Al4V, Orthopedic Implant

ÖZ

BİZMUT VE KARBONAT EKLENMİŞ HİDROKSİAPATİTİN BİYOMİMETİK YÖNTEMLE ASİTLE AŞINDIRILMIŞ Ti6Al4V PLAKASININ ÜZERİNE KAPLANARAK ORTOPEDİK İMPLANT ÜRETİMİNİN GERÇEKLEŞTİRİLMESİ; MEKANİK, YAPISAL VE BİYOLOJİK İNCELENMESİ

Hacıoğlu, Tuğçe

Doktora, Mikro ve Nano Teknoloji Bölümü

Tez Yöneticisi: Prof. Dr. Zafer Evis

Ortak Tez Yöneticisi: Prof. Dr. M. Kadri Aydınol

Ocak 2018, 135 Sayfa

Titanyum ve alaşımları, hem mühendislik hem de diş uygulamalarında kullanılmaktadır. Ti6Al4V alaşımı medikal endüstrisinde tercih edilen titanyum alaşımları arasında en yaygın kullanılanlarından biridir. Ti6Al4V'ün hidroksiapatit (HAp) ile kaplanması sıklıkla kullanılan malzeme birleşimleridir. Ancak HAp ile Ti6Al4V kaplanması ile istenilen biyouyumluluğa erişilememektedir. Titanyum alaşımını antibakteriyel nitelikli iyon ile katkılandırılmış HAp ile kaplamak önemlidir.

Bu tezde, öncelikle en iyi deneysel önişlem ve kaplama koşulları belirlenmiştir. Yeni ve üstün nitelikli Ti6Al4V implant kaplaması üretmek için, bizmut + karbonatla katkılandırılmış ve saf halde HAp ile pürüzlü yüzeye sahip Ti6Al4V plakalar biyomimetik yöntemle kaplanmıştır. Sonrasında kaplanan plakalar SEM, EDS, AFM, FTIR, XRD, ICP ve XPS vasıtasıyla incelenmiştir. Daha sonra mekanik profilometre testleri, çizik testleri ve *in vitro* hücre kültürü çalışmaları da gerçekleştirilmiştir.

Kaplamaların antibakteriyel özelliklerini araştırmak için *Staphylococcus epidermidis* bakterisinin implant yüzeyi üzerindeki canlılığı tespit edilmiştir.

Optimal önişlem prosedürü olarak üç adımlı (kumlama + asitle aşındırma+ ısıl önişlem) önişlem belirlenmiştir. AFM sonuçları sırasıyla kumlama, asit ile aşındırma ve ön ısıtma işlemlerinin yüzeyde pürüzlülüğü arttırdığını göstermiştir. Bu şekilde üç adımlı yöntemin kullanılması alttaş yüzeyinin daha çok pürüzlü hale gelmesini ve bu sayede alttaş yüzeyi ile kaplama arasında ileri derecede mekanik kenetlenme olmasına imkân sağlamıştır. Saf ve katkılandırılmış kaplamaların yapısal analizleri neticesinde HAp çekirdeklenmesinin biyomimetik kaplamanın 4. gününden sonra başlamış olduğu, çekirdeklenmenin inkübasyon süresiyle orantılı olarak arttığı ve katkı iyonunun yüzey özelliklerini önemli derecede etkilediği kanıtlanmıştır. İlaveten önişlem prosedürünün ve katkı maddelerinin plakalardaki kaplamaların mekanik özellikleri üzerinde mükemmel bir etkisi olduğu anlaşılmıştır. Üretilen kaplamaların oldukça yüksek kritik yük ve yüzey adezyonuna sahip oldukları gözlemlenmiştir. Tüm kaplama tiplerinde 100 mN değerinin üzerinde kaplamanın dayanma kuvvetinin göstergesi olan kritik yük değeri elde edilmiştir. Katkılandırılmış kaplamaların, özellikle de 0.3 mM katkılandırılmış kaplamaların, saf kaplamalara nispeten çok daha yüksek kritik yük değerlerinde sahip oldukları tespit edilmiştir.

Saf ve katkılandırılmış HAp kaplamalarda, fibroblast (l929) ve kanser kemik hücreleri (SaOS-2) proliferasyonu biyolojik özellikleri bakımından değerlendirilmiştir. Az miktarda bizmut konsantrasyonun, Fibroblast hücrelerde hücre canlılığını kısmen geliştirdiği anlaşılmıştır. SaOS-2 hücre hattı çalışmalarında ise, tüm katkılandırılmış kaplamalar arasında en yüksek yüzde redüksiyon oranına 0.1-C7 ve 0.3-C7 örneklerinin sahip olduğu gözlemlenmiştir. Mekanik test sonuçları da göz önünde bulundurulduğunda 0.3 mM katkılandırılmış kaplamaların en stabil ve koherent kaplamalar oldukları teyit edilmiştir. Katkı iyon konsantrasyonlarının 0.5 mM değerine kadar artırılması toksisitede artışa ve hücre proliferasyonda azalmaya sebep olmuştur.

SaOS-2 hücrelerinin kaplamaya yapışması ayrıca SEM analiz çalışmasıyla da incelenmiştir. Kaplamaların antibakteriyal özelliklerinin çalışılması için *S.epidermidis* bakterisi kullanılmıştır. Antibakteriyal test sonuçlarına göre 0.1-C7 ve 0.3-C7 örneklerinin en antimikrobiyal örnekler oldukları ve sonuçların hücre kültürü çalışmalarıyla uyumlu olduğu belirlenmiştir.

Anahtar Kelimeler: Bizmut, Karbonat, Hidroksiapatit, Ti6Al4V, Ortopedik İmplant

ACKNOWLEDGEMENT

Firstly, I would like to express my sincere gratitude to my advisor Prof. Dr. Zafer Evis for the continuous support of my Ph.D study and related research, for his patience, motivation, and immense knowledge. His guidance helped me in all the time of research and writing of this thesis.

Besides my advisor, I would like to thank Prof. Dr. Ayşen Tezcaner for her insightful comments and valuable help about my biological experiments.

My sincere thanks also go to my co-advisor Prof. Dr. Mehmet Kadri Aydınol, who gave access to his laboratory and research facilities. Without his precious support it would not be possible to conduct this research.

I thank my fellow labmates in for the stimulating discussions and working together.

A special thanks to my family. Words cannot express how grateful I am to my mother Yüksel Aktar, father Yusuf Aktar and my sister Tuğba Aktar for all of the sacrifices that you've made on my behalf. And most of all for my loving, supportive, encouraging, and patient husband Utku Hacıoğlu who has been a constant source of strength and inspiration for me during the all stages of this Ph.D. is so appreciated. Thank you.

TABLE OF CONTENTS

LIST OF TABLES

TABLES

LIST OF FIGURES

FIGURES

LIST OF ABBREVIATIONS

ACP   Amorphous carbonated calcium phosphate

AFM   Atomic Force Microscope

ASTM   American Society for Testing and Materials

ATCC   American Type Culture Collection

A-W   Apatite-Wollastonite

CaP   Calcium phosphate

CFU   Colony Forming Unit

c-   Control negative samples

c+   Control positive samples

DMEM   Dulbecco's Modified Eagle's Medium

EDS   Energy dispersive X-ray spectroscopy

EDTA   Ethylenediaminetetraacetic acid

FBS   Fetal Bovine Serum

fcc   Face centered cubic

FTIR   Fourier Transform Infrared Spectroscopy

HAp   Hydroxyapatite

HMDSO   Hexamethyldisiloxane

HBSS   Hank's Balanced Salt Solution

ICP-MS   Inductively Coupled Plasma-Mass Spectrophometry

ISO   International Organization for Standardization

JCPDS   Joint Committee on Powder Diffraction Standards

LB   Luria-Bertani medium

Lc   Critical load

L929   Fibroblast cells from Mouse

MIR   Mid Infrared

m-SBF   Modified Simulated Body Fluid

MTT	(3-(4,5-Dimethylthiazol-2-yl)-2,5-Diphenyltetrazolium Bromide)
PBS	Phosphate Buffered Saline
r-SBF	Revised Simulated Body Fluid
RT	Room Temperature
R_a	Roughness average
R_q	Root mean square roughness
R_z	Ten point average roughness
R_{wp}	Weighted profile factor
Saos-2	Human osteosarcoma cell line
SBF	Simulated Body Fluid
SEM	Scanning Electron Microscope
TCP	Tricalcium phosphate
Ti	None treated Ti6Al4V plate
Ti-S	Sandblasted Ti6Al4V plate
Ti-S-A	Sandblasted and acid etched Ti6Al4V plate
Ti-S-A-P	Sandblasted, acid etched and preheated Ti6Al4V plate
TRIS	Tris (hydroxymethyl) aminomethane
TTCP	Tetracalcium phosphate
XPS	X-ray Photoelectron Spectroscopy
XRD	X-ray Diffraction

CHAPTER 1

INTRODUCTION

Titanium and its alloys are commonly preferred implant materials for hard tissue applications. Statistics demonstrate that 90% of people over 40 years old have regressive illnesses among worldwide, especially in hip and knee, and both cases are costly and painful for patients. Today more than 4.4 million people have an internal fixation device and over 1.3 million people possess an artificial joint (Chen et al., 2006). Not only is there high demand for orthopedic surgeries for new patients every year, but also there is an even higher demand for patients who must receive revision surgeries. Common problems associated with patients requiring revision surgeries are instability, aseptic loosening, infection, wear, osteolysis, ingrowth failure, and periprosthetic fracture (Dobzyniak et al., 2006; Losina et al., 2004).

In order to enhance the properties of titanium based implant materials, different pretreatment and coating techniques are commonly used. Calcium-phosphate coatings are the most favorable method to upgrade the osteointegration properties of biomaterials. Porous structure of hydroxyapatite (HAp) enables osteoblast attachment, proliferation and finally leads to osteointegration of the implant. Biological performance of the coated implant can be improved by substitution of various ions.

1.1. Bone Structure and Metallic Implants

Typically, the living bone in the human musculoskeletal system is composed of 10-20% collagen, 60-70% bone mineral, and 9-20% water, by weight (Park, 1984; Doitpoms, 2011).

In addition, other organic materials, such as proteins, polysaccharides and lipids, are also present in small quantities (Lee, 1991). The basic composition of the bone mineral can be approximately defined as HAp with a chemical formula of $Ca_{10}(PO_4)_6(OH)_2$. However, when HAp has a Ca:P ratio of 1.67 (5:3), the Ca:P ratio in bone minerals actually varies between 1.37 and 1.87, indicating that bone minerals may contain other additional ions, such as strontium, zinc and carbonate, etc. (Doitpoms, 2011).

Throughout evolution, bone has preserved a fundamental hierarchical structure or building plan subdivided in organizational levels from the macroscopic to the molecular scale as shown in Figure 1 (Wang et al., 2016). This provides bone with a surprising tradeoff between stiffness and flexibility, strength and lightness, consistence and porosity, stability and self renewal. A typical human bone is composed of cortical bone, cancellous bone, periosteum, endosteum and articular cartilage in a macro scale (Suchanek and Yoshimura, 1998; Rho et al., 1998). Cortical bone, comprising 80% of the bone mass, forms a compact ectotheca surrounding the central marrow cavity, whereas cancellous bone has an open, honeycomb structure that accounts for roughly 20% of the total mass of the skeleton. Cortical bone has an high elastic modulus in order to provide sufficient mechanical strength to bear weight, while the cancellous bone possesses a much lower elastic modulus value than the cortical bone. The special alignment of the cancellous bone structure, nonetheless, is able to reduce the sudden stress.

Cartilage is a type of collagen based connective tissue composed of very large protein-polysaccharide molecules, providing a tough, flexible matrix made of entangled collagen fibers, protein, and sugar. Mechanically, articular cartilage has a very low friction coefficient that enables a smooth surface to allow for ease of joint movement with the presence of synovial fluid (Doitpoms, 2011). Periosteum is a fibrous membrane of connective tissue found on the bone surface. It contains fibroblasts and progenitor cells, which are critical to new bone formation.

Endosteum is a thin layer of lining cells present on the surface of the medullary cavity and is significant during the process of bone remodeling. The cortical bone exhibits a hierarchical structural organization composed of osteons on a micro scale, collagen fibers on a nanoscale, and collagen molecules on a sub-nanoscale.
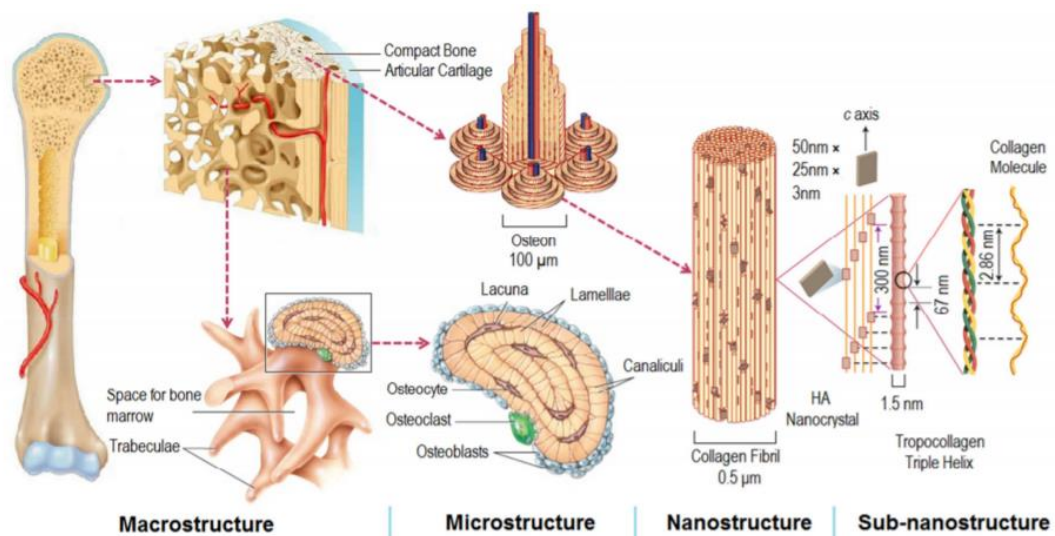
Figure 1 Hierarchical structural organization of bone (Wang et al., 2016).

The sequence of developmental events in 1850s culminated in the clinical application of Plaster of Paris (gypsum) for fracture immobilization (Mathijsen, 2007; DeMaio et al., 2012).

Today, implantable devices developed for internal and external fracture fixation and bone defect healing should respond the basic material requirements of mechanical competence (strength), rigidity, biocompatibility, and corrosion resistance to provide a suitable environment for healing. Metallic implant devices offer a wide range of mechanical features desirable for loadbearing applications including: hardness, ductility, formability, strength, and both fracture as well as corrosion resistance.

Nonetheless, metallic implant devices suffer a number of disadvantages when compared to other materials, the most limiting of which stem from a lack of inherent biological activity and a mismatch in mechanical properties between the metallic implant and peri-implant bone, a shortcoming described as stress-shielding. Furthermore, metallic implants have frequently been reported to liberate toxic corrosion products and induce wear-related effects in local tissues, impacting on long-term functionality and resulting in a combined and progressive reduction of peri-implant bone quality.

1.2. Titanium and Its Alloys

The clinical trials of titanium (Ti) have been performed since 1965, when Ödman et al. developed the titanium dental implant and introduced the concept of osseointegration (Ödman et al., 1988). Since then, pure Ti and Ti alloys have been commonly used in medical applications, mostly in orthopedic and dental implants. Compared to other traditional metallic biomaterials, such as Co-Cr alloys and stainless steels, the Ti alloys possess lower modulus, better biocompatibility and corrosion resistance (Long and Rack, 1998). These properties promote the improvement and application of new orthopedic Ti alloys in the medical field. Due to the low strength and the poor wear resistance, pure Ti is mainly restricted in many medical applications especially the ones that involve high stresses, such as orthopedic prostheses.

4

A large number of new binary Ti alloys have been developed in response to those concerns in recent years (Ho et al., 1999; Lee et al., 2002; Ho et al., 2009; Okazaki et al., 1998; Mareci et al., 2009; Cai et al., 2005; Hsu et al., 2009; Zhang, Zheng et al., 2009; Takahashi et al., 2004; Nakagawa et al., 2005; Ohkubo et al., 2003; Lin et al., 2012; Wang et al., 2013; Qiu et al., 2014).

In these binary Ti alloys, the addition of alloying elements such as Mo, Nb, Ta, Zr, V and Hf are generally used to improve the strength and lower the elastic modulus of Ti alloys. The addition of noble metal elements such as Au, Ag, Pt and Pd mainly target on developing the corrosion resistance of Ti alloys, and the fusible alloying elements Ga, Ge, In and Sn are more of emphasizing the casting procedure of Ti alloys.

In last decade, Ti6Al4V and Ti6Al7Nb alloys have been popularized in the biomedical industry for their enhanced mechanical strength and wear resistance (Lintner et al., 1986; Semlitsch et al., 1992; Geetha et al., 2009). Other favorable biomedical materials are Ti-Ni alloys which are commonly used as orthodontic wires and intravascular stents for their exclusive properties such as the superelasticity and shape memory effect (Thompson, 2000; Stoeckel et al., 2004). Main concern about Ti alloys is the release of added metallic ions and their potential toxic effects to tissues (Perl and Brody, 1980; Walker et al., 1989; Wapner, 1991; Landsberg et al., 1992; Eisenbarth et al., 2004; Biesiekierski et al., 2012; Heintz et al., 2001).

Ti6Al4V alloy is one of the most preferred implant materials according to its high mechanical properties, which ensures load transmission to bone tissues over a long time period which is significant when damaged hard tissues are replaced by prostheses (Bauer et al., 2013). Furthermore, the ASTM F136 Standard specifies the requirements of Ti6Al4V for biomedical applications. This alloy has good mechanical properties; however, it exhibits a possible toxic effect from released V and Al (Gepreel and Niinomi, 2013). For this reason, V and Al free Ti alloys were proposed for biomaterials applications.

Pure Ti and its alloys are not bioactive but they can acquire bioactivity through various surface treatments. It should be noted that there is an exceptional feature of Ti-based materials which is their air-induced passivation that cultivates a protective and stable layer of titanium oxide on its surface. The native oxide is generally thin (usually in the 3-10 nm range), amorphous, and stoichiometrically defective (Zhu et al., 2004; Sittig et al., 1999; Feng et al., 2003; Feng et al., 2002; Oh et al., 2005). The success of Ti in promoting bone growth is generally attributed to the physicochemical characteristics of the passive oxide layer that forms spontaneously at its surface. The stability of the oxide layer depends on its chemical composition, crystalline structure, and thickness, characteristics that can all be tuned by proper surface treatment. This natural inertness has two interdependent consequences: First, the implant is strongly protected against degradation by the aggressive environment occurring at the healing site (Linder and Lundskog, 1975). This assures that the implant can withstand the functional load for long periods of time without replacement. Second, the chemical stability of the layer prevents inflammation induced by particle release (Suska et al., 2005), thus avoiding the formation of soft fibrous tissue at the bone-implant interface. This reduces the risk of the implant loosening and enables new bone formation at the implant surface. Interactions between biomaterials and biological environments occur at interfaces, and they are affected by the nature of the biomaterial, such as its surface chemistry and energy, roughness, and topography (Brunski et al., 2000). It is generally accepted that rough and porous surfaces have a more positive effect on cellular activity than smooth ones. Many methods were used to modify surfaces to improve tissue repair cases, such as sand-blasting (Anselme and Bigerelle, 2006; Refai et al., 2004; Guizzardi et al., 2004), machining (Lüthen et al., 2005; Cassinelli et al., 2003; Xavier et al., 2003), anodization (Zhao et al., 2006; Das et al., 2007), lithography (Dalby et al., 2006; Andersson et al., 2003; Ismail et al., 2007), ion-implantation (Liu et al., 2004; Nayab et al., 2005; Krupa et al., 2001; Nayab et al., 2004), and chemical etching (Anselme and Bigerelle, 2005; Giordano et al., 2006; Sandrini et al., 2007). As surface is pretreated, coating step can be performed.

Mechanical and chemical processes (i.e. sand blasting and etching, respectively) were generally employed to increase the surface area of the implants, because rough surfaces with high surface area induced mechanical interlocking between the bone and the implant (Samanipour et al., 2011).

Biomimetic coating of HAp gained enormous interest because of its low deposition temperature and good step coverage. It was declared that bioactive surfaces play an important role in early stages of implantation due to better osteoconductive properties promoting good attachment and proliferation of osteoblast cells (Rønold et al., 2003).

1.3. Biomaterials

Biomaterials for prosthetic implants must replace the missing tissue and return the natural functionality. In order to achieve these phenomena, artificial materials need to interact appropriately with the biological environment and to physiologically bond to the surrounding tissues. An ideal biomaterial for prosthetic implants will promote cellular adhesion but should prevent the bacterial adhesion. The main surface properties that influence cellular and bacterial adhesion are topography, roughness, chemical composition and energy. Figure 2 lists the numerous material requirements that must be met for successful total joint replacement.

The ideal material or material combination should exhibit the following properties:

 • A biocompatible chemical composition to avoid undesirable tissue reactions
• Excellent resistance to degradation (corrosion resistance for metals or resistance to biological degradation in polymers)
• Acceptable strength to sustain cyclic loading endured by the joint
• A low modulus to minimize bone resorption
• High wear resistance to minimize wear debris generation

Requirements of implants	**Compatibility** *Tissue reactions *Change in properties (mechanical, physical, chemical) *Degradation leads to (local deleterious changes, harmful systemic effects)
	Mechanical properties * Elasticity *Yield stress *Ductility * Toughness *Time dependent deformation * Creep *Ultimate strength * Fatigue strength * Hardness * Wear resistance
	Manufacturing * Fabrication methods * Consistency and conformity to all requirements * Quality of raw materials * Superior techniques to obtain excellent surface finish or texture * Capability of material to get safe and efficient sterilization * Cost of product

Figure 2 Some requirements of implants (Davis, 2003).

Types of biomaterials:

Biomaterials can be divided into the following categories: metals, polymers, ceramics, and composites as shown in Table 1:

Table 1 Types of biomaterials (Davis, 2003; Park and Lakes, 2007).

Material	Pros	Cons	Applications
Metals and alloys 316L Stainless Steel, Cp-Ti, Ti-Al-V, Ti-Al-Nb, Ti-13Nb-13Zr, Ti-Mo-Zr-Fe, Co-Cr-Mo	Strong, Tough, Ductile	May corrode, Dense, Difficult to make	Fracture fixation, stents, surgical instruments, bone and joint replacement, dental implants, pacemaker, heart valves, bone plates, orthodontic wires
Ceramics and glasses Alumina, Zirconia, Calcium Phosphates, Bioactive Glasses, Porcelain, Carbons	Very biocompatible	Brittle, Not resilient, Weak in tension	Joint replacement, dental implants, bone repair and augmentation, surface coating on metals, bone replacement, dental restorations, heart valves
Polymers Polyethylene, Polypropylene, PTFE, PMMA, PVC, Polyamides, Polyesters, Polyurethanes, Silicones, Hydrogels	Resilient, Easy to fabricate	Not strong, Deforms with time, May degrade	Joint replacement, sutures, vascular prosthesis, soft tissue augmentation, drug delivery systems, blood contacting devices, tubing, dental restorations, intraocular lenses, soft tissue replacement, ophthalmology
Composites BIS-GMA-Quartz/Silica Filler, PMMA-Glass Fillers	Strong , Tailor made	Difficult to make	Dental restorations

Figure 3 shows various implants and devices used to replace or enhance the function of diseased or missing tissues and organs:
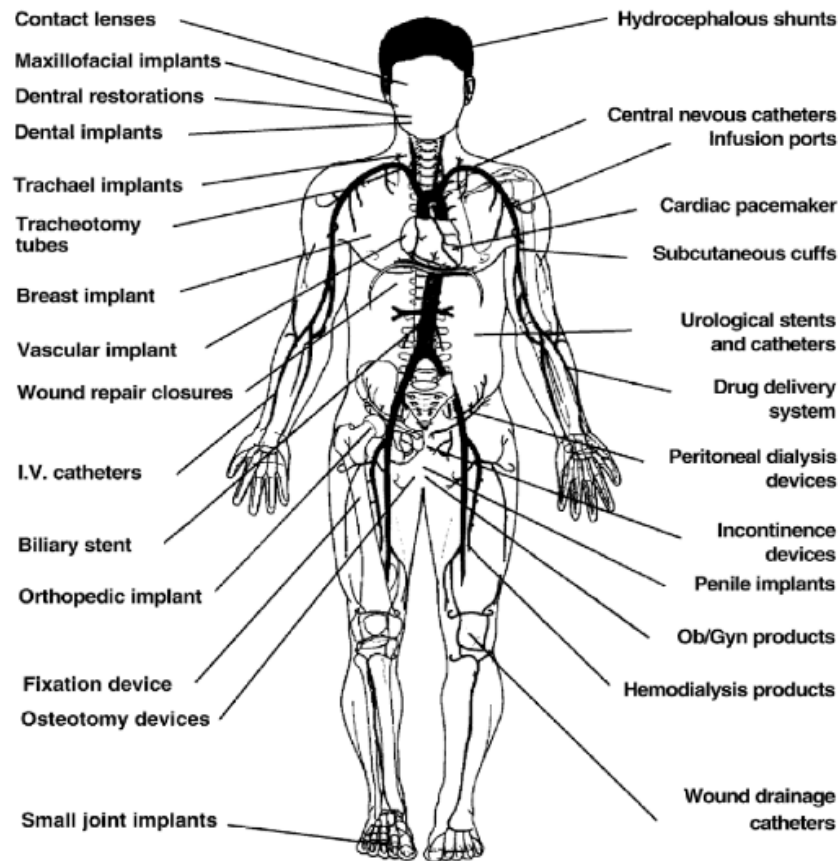
Figure 3 Some biomaterials used in human body (Park and Lakes, 2007).

1.4. Biomimetics and Simulated Body Fluid (SBF)

Ti and its alloys have been immensely used in skeletal repair and dental implant fields. They have good mechanical strength, toughness, biocompatibility and corrosion resistance. However, bioinert feature of Ti and its alloys is needed to be resolved when a strong interface bonding between implants and living bone is expected.

Most preferred approach to overcome the bioinertness of Ti and its alloys is to prepare bioactive coatings on their surfaces (Liu et al., 2004; Leeuwenburgh et al., 2005; Xie et al., 2006; Xiao et al., 2003). Many surface modifying techniques, such as plasma spraying (Feng et al., 2000), electrochemical deposition (Ban and Maruno, 1993) and sol-gel method (Cheng et al., 2006), were developed to prepare the bioactive coatings such as HAp on Ti and its alloys. Plasma-sprayed HAp coatings were extensively investigated. However, they lacked strength and reliability, as a result of the residual stresses and partial decomposition of HAp during the preparation process (Feng et al., 2000; Porter et al., 2004; Yang and Chang, 2001). In addition, this technique is not suitable to prepare uniform coatings on biomedical implants with complex geometries.

In recent years, considerable attention was given to plasma electrochemical deposition (Schreckenbach et al., 1999; Zhu et al., 2001; Zhu et al., 2002; Han et al., 2003; Frauchiger et al., 2004; Song et al., 2004; Yang et al., 2004; Song et al., 2005) and biomimetic deposition (Kim et al., 1996; Wang et al., 2000; Wang et al., 2002; Liu et al., 2002; Kokubo et al., 2003; Oliveira et al., 2003; Kim, 2003; Kawai et al., 2004; Duan and Wang, 2006; Toworfe et al., 2006) of bioactive films on Ti and its alloys. A biomimetic coating process was developed on the base of the heterogeneous nucleation of calcium phosphate (CaP) from simulated body fluid (SBF) (Zhang and Yang, 2005), in which implant materials, such as Ti implants, were soaked directly in the SBF solution and a Ca-P layer was coated on the surface. By changing the ion concentration in SBF, a different layer can be obtained, such as amorphous carbonated calcium phosphate (ACP), biomimetic carbonated apatite and octacalcium phosphate (Zhang and Yang, 2005). Biomimetic technique is a promising method to deposit apatite films on Ti and its alloys. It imitates the mode in which bone-like HAp crystals in situ form in a SBF environment. This technique includes some advantages such as low working temperature, accessibility of pore networks on the nanometer scale and suitability for complex shapes of substrates.

10

Moreover, biomimetic apatite presents some important characteristics such as carbonated structure and controllable crystallinity (Müller and Müller, 2006). Biomimetic process is considered to be one of the most promising techniques to produce a bone-like HAp apatite layer on different substrates (Song et al., 2004; Li et al., 2002). The biomimetic route utilizes supersaturated aqueous solutions with ionic composition similar to that of human blood serum, it allows to coat complex-shaped materials (Barrère et al., 2003), and to co-precipitate biologically active molecules with apatite crystals onto metal implants (Liu et al., 2001).

Biomimetic coating enables low processing temperatures, to form bone like apatite, to coat complex shapes. On the other hand, it also has some disadvantages, such as difficult to produce crack free coatings, high sintering temperatures, non uniform coating thickness.

The surfaces of materials after treatment should be able to interact with the surrounding tissue to induce direct contact of bone to implant. Kokubo treatment, also known as SBF, is a chemical method for determining a level of biocompatibility of materials that was established in 1990 (Kokubo, Ito et al., 1990). SBF simulates just the inorganic part of human blood serum and does not contain proteins, glucose, vitamins, hormones, etc. The interest in using SBF for preparation of biomimetic apatite coatings has immensely increased within the last years. Thus, several SBF solutions such as revised (r-SBF), modified (m-SBF), Hank's Balanced Salt Solution (HBSS) with ionic concentrations closer or equal to that of human blood serum have been reported (Oyane et al., 2003) and the preparation of SBF solutions will continue to evolve .

 In 1971, Hench et al. proved that some glasses in the Na_2O-CaO-SiO_2-P_2O_5 system, named Bioglass, spontaneously bond to living bone without the formation of surrounding fibrous tissue (Hench et al., 1971).

In 1980, Ogino et al. showed that a SiO_2-rich layer and CaP film form on the surface of Bioglass when implanted in the body environment, enabling bonding to living bone (Ogino et al., 1980). Kitsugi et al. claimed that the SiO_2-rich layer does not form on glass-ceramic A-W, but a CaP layer forms on its surface in the living body, allowing bonding to living bone (Kitsugi et al., 1987). Kokubo et al. identified this CaP layer as crystalline apatite by using XRD (Kokubo, Ohtsuki et al., 1990). In 1990, Kokubo et al. showed that in vivo apatite formation on the surface of glass-ceramic A-W can be reproduced in an acellular SBF with ion concentrations nearly equal to those of the human blood serum, but not in a Tris buffer solution (Kokubo, Kushitani et al., 1990; Kokubo, Ito et al., 1990). Kokubo et al. (Kokubo, Kushitani et al., 1990) and Filgueiras et al. (Filgueiras et al., 1993) confirmed the formation of apatite on the Bioglass surface in SBF. First SBF used at 1990 and 1993 by Kokubo et al. (Kokubo, Kushitani et al., 1990) and Filgueiras et al. (Filgueiras et al., 1993) lacks the SO_4^{2+} ions contained in human blood serum. A detailed recipe for preparation of SBF was reported in 1995 by Cho et al. though SBF was still richer in Cl^- ion and poorer in HCO_3^- ion than human blood serum (Cho et al., 1995). The short history of SBF usage for apatite formation is shown in Figure 4.

Tas studied biomimetic calcium hydroxyapatite powder synthesis technology for the first time in the literature, HCO_3^- ion concentration was increased from 4.2 mM to 27.0 mM and Cl^- ion concentration was decreased from 147.8 mM to 125.0 mM in order to near human blood serum (Tas, 2000). In 2003, Oyane et al. tried to decrease this difference by preparing a SBF in which the concentrations of Cl^- ion was decreased and HCO_3^- ion was increased to the levels of human blood serum. However, calcium carbonate has a strong tendency to precipitate from this SBF and they had to deal with it (Oyane et al., 2003). In 2004, Takadama et al. proposed an improved SBF in which they decreased only the Cl^- ion concentration to the level of human blood serum (Takadama et al., 2004). Bigi et al., studied a new fast biomimetic deposition of HAp onto Ti6Al4V substrate by preparing Ca/P solution (Bigi et al., 2005).

Finally in 2006, Kokubo and Takadama explained a detailed recipe for SBF preparation and biomimetic coating, furthermore they provided some information about in vivo bone activity (Kokubo and Takadama, 2006). After 2006 researchers focused on doping SBF solution with different ions to enhance SBF properties as a coating material. Researchers studied on cations such as Al^{3+}, Ln^{3+}, Cr^{3+}, Fe^{3+}, Tb^{3+} and anions such as SiO_4^{4-}, SO_4^{2-}, CO_3^{2-} as dopings into HAp structure (Boanini et al., 2010; Šupová, 2015). The short history of SBF doping with various ions (consist of last decade works) for apatite formation is shown in Table 2.

As the SBF solution was improved, the ionic composition varied due to different preparation techniques. The target for SBF composition is to obtain similar ionic concentrations of human blood serum. Some of the SBF solutions are shown in Table 3.

1971: Bioglass which spontaneously bond to living bone without the formation of surrounding fibrous tissue was prepared
1980: SiO$_2$ layer + CaP formed on a Bioglass allowing bonding to living bone
1987: SiO$_2$ not formed but CaP formed on glass-ceramic crystalline apatite and wollastonite (A-W) allowing bonding to living bone
1990: CaP determined as a crystallite apatite and formed on (A-W) glass-ceramic which reproduced in SBF
1991: Essential requirement for a material to bond living bone formation of bonelike apatite on its surface on the living body that can be repreduced in SBF
1993: Formation of apatite on the surface in SBF is confirmed
1995: A detailed SBF preparation by Cho et. al.
2000: Biomimetic calcium hydroxyapatite synthesis by Tas
2001: HAp coated Ti6Al4V in vitro study by Thian et. al.
2002: Influence of ionic strength and carbonate on the Ca-P coating formation by Barrere et al.
2003: Dissolution and mineralization behaviors of HAp coatings by Zhang et al.
2004: Biomimetic apatite formation on chemically treated titanium by Jonášová et al.
2005: Process and kinetics study of apatite formation by Kim et al.
2006: Detailed recipe for SBF preparation, biomimetic coating and vivo bone activity explained by Kokubo and Takadama
2006-Today: Tuning SBF composition by doping ions (Table 2)

Figure 4 History of SBF preparation (Hench et al., 1971; Ogino et al., 1980; Kitsugi et al., 1987; Kokubo, Kushitani et al., 1990; Kokubo, Ito et al., 1990; Ohtsuki et al., 1991; Filgueiras et al., 1993; Cho et al., 1995; Tas, 2000; Thian et al., 2001; Barrere et al., 2002; Zhang et al., 2003; Jonasova et al., 2004,; Kim et al.,2005; Kokubo and Takadama, 2006).

Table 2 Case studies of hydroxyapatite substitution.

Substituted Ion	Authors
Strontium	Avci et al., 2017
Europium(III)	Kataoka et al., 2016
Cobalt	Ignjatović et al., 2015
Titanium	Li et al., 2014
Magnesium	Onder et al., 2013
Zinc	Hu et al., 2012
Silicon	Aminian et al., 2011
Lead	Zhu et al., 2010
Chromium	Boucetta et al., 2009
Manganese	Mayer et al., 2008
Cerium	Lin et al., 2007

Table 3 SBF solutions in the literature.

Ionic Conc. (mM)	Na^+	K^+	Mg^{2+}	Ca^{2+}	Cl^-	HCO_3^-	HPO_4^{2-}	SO_4^{2-}
Human Blood Serum (Gamble, 1952)	142	5	1.5	2.5	103	27	1	0.5
(Kokubo, Ito et al., 1990)	142	5	1.5	2.5	148.8	4.2	1	0
(Ohtsuki et al., 1991)	142	5	1.5	2.5	147.8	4.2	1	0.5
(Tas, 2000)	142	5	1.5	2.5	125	27	1	0.5
(Oyane et al. 2003)	142	5	1.5	2.5	103	27	1	0.5
(Takadama et al., 2004)	142	5	1.5	2.5	103	4.2	1	0.5
(Bigi et al., 2005)	25.5	0	0	2.5	5	18	1	0
(Kokubo and Takadama, 2006)	142	5	1.5	2.5	147.8	4.2	1	0.5

1.5. Hydroxyapatite Coatings and Dopants

Ti and its alloys are widely used as orthopedic and dental implant materials though they have poor surface biocompatibility, the surface of Ti and its alloys has to be modified to improve their surface osteoinductivity. Coating can be improved by applying HAp coating. HAp acts as reinforcement in hard tissues and is responsible for stiffness of bone, dentin and enamel.

Furthermore, HAp coating enables direct bone formation on implant surfaces by attachment, proliferation and differentiation of bone forming cells (Ducheyne and Qiu, 1999) due its structure resemblance to the mineral constituent of human bone (Boretos, 1987; Geesink et al., 1987; Zeng et al., 1993). Due to these reasons, synthetic HAp exhibits strong affinity to host hard tissues. Though, it possesses poor antibacterial property, crystallinity and stability (Fu and Chen, 2005). HAp coatings are also susceptible to fatigue failure, making it unsuitable for load bearing implants (Thomas et al., 1980; With et al., 1981). To overcome the disadvantages of HAp, many researchers focused on modification of the structure. Apatite compounds are calcium ortho phosphates with a formula of $Ca_{10}(PO_4)_6(OH)_2$. It crystallizes in the hexagonal rhombic prisms shape with $P6_3/m$ symmetry. The theoretical density of HAp is 3.16 g/cm^3 (Park and Lakes, 2007). The structure of HAp and its cell dimensions are shown in Figure 5.
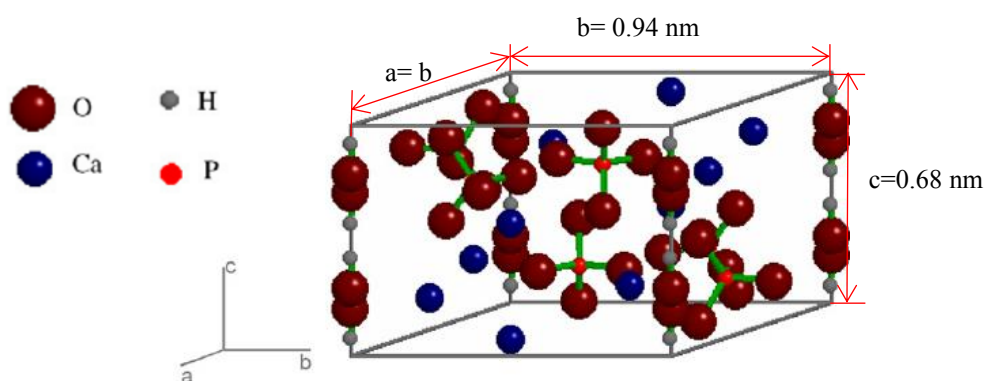
Figure 5 HAp structure and lattice parameters (Park and Lakes, 2007).

In the crystal lattice formed by corner-connected Ca-O octahedra and P-O tetrahedra the divalent metal ions occupy two nonequivalent crystallographic sites (4f (Ca1), 6h (Ca2)). It is known that other divalent cations with a similar charge-to-size ratio to calcium can be readily substituted in the lattice of HAp. The three dimensional network structure exhibits flexibility in accommodating variety of ions, such as monovalent, divalent, trivalent ions (Na, K, Ag, Cd, Mn, Sr, Cu, Co, Zn, Mg, Bi, Ln, etc.) in calcium site. PO_4^{3-} can be substituted by SiO_4^{4-} or CO_3^{2-}.

16

These ionic substitutions can alter properties of HAp (such as solubility and mechanical) either causing or inhibiting normal function, e.g., excessive fluoride can weaken bone (Kaplan et al., 1994; Hall, 2011). For example, substitution improved apatite properties in various applications such as catalysis (Sebti et al., 2001), protein adsorption (Fujii et al., 2006), ion exchangers (Suzuki et al., 1981) and biomaterials etc. (Hench, 1991).

Some researchers focused on antibacterial activity of Ag, Cu and Zn ion substituted ceramics (Kim et al., 1998). Ag, Cu and Zn ion co-doped with β-tricalcium phosphate synthesized by conventional high temperature solid state method is reported for its antibacterial activity and cytotoxicity (Matsumoto et al., 2009). Even though not commonly used like HAp, oxyapatite structures are more widespread in substituted compositions. For example, lanthanum and vanadium-containing oxyapatite compounds (Bouhaouss et al., 2001) were reported as fast oxide ion conductors (Tolchard et al., 2005). Silicate oxy apatite compounds are known for its luminescent activity (Lakshminarasimhan and Varadaraju, 2005) and electrical conductivity (Tolchard et al., 2003). Coated implants should possess similar properties to the human bones. The implants can be made into different shapes such as plates, rods, screws and pins (Kawagoe et al., 2000). Osteoblasts adhere to the apatite and produce a network of collagen fibers, which constitute the organic part of bone. This collagen network is mineralized by apatite and new bone is formed.

HAp's chemical structure can be substituted by cations and anions in order to tune its properties. Several researchers studied multi-ionic substitutions; cationic, anionic and mutual combinations of substitutions in anionic and cationic sites have been formed. These mutual substitutions of trace elements into HAp were introduced new physico-chemical, mechanical and biological properties in comparison to pure HAp or monoionic substituted HAp materials. Table 4 indicates a detailed information about ionic substitutions occurred in HAp structure (Boanini et al., 2010; Šupová, 2015).

Table 4 The ionic substitutions occurred in HAp structure.

Substitution Type	HAp Formula:			$Ca_{10}(PO_4)_6(OH)_2$	
	Cationic Substitution			**Anionic Substitution**	
	Substitutes with Ca^{2+}			**with PO_4^{2-}**	**with OH^-**
Monoionic substitution	Quadrivalent	Ti^{4+}		VO_4^{3-} AsO_4^{3-} SiO_4^{4-} SO_4^{2-} CO_3^{2-} (B type substitution) SeO_4^{2-} SeO_3^{2-}	F^- Cl^- Br^- CO_3^{2-} (A type substitution) SeO_4^{2-} SeO_3^{2-}
	Trivalent	Al^{3+} Ln^{3+} Cr^{3+} Fe^{3+} Tb^{3+}	Nd^{3+} Sm^{3+} Ce^{3+} Eu^{3+} La^{3+} Pr^{3+}		
	Divalent	Sr^{2+} Ba^{2+} Cd^{2+} Pb^{2+} Cu^{2+}	Zn^{2+} Mg^{2+} Mn^{2+} Ni^{2+} Fe^{2+} Co^{2+}		
Monoionic substitution	Monovalent	Na^+ K^+	Ag^+ Li^+		
Cationic co-substitution	Na^+/ Mg^{2+} Mg^{2+}/Zn^{2+} $Sr^{2+}/Mg^{2+}/Zn^{2+}$ Sr^{2+}/Ce^{3+} Ag^+/Mg^{2+}	Ti^{4+}/Ag^+ Ti^{4+}/Cu^{2+} Ti^{4+}/Zn^{2+} Fe^{3+}/Mn^{2+}		-	-
Anionic co-substitution	-			Cl^-/F^- (OH⁻ subs.) CO_3^{2-} (PO_4^{2-} subs.) /F^- (OH⁻ subs.) SeO_4^{2-}(PO_4^{2-} subs.)/ CO_3^{2-} (PO_4^{2-} subs.)	
Anionic-cationic co-substitution	Na^+/ CO_3^{2-} Zn^{2+}/ CO_3^{2-} Zn^{2+}/ F^- Na^+/ F^- Mg^{2+}/ F^- Mg^{2+}/ SiO_4^{4-}	Mg^{2+}/ CO_3^{2-} Sr^{2+}/ CO_3^{2-} Sr^{2+}/ F^- Na^+/ Cl^- Mn^{2+}/ CO_3^{2-} Sr^{2+}/ SiO_4^{4-}		$Na^+/ Mg^{2+}/ CO_3^{2-}$ $Zn^{2+}/ Sr^{2+}/ CO_3^{2-}$ $Na^+/ SiO_4^{4-}/ CO_3^{2-}$ $Na^+/ Cl^-/ CO_3^{2-}$ $Mg^{2+}/ SiO_4^{4-}/ CO_3^{2-}$ $Na^+/ Mg^{2+}/ F^-$	

1.6. Effect of Bismuth Ion in HAp Structure

Bismuth is one of the heavy metals with low toxicity and known for its antibacterial activity for more than 200 years (Li and Sun, 2012). Bi compounds were primarily used clinically for the treatment of ulcers, and they also have anti-cancer activity (Maier and Klapötke, 1988; Desoize, 2004; Tiekink, 2002). Due to the similarity in composition with the biological apatite, doped HAp compounds may be a better choice compared to pure HAp.

Not long ago, bismuth doped CaP was found to be potent antimicrobial agent for many applications specially for root canal filling (Chen et al., 2010). It is also proven that Bi^{3+} enhanced the long-term calcium-containing mineral deposition of osteoblasts more than other cations (Webster et al., 2004). Thus, it was claimed that Bi^{3+} release might have a positive influence on osteogenesis.

Standard lattice parameter values of an undoped HAp hexagonal crystal, a and c; are 0. 94 nm and 0.68 nm, respectively (Park and Lakes, 2007). Changes in overall volume may imply that dopant substituted for calcium in the HAp lattice since cations smaller than calcium (Mg^{2+}, Zn^{2+}, In^{3+}, Y^{3+}) corresponding to a shrinkage in crystal volume, while cations larger than calcium (Bi^{3+}, La^{3+}) corresponding to an increase in crystal volume (Webster et al., 2004). As Bi^{3+} ion has larger ionic radius (1.60 Å) than Ca^{2+} ionic radius (1.00 Å), it is expectable that Bi^{3+} substitution in calcium site will result in increase in the lattice unit parameters. Bi ions can push surrounding atoms and cause local distortions. (Sumathi and Buvaneswari, 2012). Substitution of bismuth ion in HAp structure is shown in Figure 6.
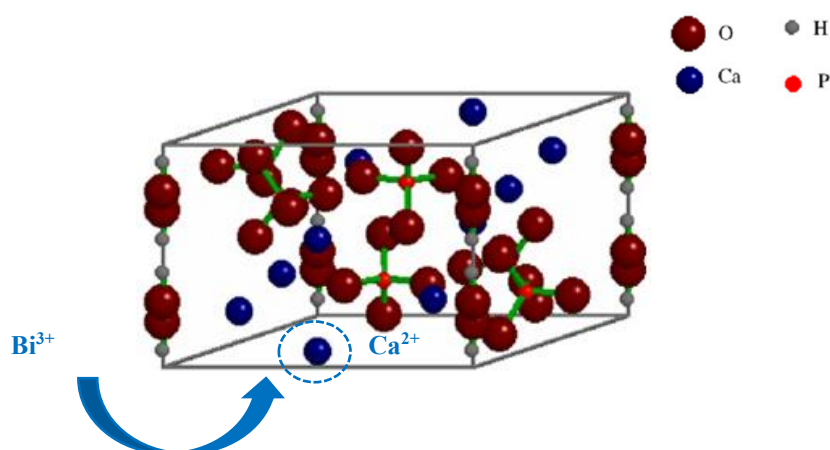
Figure 6 The substitution of bismuth ion into HAp structure (Park and Lakes, 2007).

Bismuth doped HAp would have the following chemical formula:

$Ca_{10-x}Bi_x(PO_4)_6(OH)_2$,   where, x = Doping molarity

HAp doped with Bi is mainly composed of single phase HAp. In general, no other secondary phases such as tricalcium phosphate (TCP), tetracalcium phosphate (TTCP) or calcium oxide (CaO) were detected up to certain bismuth concentration. Though in cases of larger than 1.0 wt.% Bi doping a-TCP phases can be detected. In addition, Bi addition (>0.3 wt%) into HAp structure leads to exhibit higher densification (Ramesh et al., 2011).

The effect of substitution of Bi on HAp's thermal stability was investigated in literature. It was found out that Bi and K substituted HAp was stable up to 1000°C. However, the thermal stability could not be compared exactly with the reported literature because of the different levels of substitution (Shanmugam and Gopal, 2014).

1.7. Effect of Carbonate Ion in HAp Structure

SBF solutions mentioned in literature differ mostly in the concentrations of HCO_3^- and Cl^- compared to human blood serum. The addition of more carbonate ion into SBF may make SBF composition more familiar to human blood serum. Introduction of carbonate ions in HAp improves dissolution and could enhance the osteointegration rate. In addition, carbonate doped HAp can be resorbed by osteoclasts and be replaced with new bone. Therefore, carbonate-substituted HAp is a prospective candidate for bone-substitute material (Bang et al., 2015). Bone mineral contains a minor amount (3 wt. %) of carbonate ion which substitutes hydroxide (OH^-) ions in the A sites (A-type substitution) and phosphate (PO_4^{3-}) ions in the B sites (B-type substitution) of the apatite structure (Elliott et al., 1985). Carbonate is valuable and crucial constituent of the HAp of human dental enamel and cortical bone (Fleet and Liu, 2007). The ratio of A/B type substitution varies depending on the individual (Elliott et al., 1985; Burnell et al., 1980; Rey et al., 1991). A-type CHA is found in old bone tissue while B-type is in young bone tissue.

B-type of carbonate substitution is preferred because it is commonly found in young tissue and responsible for the decrease of crystallinity and subsequently resulting in increases its solubility (Wong and Noor, 2016). Although these levels of substitution are limited, different ions play an important role in the biochemistry of the hard tissue (Ginty et al., 1998; Ergun et al., 2002; Wiesmann et al., 1998; Kim et al., 2003; Farley et al., 1983; Neuman and Neuman, 1958). The incorporation of carbonate into the apatite structure can happen by substitution for the monovalent anion (A-type substitution of one CO_3^{2-} for two OH^-) or by substitution for phosphate (B-type substitution CO_3^{2-} for PO_4^{3-}), the latter of which requires loss of both monovalent anions and cations to preserve charge neutrality (Yoder et al., 2012). These types of apatite structures form a bioactive apatite with higher dissolution and osteoclast mediated resorption features (Fleet and Liu, 2003). Moreover, the existence of carbonate into the apatite structure leads to a decrease in crystallinity, a change in crystal morphology, and an enhancement of chemical reactivity due to the weak bonding of carbonates geometry (Vignoles et al., 1988; Nikčević et al., 2004). The presence of defects and molecular substitution might also affect the mechanical properties of HAp coatings. In fact, the carbonated apatite increases the local concentration of calcium and phosphate ions that are necessary for new bone formation (Fathi and Zahrani, 2009). The carbonate substitution is related to the calcium vacancy and mechanical properties of the apatite. Regarding to all these reasons, the production of CHA and carbonated fluorapatite is of great value and has been broadly scrutinized using different synthesis processes such as precipitation, sol-gel, solid state reaction, and hydrothermal treatment.

According to literature, CO_3^{2-} ion substitutes with both OH^- (A-type) and PO_4^{3-} (B-type), thus the formula of dual doped HAp can be written as: $Ca_{10-x-y}Bi_y(HPO_4)_{x-z}(CO_3)_z(PO_4)_{6-x}(OH)_{2-x}$ assuming that $0 \leq x, y, z \leq 1$. It can be supposed that as long as the (HCO_3^-) concentration in SBF is below 20 mmol/l, only B-type HAp precipitates. At higher (HCO_3^-) concentration, it can be assumed that A-type HAp also forms (Müller et al., 2007).

Substitution of carbonate ion in HAp structure is shown in Figure 7.

A-type substitution   **B-type substitution**
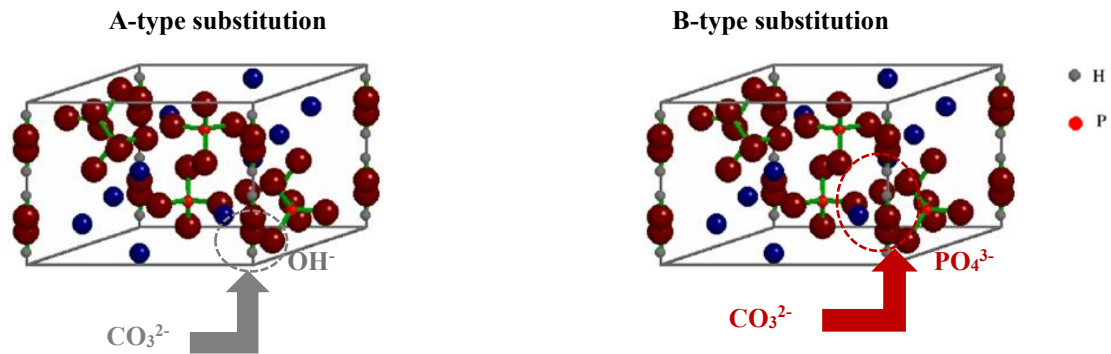
Figure 7 The substitution of carbonate ion into HAp structure (Park and Lakes, 2007).

Studies on tooth enamel and apatites synthesized at high temperatures showed carbonate groups located in the hydroxy channels, replacing the hydroxy ions, leading to an increase in the a-parameter of the apatite lattice. Substitutional carbonate groups in phosphate locations were observed in human bone mineral and again in high-temperature synthetic apatites, which was accompanied by a shrinkage in the a-parameter of the lattice due to its smaller size. Many structural characteristics of HAp were observed as a mixture of these two carbonate defects within the same lattice, as well as a mixture of carbonate and other defects (Peroos et al., 2006). Furthermore the addition of carbonate into HAp/A-type substitution caused a decrease in crystallinity and, as the bonding in the apatite became weaker, the chemical reactivity in these apatites was increased (Tônsuaadu et al., 1995). On the other hand, addition of carbonate into HAp/AB-type substitution caused an increase in the crystallinity (Müller and Müller, 2006). It is claimed that CO_3^{2-} ion substituted HAp samples had a similar structure as the hexagonal $P6_3/m$ space group but with a slight difference in the value of the lattice constants, which were a=9.389 Å and c=6.901 Å (Mohammad et al., 2015).

It was found that CO_3^{2-} ion substituted HAp was stable up 800 °C, above 900 °C carbonated HAp decomposed to $CaCO_3$ phase in the CO_2 gas atmosphere (Bang et al., 2015). No intermediate phase, such as the formation of tricalcium phosphate, was observed for CO_3^{2-} ion substituted HAp (Mohammad et al., 2015).

Carbonate ions were reported not to affect the grain growth and to enhance sinterability of HAp if they replaced only phosphate groups in the HAp lattice. On the other hand, carbonate ions for hydroxyl groups substitution had no effect on sintering (He et al., 2005).

1.8. Aim of the Study

The aim of this thesis was to reduce implant rejection caused by the human body and increase the implants lifetime as this new generation orthopedic implant coatings were produced. Mimicking the bone structure by coating metallic scaffold with HAp, $(Ca_{10}(PO_4)_6(OH)_2)$ in an effective way enable strong bone-implant integration. The aim was to prepare a new generation coating on Ti6Al4V implant. Three steps pretreatment procedure (sandblasting, acid etching and heating), bismuth and carbonate ions doping in the structure of HAp as coating material constitute originalities of this study. Coated plates were evaluated in terms of their structural properties by SEM, EDS, AFM, FTIR, XRD, ICP and XPS. Furthermore, mechanical tests and in vitro cell studies were carried out to study mechanical and biological properties of coatings, respectively to investigate the antibacterial property of the coating, the survival of the *Staphylococcus epidermidis* on the surface of the implant were determined.

CHAPTER 2

MATERIALS AND METHODS

The Ti alloy, Ti6Al4V (Grade 5 ELI ASTM B265-10), was selected as the substrate material because of its widespread use in orthopedic area. Experimental procedure can be summarized into three main parts as shown in Figure 8.
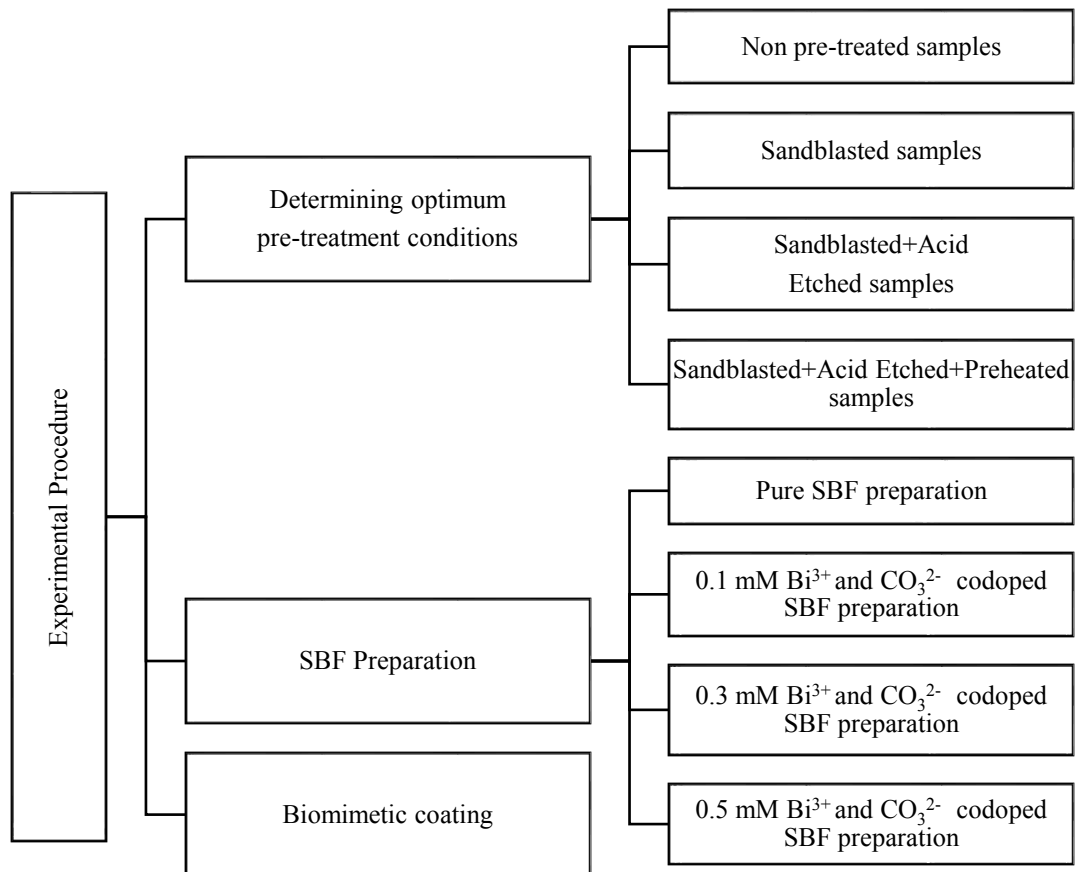
Figure 8 Schematic presentation of experimental procedure.

In order to follow up this thesis more easily samples were coded as shown in Table 5.

Table 5 Codes used for coated samples.

Code	Explanation
P4	Ti-S-A-P plates after soaking in pure 1.5×SBF for 4 days
P7	Ti-S-A-P plates after soaking in pure 1.5×SBF for 7 days
P14	Ti-S-A-P plates after soaking in pure 1.5×SBF for 14 days
P21	Ti-S-A-P plates after soaking in pure 1.5×SBF for 21 days
0.1-C4	Ti-S-A-P plates after soaking in 0.1 mM co-doped 1.5×SBF for 4 days
0.1-C7	Ti-S-A-P plates after soaking in 0.1 mM co-doped 1.5×SBF for 7 days
0.1-C14	Ti-S-A-P plates after soaking in 0.1 mM co-doped 1.5×SBF for 14 days
0.1-C21	Ti-S-A-P plates after soaking in 0.1 mM co-doped 1.5×SBF for 21 days
0.3-C4	Ti-S-A-P plates after soaking in 0.3 mM co-doped 1.5×SBF for 4 days
0.3-C7	Ti-S-A-P plates after soaking in 0.3 mM co-doped 1.5×SBF for 7 days
0.3-C14	Ti-S-A-P plates after soaking in 0.3 mM co-doped 1.5×SBF for 14 days
0.3-C21	Ti-S-A-P plates after soaking in 0.3 mM co-doped 1.5×SBF for 21 days
0.5-C4	Ti-S-A-P plates after soaking in 0.5 mM co-doped 1.5×SBF for 4 days
0.5-C7	Ti-S-A-P plates after soaking in 0.5 mM co-doped 1.5×SBF for 7 days
0.5-C14	Ti-S-A-P plates after soaking in 0.5 mM co-doped 1.5×SBF for 14 days
0.5-C21	Ti-S-A-P plates after soaking in 0.5 mM co-doped 1.5×SBF for 21 days

2.1. Determining Optimum Pre-Treatment Conditions

None treated samples (Ti): None pretreated samples were prepared by cutting the bulk Ti6Al4V plates into 10x10x1.2 mm^3 dimensions (Figure 9).
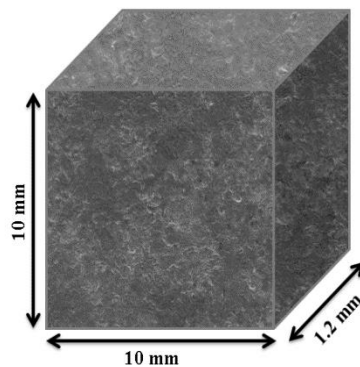
Figure 9 None treated Ti plate.

Sandblasted Samples (Ti-S): Sandblasted samples were prepared by exposing the cut plates to sandblasting process via sandblasting gun or sandblasting drum.

In both cases SiO_2 particles used were at spherical form with an average diameter of 250-300 μm. Sandblasted plate is shown in Figure 10.
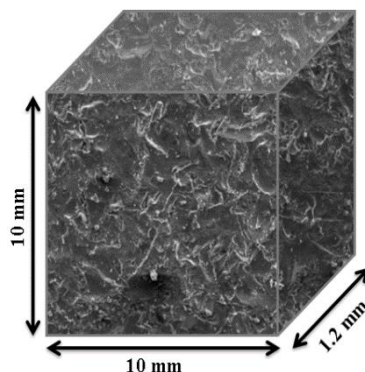
Figure 10 Sandblasted Ti plate.

Sandblasted + Acid Etched Samples (Ti-S-A): Sandblasted + Acid etched samples were prepared by acid etching process of sandblasted plates in H_2SO_4 (48% wt.) solution as an etchant. Etching was performed at 200ºC for 30 min by using a heater (Figure 11).

Figure 11 Acid etching process.

Acid etching process was followed by washing the plates in distilled water and drying them in a desiccator at room temperature (RT).

The acid etching reaction is shown in Equation (1):

$$Ti + 2H_2SO_4 \rightarrow Ti(SO_4)_2 + 2H_2 \qquad (1)$$

Sandblasted + Acid Etched + Preheated Samples (Ti-S-A-P): Sandblasted + Acid etched + Preheated samples were prepared via preheating of acid etched plates. Preheating process was carried out in a furnace at 600ºC for 1 h. After preheating, samples were kept in a furnace (Figure 12) in overnight period for cooling.

Figure 12 Preheating process.

2.2. SBF Preparation

2.2.1. Pure SBF Preparation

In order to prepare the simulated body fluid (SBF), a method by Kokubo and Takadama was followed (Kokubo and Takadama, 2006). For the preparation of 1000 ml of 1.5xSBF, the reagents given in Table 6, was dissolved in 700 ml ion-exchanged distilled water at 36.5±1.5°C, by adding in the order from the 1st to the 8th under constant stirring. Each weighing bottle was washed with several drops of ion-exchanged distilled water, which was added to the solution.

After the first eight reagents were dissolved, TRIS and small amount of HCl were dissolved in the process of pH adjustment. Just before dissolving the TRIS, the pH of the solution should be between 2.0±1.0. 1M HCl and TRIS were added alternately into the solution until the whole amount of TRIS was dissolved keeping the pH within the range of 7.42-7.45. Lastly, the pH of the solution was adjusted to 7.40 exactly at 36.5°C by adding 1 M HCl dropwise. The resulting solution was used in biomimetic coating immediately after the preparation without delay or storing. Amounts for SBF preparation are given in Table 6.

Table 6 SBF ingredients formula and amounts for 1000 ml of SBF.

Order	Reagent	Formula	Amount for 1xSBF	Amount for 1.5xSBF
1	Sodium chloride	$NaCl$	8.035 g	12.0525 g
2	Sodium hydrogen carbonate	$NaHCO_3$	0.355 g	0.5325 g
3	Potassium chloride	KCl	0.225 g	0.3375 g
4	Di-potassium hydrogen phosphate trihydrate	$K_2HPO_4.3H_2O$	0.231 g	0.3465 g
5	Magnesium chloride hexahydrate	$MgCl_2.6H_2O$	0.311 g	0.4665 g
6	Hydrochloric acid	1.0 M HCl	39 ml	58.5 ml
7	Calcium chloride	$CaCl_2$	0.292 g	0.438 g
8	Sodium sulfate	Na_2SO_4	0.072 g	0.108 g
9	TRIS hydroxymethyl aminomethane	$(CH_2OH)_3CNH_2$	6.118 g	9.177 g
10	Hydrochloric acid	1.0 M HCl	0-5 ml	0-10 ml

The dissolution reactions are shown in Equations (2-8):

$$NaCl \rightarrow Na^+ + Cl^- \tag{2}$$
$$NaHCO_3 \rightarrow Na^+ + HCO_3^- \tag{3}$$
$$KCl \rightarrow K^+ + Cl^- \tag{4}$$
$$K_2HPO_4{\cdot}3H_2O \rightarrow 2K^+ + HPO_4^{2-} \tag{5}$$
$$MgCl_2{\cdot}6H_2O \rightarrow Mg^{2+} + 2Cl^- \tag{6}$$

$$CaCl_2 \rightarrow Ca^{2+} + 2Cl^- \tag{7}$$

$$Na_2SO_4 \rightarrow 2Na^+ + SO_4^{2-} \tag{8}$$
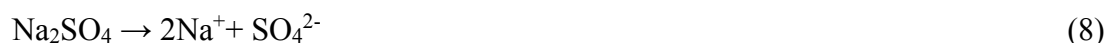
The ionic concentrations of human blood serum and 1.5×SBF are reported in Table 7. According to the given ionic concentrations, the amounts of reagents were raised. The same procedure for the preparation of SBF with conventional ionic concentration was followed while preparing the more concentrated solution. The resulting solution was used immediately after the preparation without delay or storing.

Table 7 The ionic concentrations of human blood serum and 1.5×SBF.

Ion	Blood Serum	Concentration in 1.5×SBF (mM)
Na^+	142.0	212.3
K^+	5.0	7.5
Mg^{2+}	1.5	2.3
Ca^{2+}	2.5	3.8
Cl^-	103.0	186.8
HPO_4^{2-}	1.0	1.5
SO_4^{2-}	0.5	0.75
HCO_3^-	27.0	40.5

SBF solution was prepared at 37°C, 710 rpm on a magnetic stirrer and the final pH value was set to 7.4 (Figure 13).
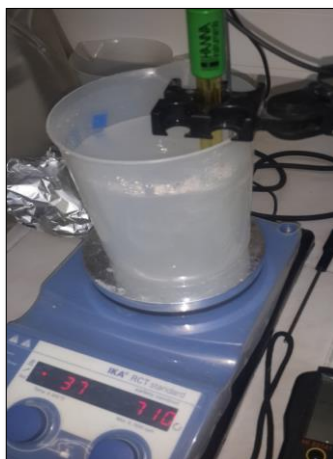
Figure 13 SBF preparation system.

2.2.2. Bismuth and Carbonate Co-Doped SBF Preparation

Bismuth (III) chloride ($BiCl_3$) was selected as bismuth source. Bismuth (III) chloride is soluble in HCl which already presents in SBF solution. Three different concentrations; 0.1 mM, 0.3 mM and 0.5 mM of Bismuth ion were introduced into SBF solutions.

Sodium bicarbonate ($NaHCO_3$) which already exists in SBF formulation was used as a carbonate source. Carbonate ion concentration was raised up to the 40.50 mM in order to equalize the concentration to the natural human blood serum.

Sand blasted + acid etched + preheated plates (Ti-S-A-P) were used as substrate. Amounts used to prepare co-doped SBF solutions are shown in Table 8.

In addition to previously mentioned dissolution (2-8) reactions, reaction (9) occurs:

$$BiCl_3 \rightarrow Bi^{3+} + 3Cl^- \tag{9}$$
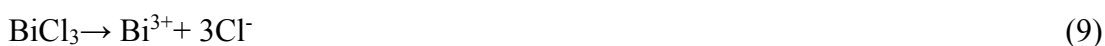
The ionic concentrations of prepared solutions are shown in Table 9.

31

Table 8 Order, formulas and amounts of chemicals used to prepare Bismuth and Carbonate co-doped 1.5xSBF for 1000 ml.

Order	Reagent	Formula	Amount used for		
			0.1 mM co-doped 1.5xSBF	0.3 mM co-doped 1.5xSBF	0.5 mM co-doped 1.5xSBF
1	Sodium chloride	NaCl	10.0563 g	10.0563 g	10.0563 g
2	Sodium hydrogen carbonate	$NaHCO_3$	3.4023 g	3.4023 g	3.4023 g
3	Potassium chloride	KCl	0.3375 g	0.3375 g	0.3375 g
4	Di-potassium hydrogen phosphate trihydrate	$K_2HPO_4.3H_2O$	0.3465 g	0.3465 g	0.3465 g
5	Magnesium chloride hexahydrate	$MgCl_2.6H_2O$	0.4665 g	0.4665 g	0.4665 g
6	Bismuth (III) chloride	$BiCl_3$	0.0315 g	0.0946 g	0.1577 g
7	Hydrochloric acid	1.0 M HCl	58.50 ml	58.50 ml	58.50 ml
8	Calcium chloride	$CaCl_2$	0.4380 g	0.4380 g	0.4380 g
9	Sodium sulfate	Na_2SO_4	0.1080 g	0.1080 g	0.1080 g
10	TRIS	$(CH_2OH)_3CNH_2$	9.1770 g	9.1770 g	9.1770 g
11	Hydrochloric acid	1.0 M HCl	0-10 ml	0-10 ml	0-10 ml

Table 9 Ionic concentrations of 1.5xblood serum, 1.5×SBF and Bismuth and Carbonate co-doped 1.5xSBF.

Ion	1.5 x Blood Serum (mM)	Pure 1.5xSBF (mM)	0.1 mM co-doped 1.5xSBF (mM)	0.3 mM co-doped 1.5xSBF (mM)	0.5 mM co-doped 1.5xSBF (mM)
Na^+	213.00	214.09	214.09	214.09	214.09
K^+	7.50	7.56	7.56	7.56	7.56
Mg^{2+}	2.25	2.29	2.29	2.29	2.29
Ca^{2+}	3.75	3.95	3.95	3.95	3.95
Bi^{3+}	-	-	0.10	0.30	0.50
Cl^-	154.50	223.24	189.08	189.08	189.08
HCO_3^-	40.50	6.34	40.50	40.50	40.50
HPO_4^{2-}	1.50	1.52	1.52	1.52	1.52
SO_4^{2-}	0.75	0.76	0.76	0.76	0.76

SBF solution was prepared at 37ºC by adding the constituents one by one and mixing with a magnetic stirrer set at 710 rpm and the final pH value was set to 7.4.

2.3. Biomimetic Coating

Ti6Al4V substrates were soaked in prepared SBF solution separately at 37°C for apatite depositing. The plates, after being placed into plastic beaker, were soaked in 50 ml of simulated body fluids per plate. In every two days, new solutions were prepared and freshened. In each renewal of the solutions, by considering the possible precipitation on the walls, the plastic beakers were replaced with the clean ones. The solutions, in which the plates were soaked, were kept at 37°C by using a shaking water bath (Figure 14).

Figure 14 The shaker used for biomimetic coating.

Coated samples were taken out at days 4, 7, 14 and 21 for analysis. Coated plates were dried in a furnace at 200ºC for 2 h and left for cooling overnight before analysis.

2.4. Sterilization

The preparation of SBF solutions was carried out with autoclaved distilled water and the coated plates were sterilized after biomimetic deposition process.

The coated Ti6Al4V plates were sterilized in a dry-heat furnace at 200°C for 2 h. In order to prevent spontaneous crack formation on the HAp coatings, the samples were left to cool slowly in the furnace during overnight.

2.5. Analysis

In order to obtain information about the properties of samples, analysis were performed as summarized in Figure 15.
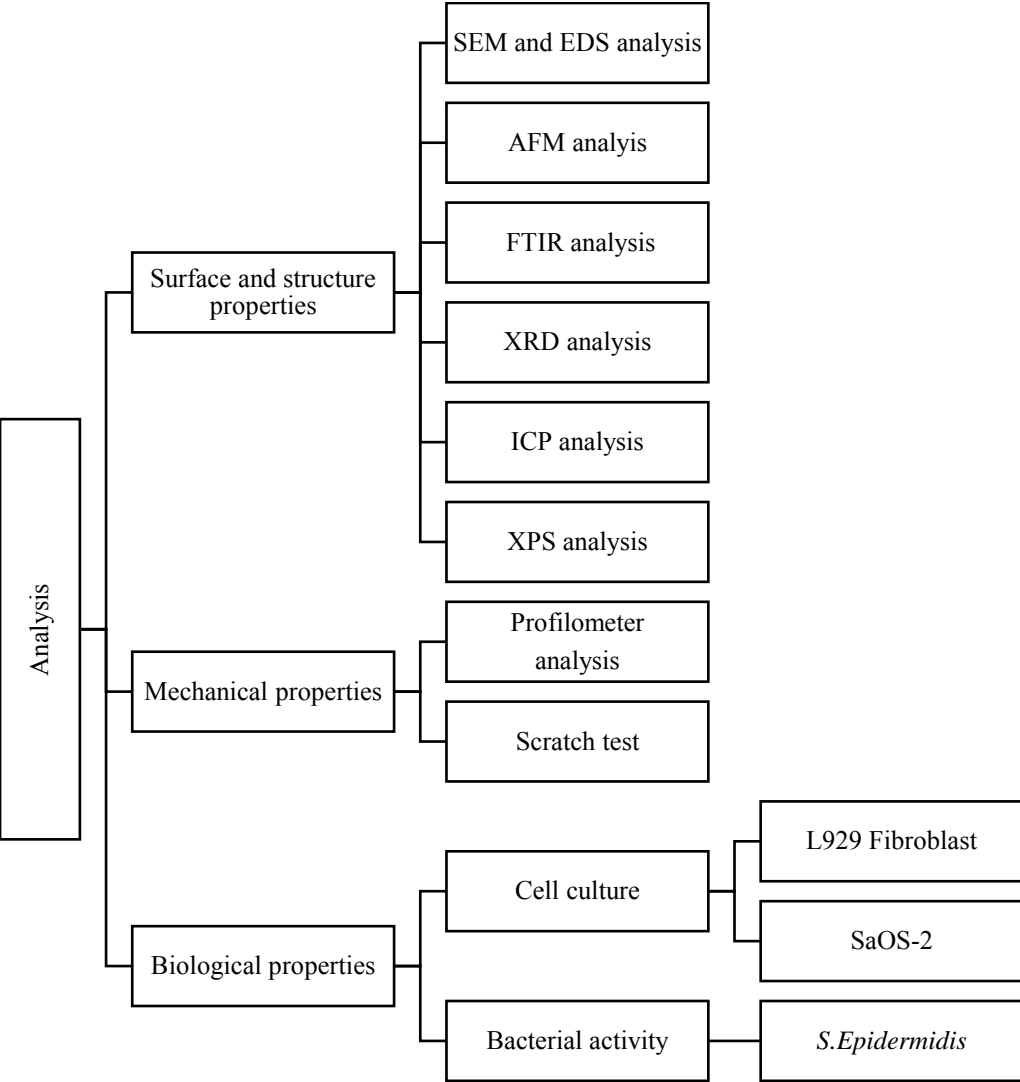
Figure 15 Summary of analysis performed.

2.5.1. Surface and structure properties

The surface morphology of the abraded, pretreated, biomimetically coated and cell seeded plates were observed with a scanning electron microscope (QUANTA 400F Field Emission SEM). The plates were first sputter-coated with Au/Pd in order to obtain a thin layer of conducting material. In addition, elemental composition of the coatings was analyzed by using the energy dispersive X-ray spectroscopy (JXA - 8230 EDS) set up.

The surface topography and roughness of abrade and pretreated samples were examined with an atomic force microscope (Veeco MultiMode V model, AFM). AFM was used in tapping mode. Area of investigation was selected as 50 μm x 50 μm. Roughness parameters were evaluated in terms of R_a, R_z and R_q. R_a stands for arithmetic mean of the area between the roughness and its mean line, while R_z stands for arithmetic mean of the five highest peaks plus the depth of the five deepest valleys over the evaluation length. R_q is the root mean square average of the profile heights over the evaluation length (Borsari et al., 2005).

For Fourier transform infrared spectroscopy (FTIR) analysis, a spectrometer (Perkin Elmer 400, Germany) was used with scan rate of 16 and selected resolution was 4 cm^{-1}. The samples were examined in the mid-infrared (MIR) range (4000-400 cm^{-1}). Baseline correction was applied.

X-Ray Diffraction (XRD) analysis was performed with a diffractometer (Rigaku Ultima-IV, Japan) with Cu-Kα radiation at 40 kV and 30 mA. A pretreated plate without a coating was introduced as blank and therefore, the pattern of substrate itself would be subtracted from XRD data of the coated samples. XRD data were also assessed by the Rietveld method.

The Rietveld method is a full pattern analysis approach in which all factors contributing to the intensity measured for each 2θ can be refined until the difference between the observed and calculated pattern is minimized.

Inductively coupled plasma-mass spectrophometry (ICP-MS) analysis was performed by using a Thermo Electron X7 device (Thermo Fisher Scientific, USA). For ICP-MS analysis, the coatings on the Ti6Al4V plate surfaces were scraped by using a spatula and each powder was dissolved in 2% nitric acid (HNO_3) solution.

X-ray photoelectron spectroscopy (XPS) was performed by using a PHI 5000 VersaProbe. X-ray photoelectron spectroscopy is a technique for analyzing the surface chemistry of a material. XPS can measure the elemental composition, empirical formula, chemical state and electronic state of the elements within a material.

2.5.2. Mechanical properties

Thickness analyses were run with a profilometer (Dektak 6M Stylus Surface Profilometer). It provides topographic information of the sample by measuring vertical pattern of the surface using stylus tip. Hills and valleys profile mode was selected within 2000 μm scan length. The test was repeated 5 times for each sample in order to obtain an average thickness value.

Scratch tests were run with a scanning scratch tester (Shimadzu SST-W101, Japan). The scratch test was used to evaluate the adhesion of the pure and doped HAp coating to the underlying substrate. The scratch tests were conducted using a scratch tester with a linear and progressive load, with the following test parameters: scratch pre load of 0.05 N, load speed of 0.47 N/min, end load of 1 N. The scratch length was 4 mm.

The scratch test consisted of generating scratches using a Rockwell diamond tip with 100 μm radius (serial number I-128) maintained at a constant speed over the surface under different test loadings. The test was repeated 5 times for each sample and the measured values of the critical lateral force were averaged. Series of scratch tests were performed with normal loads on a coating to obtain a load where the coating exhibited failure. Each scratch was evaluated by the use of an optical microscope for failure. The load at which such failure of the coating occurs is termed as the critical load (Lc). Critical loads were determined from ossilations in friction coefficent graph.

2.5.3. Biological properties

L929 Fibroblast cells were seeded into 96-well plates at a density of 1.0×10^4 cells/well. Cells were allowed to attach to the surfaces in an incubator for 24 h. Plates were weighed as 0.1 g/ml and then left in an incubator at an atmosphere of 5% CO_2 at 37°C in serum-free culture medium for 72 h. Prepared extracts were applied to cells untreated with extract and left in an incubator for 24 h. Nutrient medium was used as control. Elisa plate reader was used at 570 nm wavelength in order to determine cell viability. In order to determine cytotoxicity, MTT tests were performed according to ISO 10993-5 standard. MTT assay is a sensitive technique that uses 3-(4,5-dimethylthiazol-2-yl)-2,5-diphenyltetrazolium bromide. Calculation of cytotoxicity is shown in equation (10). If the percentage of viability is lower than 70%, sample has potential to be cytotoxic.

$$\text{Viability \%} = (100 \times OD_{570e})/ OD_{570b} \tag{10}$$

Where,

OD_{570e}: Optical density of the sample

OD_{570b}: Optical density of control group

Osteogenic committed cell line Saos-2 (CRL-7939, ATCC, USA) were obtained in the cryopreserved form in a cryovial. Upon receipt, the cells were removed from dry ice packaging and thawed by gentle agitation in a 37°C water bath immediately. The base medium of this cell line is Dulbecco's Modified Eagle Medium (DMEM). In order to obtain a complete growth medium, 10% Fetal Bovine Serum (FBS) (Biowest, France) and 1% penicillin/streptomycin solution (Biowest, France) were added to DMEM (Biowest, France). After thawing the cryopreserved cells for 2 min, the vial content was transferred to a centrifuge tube containing 11.5 ml complete culture medium and centrifuged at 2000 rpm for 5 min. The cell pellet was resuspended in complete medium, transferred to a cell culture flask (T-75 type) and incubated at 37°C in a humidified incubator with 5% CO_2. In every two day, medium solution in the cell culture flask was refreshed. When the cells reached 80% confluency, they were subcultured. The medium was removed and the cells were rinsed with PBS. The cells were detached by using 0.25% trypsin/EDTA (Gibco, USA) solution at 37°C. Trypsin was neutralized with growth medium and the detached cells were centrifuged at 2000 rpm for 5 min. The cells were diluted in growth medium, seeded to flasks with a subcultivation ratio of 1:3 and incubated in a 37°C, humidified incubator with 5% CO_2. The medium was refreshed twice per week. Elisa plate reader was used at 570 nm and 600 nm wavelength in order to determine cell viability. To investigate the ability of the coating surfaces to induce biominerals, SaOS-2 cells were seeded onto coatings at a density of 50 000 cells/ sample. The Alamar Blue test was performed to assess cytotoxicity. In order to obtain background corrected absorbance data the following calculations were made. The absorbance at 600 nm was subtracted from the absorbance at 570 nm for each individual well. Then, the absorbances of the media only control wells were averaged and the average control well value was subtracted from the absorbance of the each experimental well. By doing this, the background (absorbance of culture media) was corrected. The number of replicates for each group was 5 (n=5). Statistical comparison of the results was performed using the ANOVA test. To calculate percentage of reduction Equation (11) was used due to U.S. Patent No. 5501959:

$$\text{Reduction}(\%) = \frac{(117216 \times \text{Sample at 570 nm}) - (80586 \times \text{Sample at 600 nm})}{(155677 \times (c\text{-}) \text{ at 600 nm}) - (14652 \times (c\text{-}) \text{ at 570 nm})} \times 100 \qquad (11)$$

Control negative samples (c-) were composed of medium and Alamar Blue (no cells, no plates). On the other hand Control positive samples (c+) were cells seeded on culture plates. Samples were analyzed at day 1, day 3 and day 7 after seeding. The absorbance is a direct measure of cellular viability since it is a result of the ability of the cells to reduce the active ingredient.

2.5.3.1. Determination of Cell Morphology with SEM Imaging

In order to examine the morphology and attachment of SaOS-2 cells on the pure and bismuth added HAp coatings, SEM studies were performed. After growing in T-75 flasks to 90-95% confluency, the cells were detached from the surface by 0.25% trypsin/EDTA solution. 50 000 cells were seeded on each sample in DMEM medium containing 10% FBS and 1% penicillin/streptomycin. The plates were incubated in 24-well plates for 1 day and 7 days. After incubation, the medium in the wells were aspirated and the cells were washed with PBS. The plates were immersed in 4% paraformaldehyde solution for 15 min at RT in order to preserve the cell morphology by fixation. After fixation, the cells were gently rinsed with PBS and the cells were dehydrated with graded series of ethanol (50%, 70%, 80%, 90% and 100%) for 10 min of immersion in each solution. For complete dehydration, hexamethyldisiloxane (HMDSO, Sigma, USA) was dropped onto the plates and they were left in a laminar flow cabin for 10 min. Plates were coated with platinum (Pt) prior to SEM examinations. Sputter coated samples were observed by SEM (JEOL, JSM 6400, Japan) operating at an acceleration voltage of 15 kV.

2.5.3.2. Antimicrobacterial Activity Test

Staphylococcus epidermidis is one of the members of normal bacterial flora of the human skin. It accounts for most of the device-related infections; it is one of the most common factors of primary bacteremia due to the formation of biofilm adherent to the implants.

Prior to the antibacterial test, *Staphylococcus epidermidis* bacteria (ATCC 12228) were cultured on nutrient agar plates at 37°C. A 10^6 colony-forming unit (CFU)/ml bacterial suspension was prepared using a 1:500 diluted nutrient broth (NB). The coated Ti6Al4V plates were sterilized in a dry-heat furnace at 200°C with for 2 h. In order to prevent spontaneous crack formation on the HAp coatings, the samples were left to cool slowly during overnight in the furnace. The antibacterial tests were performed with 3 replicates from each group (n = 3). A 50 µl aliquot of the bacterial suspension was dispensed into the sterilized specimens and covered with a 15×15 mm cover glass. The specimens were subsequently placed into an incubator set at 37°C with 95% humidity and incubated for 4 h. After the incubation period the samples were washed with 5 ml of PBS solution and subsequently cultivated on the surface of a nutrient agar plate (100 µl). The colonies formed on the plates surface were counted and the results were obtained in CFU/ml (Ohtsu et al., 2017; Chen et al., 2006).

CHAPTER 3

RESULTS & DISCUSSION

3.1. Surface and Structure Properties

3.1.1. Effect of Pre-Treatment

SEM images of as received and pretreated plates are shown in Figure 16. As seen from the image at Figure 16 (a), as received Ti6Al4V plate (Ti) surface is quite smooth. In order to enhance the mechanical interlock between the coating and metal plate surface by changing the surface topography, abrading was applied to the Ti6Al4V plates (Ti-S). As represented in Figure 16 (b), Ti6Al4V sandblasted plate surface became rougher by sandblasting process. To remove the sand particles observed on the surface, acid etching process was applied on these samples. As seen from Figure 16 (c), Ti6Al4V sandblasted + acid etched plate (Ti-S-A) surfaces were substantially treated by acid etching process. Material became rougher and much more porous. Crystal titanium salts also existed on the plate surface. Acid etching process was followed by the preheating step. Figure 16 (d) shows SEM images of Ti6Al4V sandblasted + acid etched + preheated plates (Ti-S-A-P). The plate surface was oxidized by preheating process. It was claimed that grain boundaries were shrank and got oxidized.

EDS Spectra of as received and pretreated plates are shown in Figure 17. EDS spectrum in Figure 17 (a) proved that Ti alloy used as a substrate is mainly composed of TiKα. EDS spectrum in Figure 17 (b) supported the presence of sand particles on the surface. Moreover, Si and Al peaks were observed.
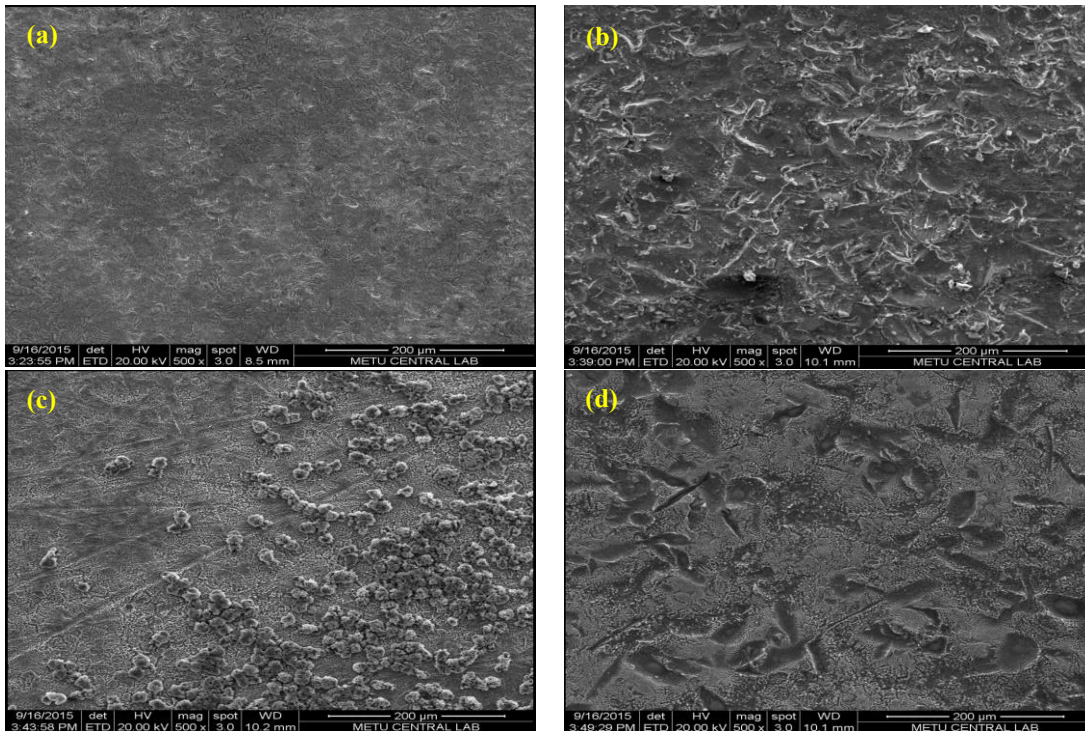
Figure 16 SEM images of a) Ti, b) Ti-S, c) Ti-S-A, d) Ti-S-A-P (500x).

EDS spectra shown in Figure 17 (c) and (d) show the presence of titanium salt crystals. EDS spectra demonstrated that titanium salt is composed of sulfur (S), oxygen (O) and titanium. According to this information reaction (1) occurs and as a result the crystal salt formed was $TiSO_4$. According to Ban et al., 30 min period is optimum for acid etching process (Ban et al., 2006). For 30 min time, the grain boundaries were obvious and the crystal grains were distinguishable. The grain surface showed micro-porosities owing to the formation of micro-pits smaller than 1µm in diameter (Ban et al., 2006). Moreover, EDS spectra of Ti-S-A (Figure 17 (c) and (d)) verified that sand particles were removed by acid etching (Si and Al peaks were lost). As expected, after the preheating step, sulfur content was decreased while Ti content increased as seen in Figure 17 (e).
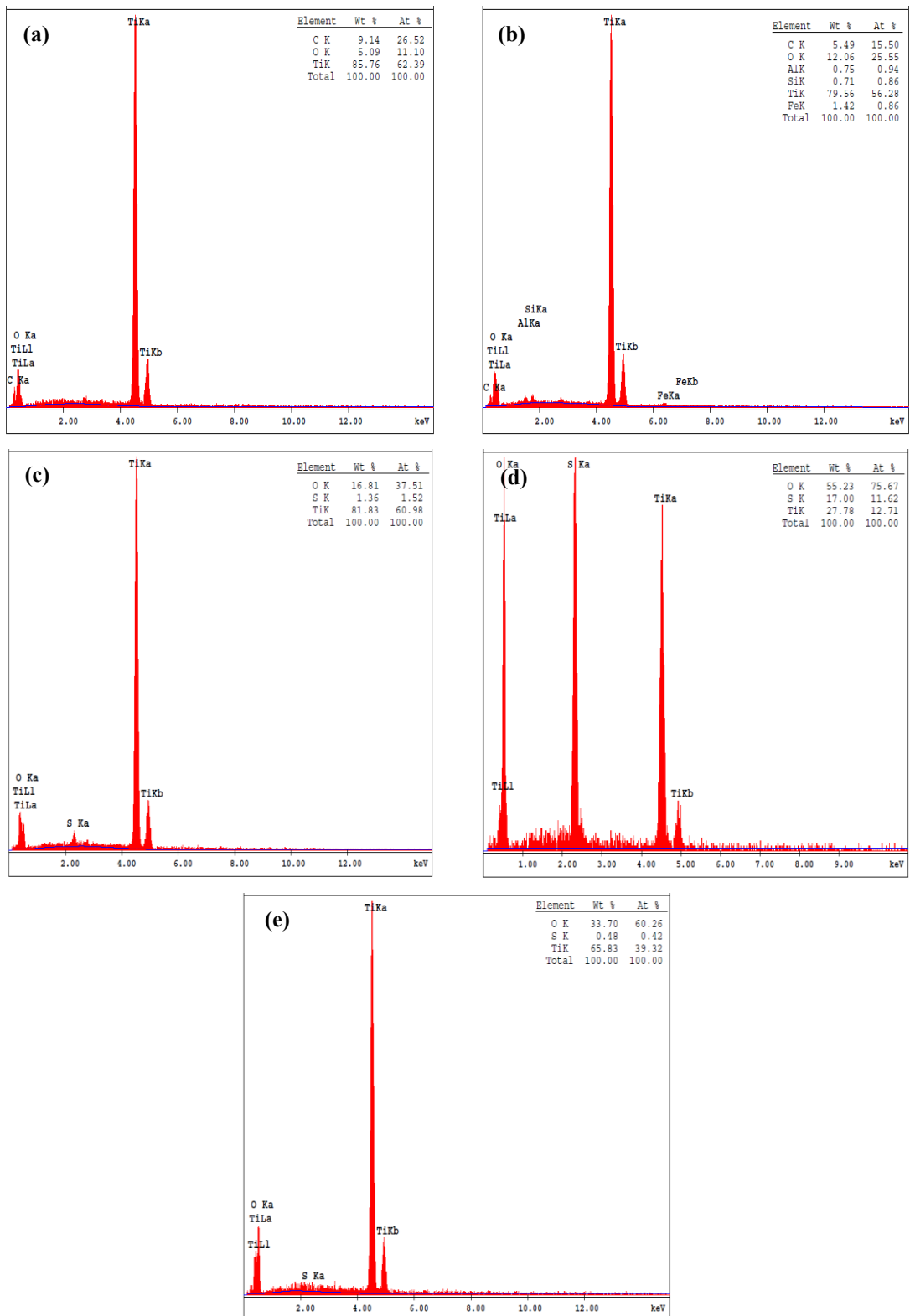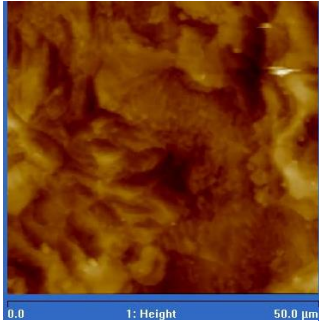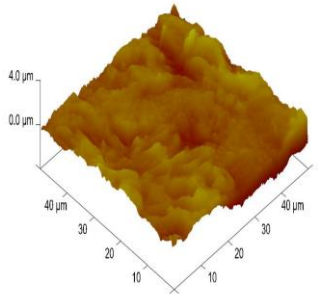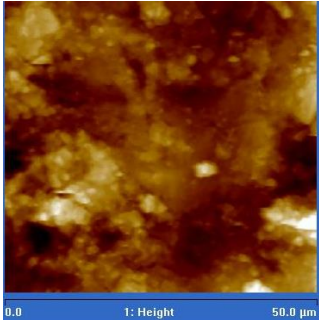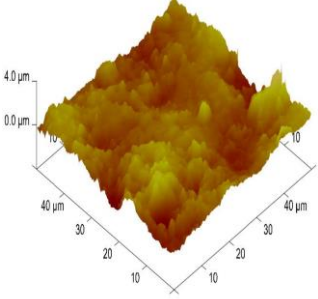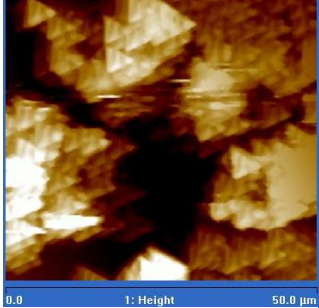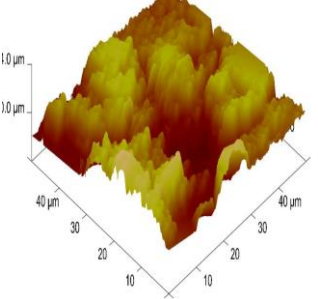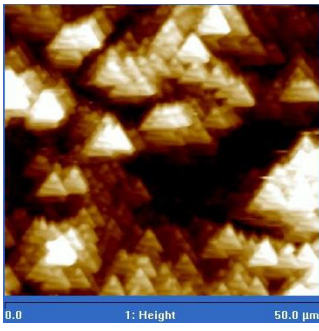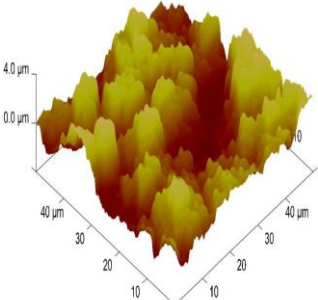
Figure 17 EDS Spectra of a) Ti, b) Ti-S, c) Ti-S-A pore side, d) Ti-S-A crystal side, e) Ti-S-A-P.

Surface roughness was increased due to pretreating routine. Roughness parameters and topography are shown in Table 10. R_a value provides average roughness information. According to R_a values and the topographic images, the surface became rougher and porous as the pretreatment procedure proceeded. As received titanium alloy (Ti) had a roughness degree (about 180-300 nm) which is similar to a literature work (Yang et al., 2017). Sandblasting process (Ti-S) evoked an increment in small pits and decrement in large pits by smoothing them (Henriques et al., 2017). It was observed that acid etching process (Ti-S-A) caused enormous deformation on the surface, meanwhile (111) face centered cubic (fcc) planes were also clearly seen in 2D image (Baek et al., 2017). Finally preheating step (Ti-S-A-P) caused surface oxidation and increased roughness up to 953 nm, thus still (111) fcc plates dominated the surface (Li et al., 2016).

FTIR spectra of untreated and pretreated plates are shown in Figure 18. Ti plate had no detectable functional group as shown in FTIR spectrum. The characteristic bands observed in Ti-S samples belong to Si-O-Si stretching mode at 1083-1089 cm^{-1} (Shokri et al., 2009). Bands observed in Ti-S-A and Ti-S-A-P samples at 1172-1214 cm^{-1} and 1443-1446 cm^{-1} were attributed to S=O stretching (Givan et al., 2002). Ti-OH stretching mode is observed at 1637-1641 cm^{-1} (Hamadanian et al., 2010). Furthermore, the weak bands at 3500-3700 cm^{-1} were attributed to absorbed water vapor (moisture) (Chemistry Libretexts, 2014). In most cases, a weak peak around 2349 cm^{-1} is due to the CO_2 in the beam (poor background correction). In samples except Ti plate, a weak peak around 1600 cm^{-1} was observed due to O-H stretching (Yilmaz et al., 2014). Upward peaks are the result of inadequate background correction.

Table 10 Roughness and topography of Ti, Ti-S, Ti-S-A and Ti-S-A-P.

Sample	Roughness (nm)			2D image	3D image
	R_a	R_q	R_z		
Ti	260±4.3	337±7.1	228±2.3		
Ti-S	397±3.0	507±8.7	196±1.5		
Ti-S-A	848±7.2	1057±9.3	747±7.7		
Ti-S-A-P	953±2.8	1148±5.2	973±4.1		
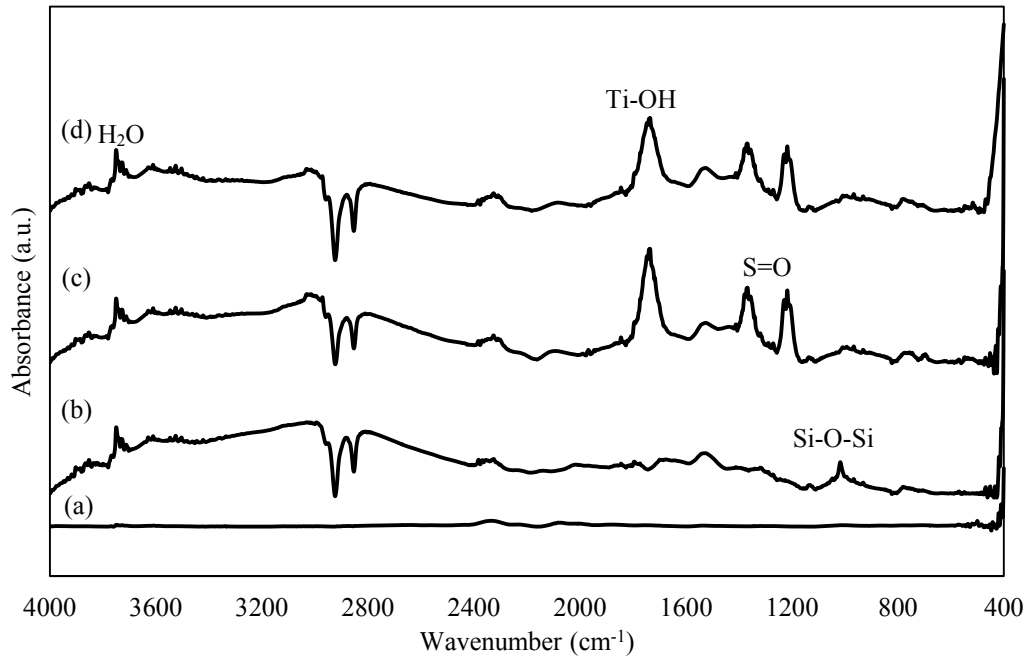
Figure 18 FTIR spectrum of a) Ti, b) Ti-S, c) Ti-S-A, d) Ti-S-A-P.

The XRD patterns of the as received Ti6Al4V plate and pretreated plates are represented in Figure 19. Since there is no JCPDS standard for Ti6Al4V, fitting results to those reported for the hexagonal α-Ti (JCPDS file #44-1294) and for the cubic β-Ti (JCPDS file #44-1288) were performed. As observed from Figure 19, all plates (Ti, Ti-S, Ti-S-A and Ti-S-A-P) indicated mainly α-Ti peaks. β-Ti peaks were weak. Both rutile and anatase peaks were present in preheated plates (Ti-S-A-P) due to high temperature oxidation (Teker et al., 2015). Furthermore, TiH_2 peaks (ICDD # 09-037) were present in acid etched (Ti-S-A) and preheated (Ti-S-A-P) plates. The intensity of TiH_2 was the sum of the intensities of the (110) shoulder peak at 40.9° and the (200) peak at 59.6° for 2θ. Though TiH_2 (200) peak lost after preheating step. This suggests that secondary reaction occurs with reaction (1). Secondary reaction is given in Equation 12 (Ban et al., 2006).

$$Ti+H_2 \rightarrow TiH_2 \tag{12}$$

46
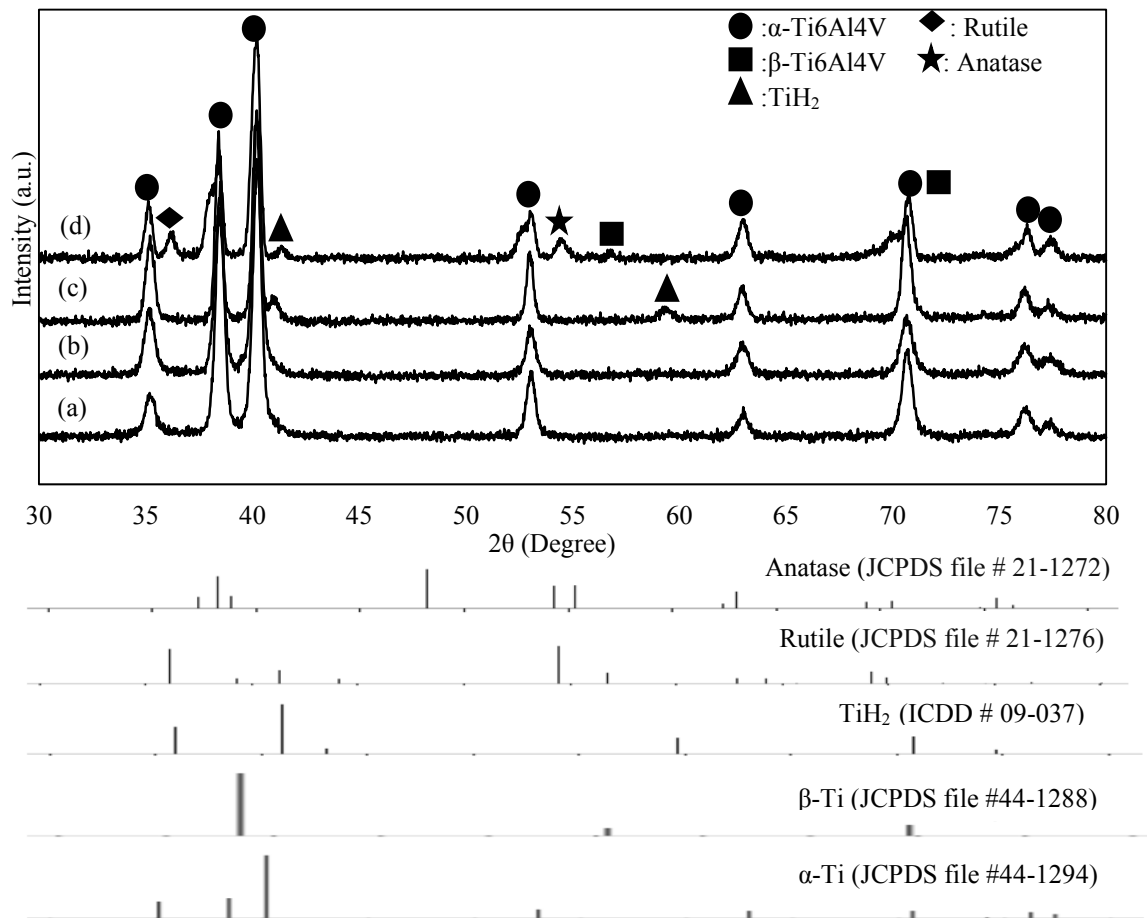
Figure 19 XRD patterns of a) Ti, b) Ti-S, c) Ti-S-A, d) Ti-S-A-P.

3.1.2. Effect of Coating Time

Pure 1.5xSBF:

SEM images of Ti-S-A-P plates after soaking in pure 1.5×SBF for a period of 4 days (P4), 7 days (P7), 14 days (P14) and 21 days (P21) are shown in Figure 20. As observed from Figure 20, HAp nucleation started in 4 days period. HAp particles were present in globular form. HAp precipitation was drastically improved with increasing the incubation period in SBF. The surface of the Ti6Al4V plates was entirely covered with numerous and almost spherical granular CaP precipitates after 7 days in 1.5×SBF.
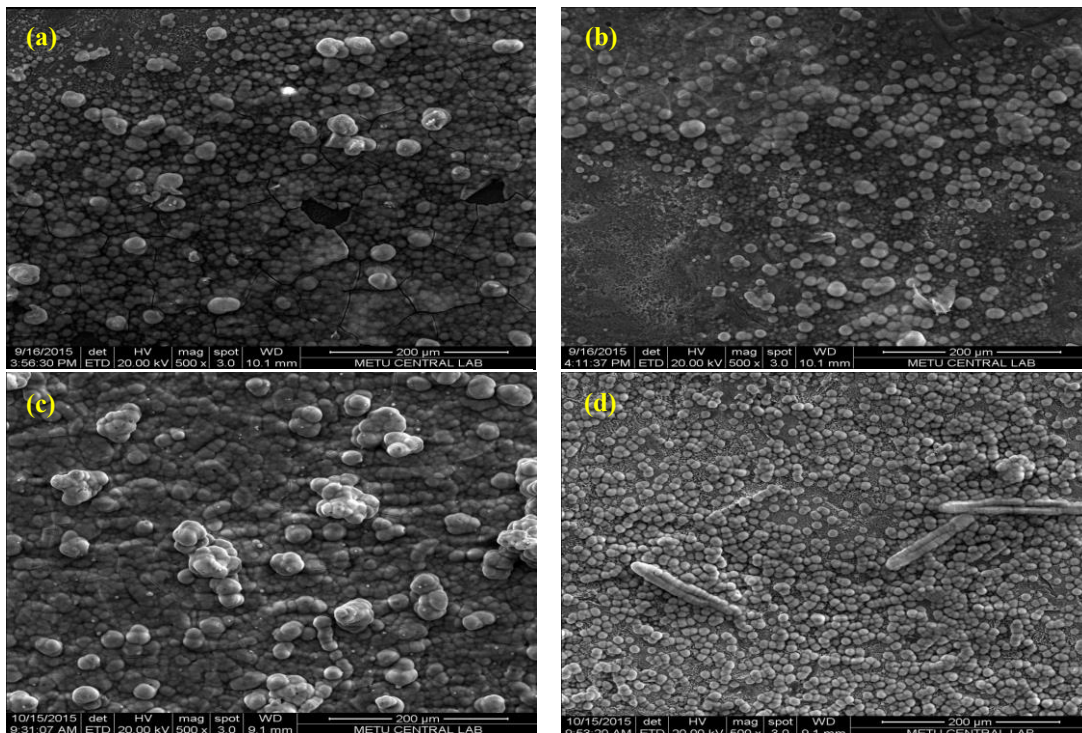
Figure 20 SEM images of a) P4, b) P7, c) P14, d) P21 (500x).

For 14 days soaking period, HAp crystals were vertically nucleated all over the surface while for 21 days soaking period HAp particles almost fully covered the surface and horizontal growth even occurred. SEM images given in Figure 20 showed that the CaP layer was grown steadily as a result of this process. The EDS analysis results obtained from SEM images, mass and atomic ratios of the elements in the coatings are listed in Figure 21. The CaP composition of the coatings can be determined from the EDS analysis results. The Ca/P molar ratios of the coatings obtained from the 1.5×SBF with normal ionic concentration were calculated as follows: 1.44 on day 4, 1.47 on day 7, 1.48 on day 14 and 1.25 on day 21. Sudden decrease in Ca/P ratio on day 21 could be due to the analysis error related to local data collection.
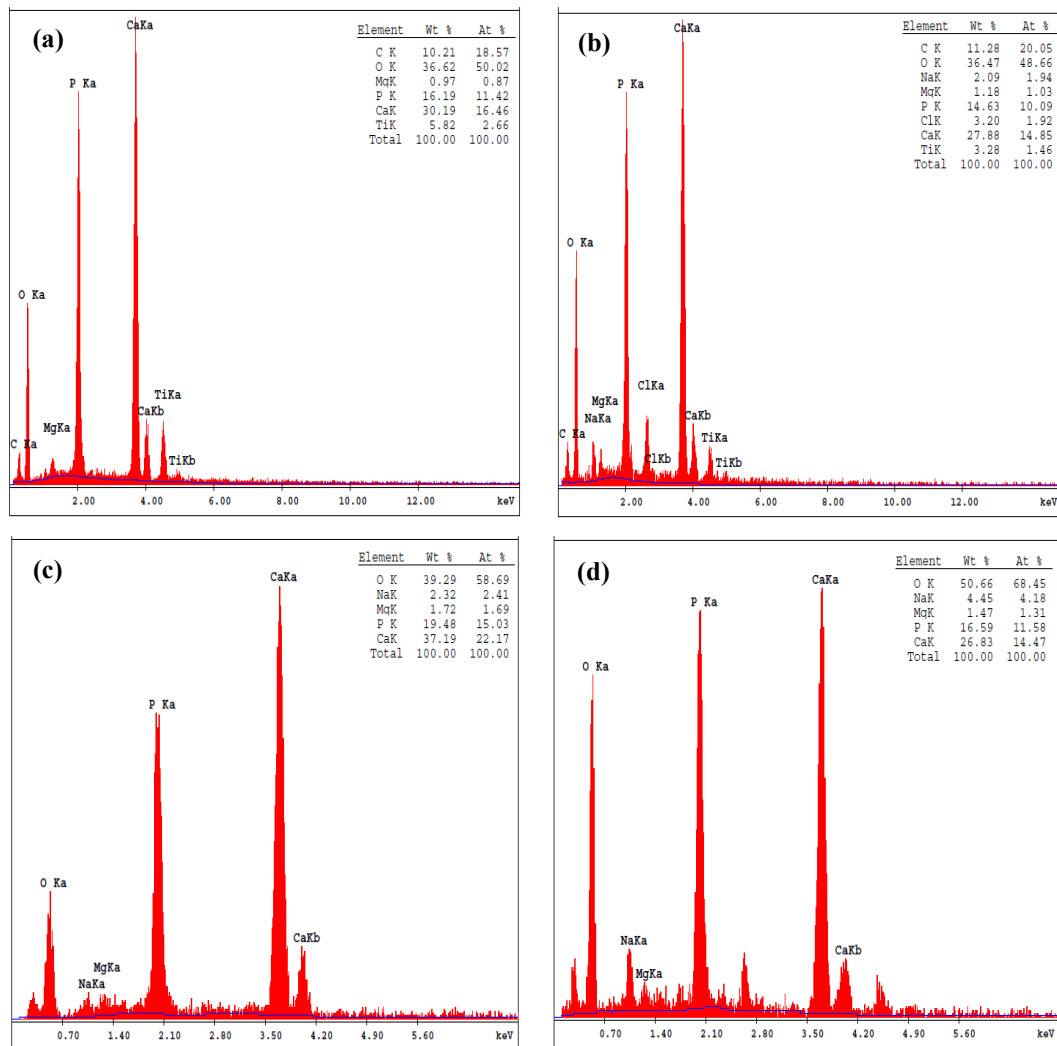
Figure 21 EDS Spectra of a) P4, b) P7, c) P14,d) P21.

Figure 22 represents FTIR spectra of Ti-S-A-P plates coated with pure SBF for different time periods. In all cases, the bands belonging to $v_4PO_4^{3-}$ bending mode with a maximum at 560 cm^{-1} and a shoulder at 600 cm^{-1} of the phosphate ion in the structure of HAp were obviously observed. The bands around 1020 cm^{-1} were due to $v_3PO_4^{3-}$ stretching mode while the bands around 1400 cm^{-1} were attributed to $v_3CO_3^{2-}$ mode of carbonate (Avci et al., 2017; Silva et al., 2003; Pylypchuk et al., 2016). All characteristic bands of HAp were obtained from each coating periods (Hazmi, 2016). The weak bands seen between 1800 cm^{-1}-2300 cm^{-1} were derived from ATR crystal which was used during FTIR analysis.
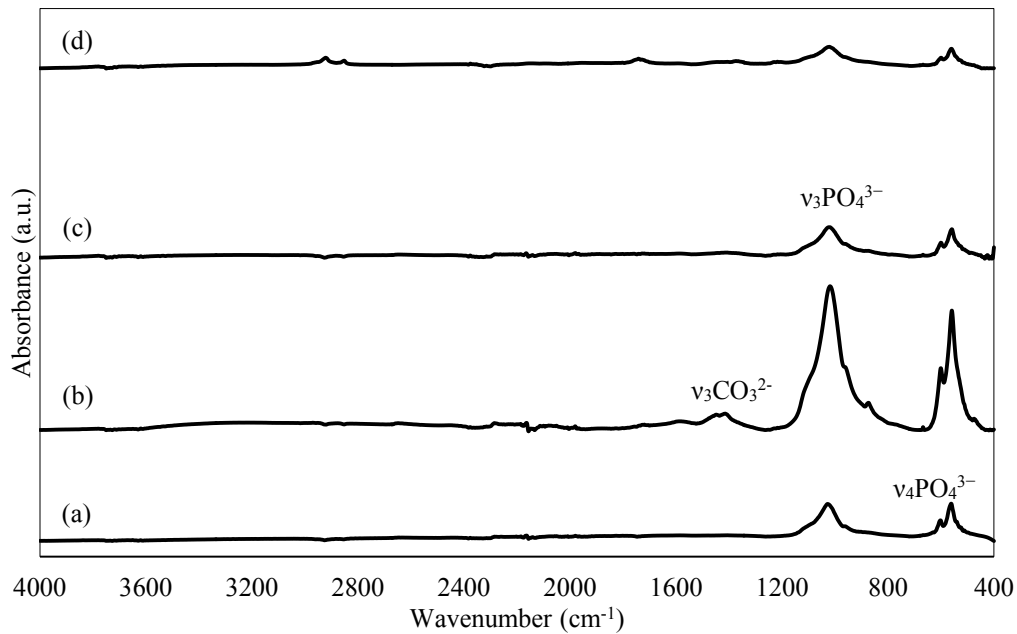
Figure 22 FTIR spectrum of a) P4, b) P7, c) P14, d) P21.

XRD patterns of pure SBF coated plates for 4 days, 7 days, 14 days and 21 days plates are presented along with the standard HAp spectrum (ICDD card No. 1-1008) in Figure 23. All coatings exhibited the standard HAp XRD peaks. As the immersion time increased, XRD peaks sharpened due to the increase in coating thickness and crystallization. HAp crystallizes in hexagonal crystal system. It should also be noted that preferred orientation of HAp growth occurred on surfaces resulted in modified intensity of HAp peaks when compared to the standard peaks.
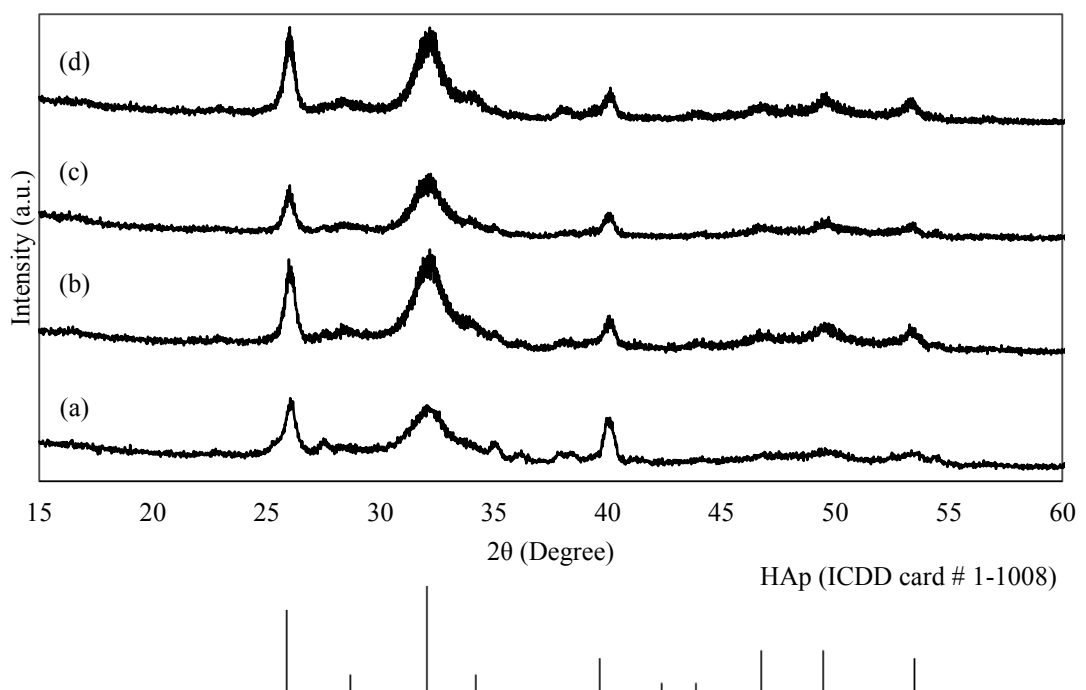
Figure 23 XRD patterns of a) P4, b) P7, c) P14, d) P21.

The results of Rietveld analysis obtained from XRD data are shown in Table 11. R_{wp} stands for weighted profile factor and it should be less than 20.00, for good fitting. Thus, in all cases it was less than 20.00. The mean lattice parameters were approximately a=9.4492 Å and c=6.8739 Å. The calculated lattice parameters were consistent with HAp cif. file (code:1617565) where a=9.4232 Å and c=6.8833 Å. Slight difference in parameter values were negligible. Similar to this study, Sumathi & Buvaneswari determined the lattice parameters of the compound by least square fitting of high angle lines. The unit cell parameters were: a = 9.4122 Å , c = 6.922 Å and the unit cell volume is 530.9 Å^3 (Sumathi and Buvaneswari, 2012).

Table 11 Rietveld analysis results of Ti-S-A-P plates after soaking in pure SBF.

Sample	Lattice parameters			Volume, V (Å³)
	R_{wp}	a (Å)	c (Å)	
P4	12.5500	9.4231	6.8526	608.4753
P7	13.5800	9.4622	6.8814	616.1139
P14	14.1500	9.4514	6.8773	614.3421
P21	15.9000	9.4602	6.8843	616.1131

51

XPS spectrum of P14 is shown in Figure 24. As seen in Figure 24, XPS provided not only spectrum but also atomic ratios. From the atomic ratios chemical composition of the surface coating can be determined. Spectroscopy technique does not provide reliable oxygen content. Moreover, it does not allow calculating amount of hydrogen. According to the spectroscopy results, $Ca_9(PO_4)_{7.2}(OH)_x$ compound formula was obtained as a coating material.
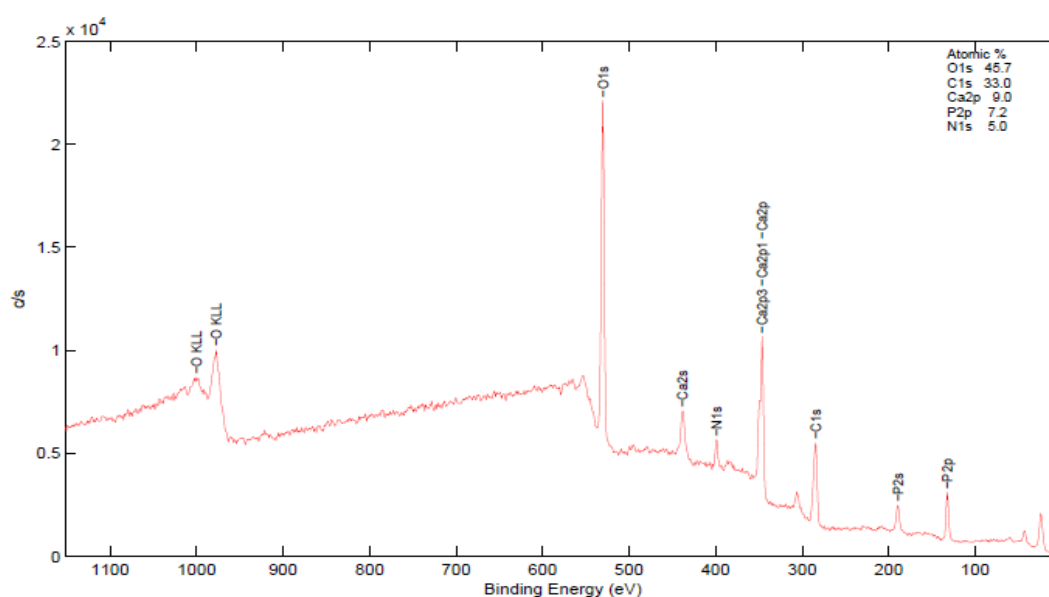
Figure 24 XPS spectrum of P14.

3.1.3. Effect of Dopants

0.1 mM Bismuth and Carbonate doped 1.5xSBF:

SEM images of Ti-S-A-P plates after soaking in 0.1 mM Bismuth and Carbonate doped 1.5×SBF for a period of 4 days (0.1-C4), 7 days (0.1-C7), 14 days (0.1-C14) and 21 days (0.1-C21) are shown in Figure 25. It was observed that the nucleation started on the surfaces coated in co-doped 1.5×SBF on day 4, just as for the coatings obtained from the 1.5×SBF. Brighter areas shown in Figure 25 represented highly doped area due to heavier atomic mass of bismuth. It was obvious that the deposition of HAp around the nuclei continued during the soaking period.

Precipitation started with the formation of uniform globular structure of HAp followed by nano-flake shaped clusters formation after 14th day of coating. The SEM images taken at high magnification revealed that the spherical structures of the co-doped coatings were composed of nano-spheres.

The EDS analysis results obtained from SEM images, mass and atomic ratios of the elements in the coatings are listed in Figure 26. The CaP composition of the coatings can be determined from the EDS analysis results. The Ca/P molar ratios of the coatings obtained from the 0.1 mM Bismuth and Carbonate doped 1.5×SBF were calculated as follows: 1.35 on day 4, 1.32 on day 7, 1.42 on day 14 and 1.35 on day 21. Maximum ratio obtained on day 14. All EDS results showed the presence of bismuth ion, amount of this ion varied between 0.74-0.98 (at)%.

Figure 27 presents FTIR spectra of Ti-S-A-P plates coated with 0.1 mM Bismuth and Carbonate co-doped 1.5×SBF for different time periods. The FTIR spectra of 0.1 mM co-doped coatings were found to exhibit no remarkable difference than pure HAp spectrum. This result is consistent with the XRD analyses and showed that the coatings were phase pure. As the bismuth was at ppm level, it was expected to have no obvious peak for bismuth bonding in HAp structure. It should also be noted that the weak peaks observed between 1400-1500 cm^{-1} were assigned to CO_3^{2-} coming from co-deposition of carbonate ion (Pazarçeviren et al., 2018; Adams et al., 2013).

The XRD patterns of 0.1 mM Bismuth and Carbonate doped 1.5xSBF coated for 4 days, 7 days, 14 days and 21 days plates are presented in Figure 28. All coatings exhibited the standard HAp XRD peaks. However, the broad diffraction peaks displayed that the obtained HAp was neither well crystallized nor was in nano-scales (Zhang, Zou et al., 2009). Thus, surfaces were not fully covered homogenously with HAp. This could be confirmed by rutile, Ti6Al4V and TiH$_2$ presence (Teker et al., 2015). The peaks shown at (b) at 26° and 53° belonged to carbonated apatite that comes from carbonate doping into SBF (Müller and Müller, 2006).

Figure 25 SEM images of a) 0.1-C4 (500x), b) 0.1-C4 (3000x) c) 0.1-C7 (x500), d) 0.1-C7 (3000x), e) 0.1-C14 (500x), f) 0.1-C14 (3000x), g) 0.1-C21 (500x), h) 0.1-C21 (3000x). Insets show particles in high magnification (40 000x).
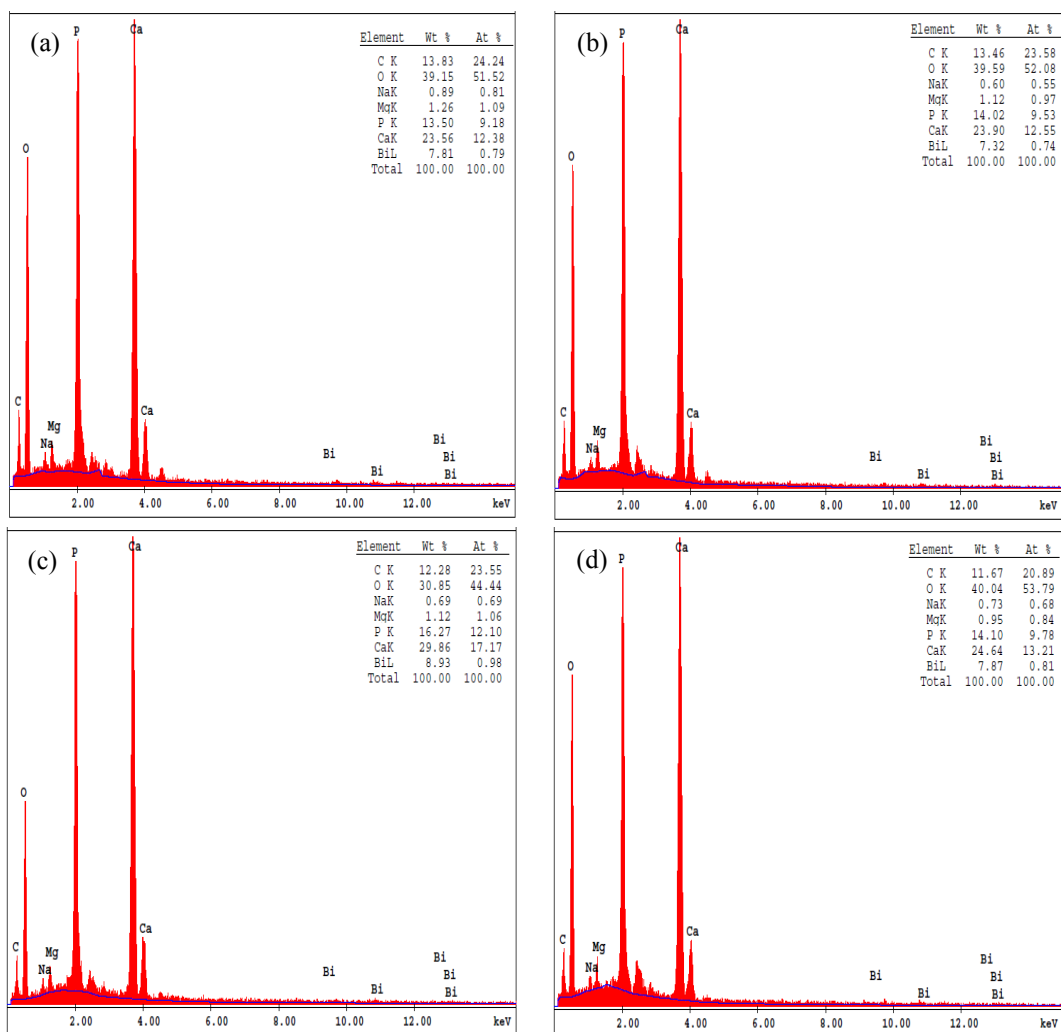
Figure 26 EDS Spectra of a) 0.1-C4, b) 0.1-C7, c) 0.1-C14, d) 0.1-C21.
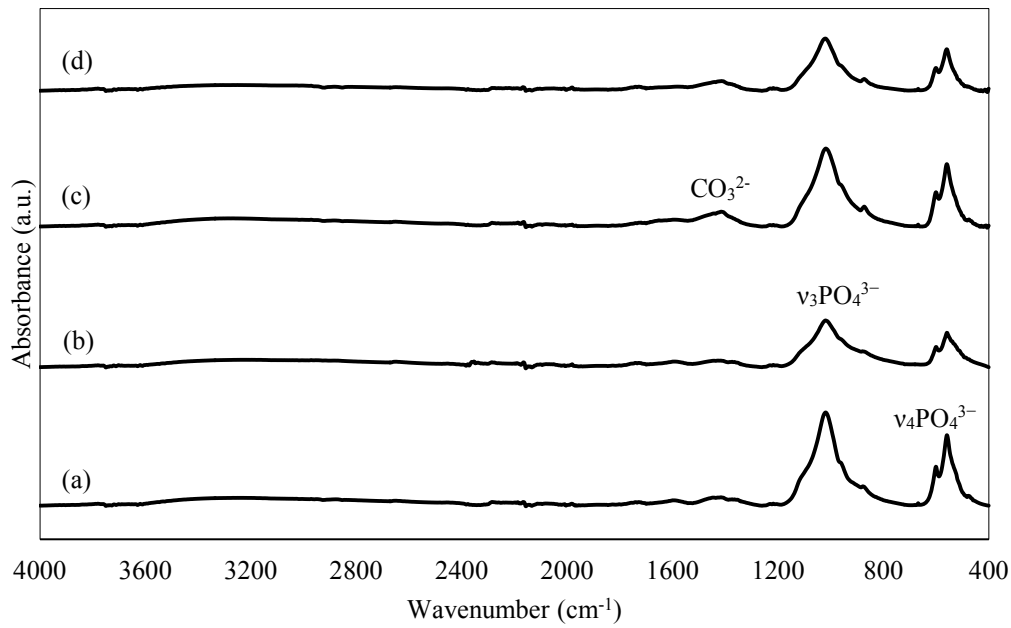
Figure 27 FTIR spectrum of a) 0.1-C4, b) 0.1-C7, c) 0.1-C14, d) 0.1-C21.
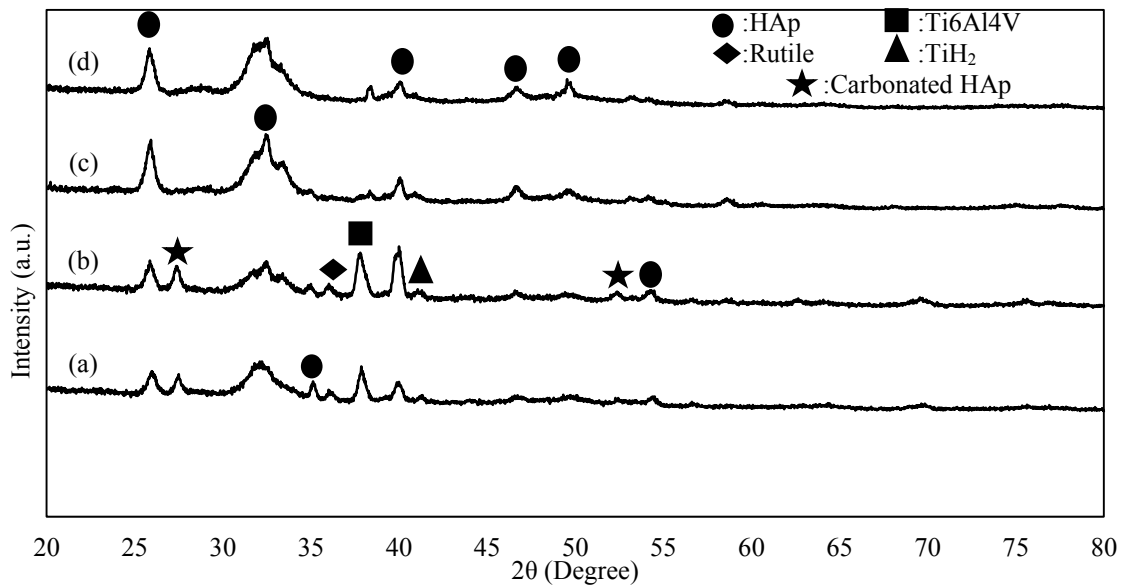
Figure 28 XRD patterns of a) 0.1-C4, b) 0.1-C7, c) 0.1-C14, d) 0.1-C21.

The results of Rietveld analysis obtained from XRD data are shown in Table 12.

R_{wp} was less than 20.00 in all cases. Mainly 'a' and 'c' lattice parameters decreased in case of 0.1 mM bismuth and carbonate co-doped coating compared to pure coating. Slight changes in parameters are negligible. Decrease in lattice parameters led to decrease in unit cell volume.

Table 12 Rietveld analysis results of Ti-S-A-P plates after soaking in 0.1 mM Bismuth and Carbonate co-doped SBF.

Samples	Lattice parameters				Reference (P4, P7, P14, P21)		
	R_{wp}	a (Å)	c (Å)	V(Å³)	a (Å)	c (Å)	V (Å³)
0.1-C4	14.2548	9.4393	6.7987	605.7668	9.4231	6.8526	608.4753
0.1-C7	17.9880	9.3607	6.8029	596.0885	9.4622	6.8814	616.1139
0.1-C14	13.2877	9.4315	6.8990	613.6881	9.4514	6.8773	614.3421
0.1-C21	12.8153	9.4054	6.8579	606.6605	9.4602	6.8843	616.1131

The Ca/Bi atomic ratios of the coatings obtained by soaking the pretreated Ti6Al4V plates into 0.1 mM bismuth and carbonate added 1.5×SBF for a period of 4, 7, 14 and 21 days are given in Table 13. As can be seen in Table 13, all of the coatings on the Ti6Al4V plates soaked into the 0.1 mM Bismuth and Carbonate co-doped 1.5×SBF contained bismuth ion. Since the plates were washed with distilled water after removal from the SBF solutions, the unbound precipitates were removed from the surface and the detected bismuth was only coming from the content of the coatings. It is noticeable that the Ca/Bi ratio decreased with increasing the soaking time because the doped bismuth amount was increasing.

Table 13 Calculated Ca/Bi atomic ratios of 0.1-C4, 01.-C7, 0.1-C14, 0.1-C21.

Sample	Ca/Bi
0.1-C4	32.73±0.58
0.1-C7	34.21±0.84
0.1-C14	17.24±0.08
0.1-C21	16.00±0.04

XPS spectrum of 0.1-C14 is shown in Figure 29. Due to the spectroscopy results, $Ca_{7.2}Bi_{0.3}(HPO_4)_{2.4}(CO_3)_{0.1}(PO_4)_{3.5}$ compound formula was obtained as a coating material. XPS results proved that bismuth ion substitutes with calcium while carbonate ion substitutes with both phosphate and hydroxide.
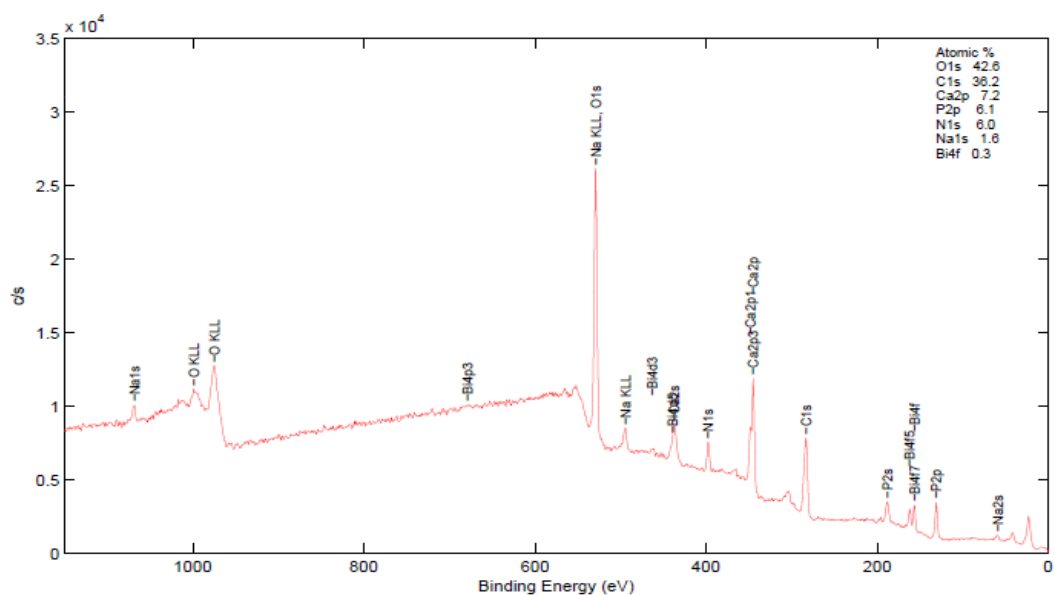
Figure 29 XPS spectrum of 0.1-C14.

0.3 mM Bismuth and Carbonate doped 1.5xSBF:

SEM images of Ti-S-A-P plates after soaking in 0.3 mM Bismuth and Carbonate doped 1.5×SBF for a period of 4 days (0.3-C4), 7 days (0.3-C7), 14 days (0.3-C14) and 21 days (0.3-C21) are shown in Figure 30. SEM images proves that the nucleation started on the surfaces coated in 0.3 mM co-doped 1.5×SBF on day 4, similarly to 0.1 mM co-doped 1.5×SBF and 1.5×SBF coatings. Brighter areas represented in the images are referred to bismuth. It was obvious that the deposition of HAp around the nuclei continued during the soaking period. Co-doped HAp particles precipitated in globular form in all soaking periods.
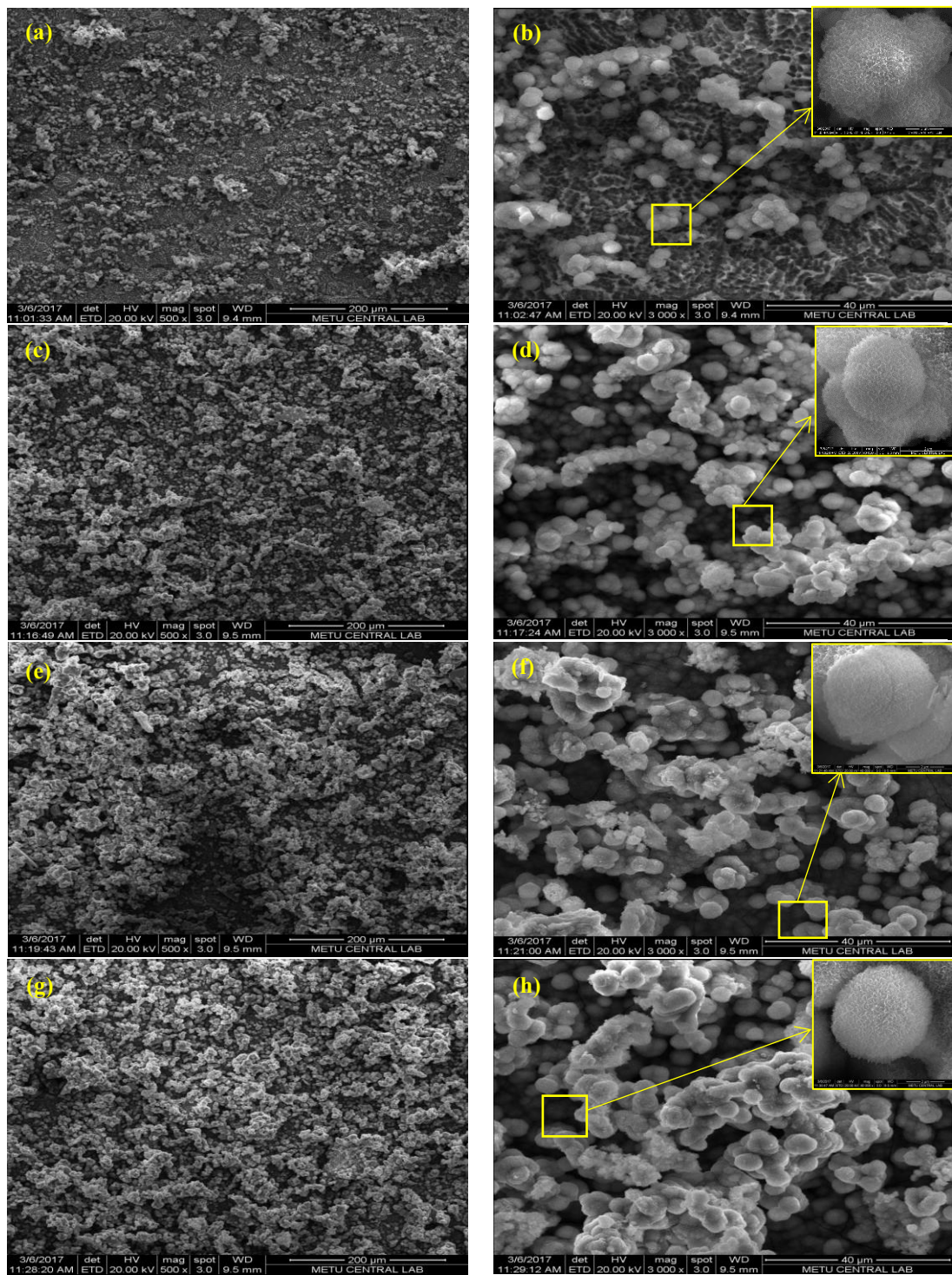
Figure 30 SEM images of a) 0.3-C4 (500x), b) 0.3-C4 (3000x), c) 0.3-C7 (500x), d) 0.3-C7 (3000x), e) 0.3-C14 (500x), f) 0.3-C14 (3000x), g) 0.3-C21 (500x), h) 0.3-C21 (3000x). Insets show particles in high magnification (40 000x).

The EDS analysis results obtained from SEM images, mass and atomic ratios of the elements in the coatings are listed in Figure 31. The Ca/P molar ratios of the coatings obtained from the 0.3 mM Bismuth and Carbonate doped 1.5×SBF were calculated as follows: 1.43 on day 4, 1.58 on day 7, 1.71 on day 14 and 1.64 on day 21. Maximum ratio of Ca/P was obtained on day 14. All EDS results showed the presence of bismuth ion, amount of this ion varied between 0.48-1.39 (at)%.
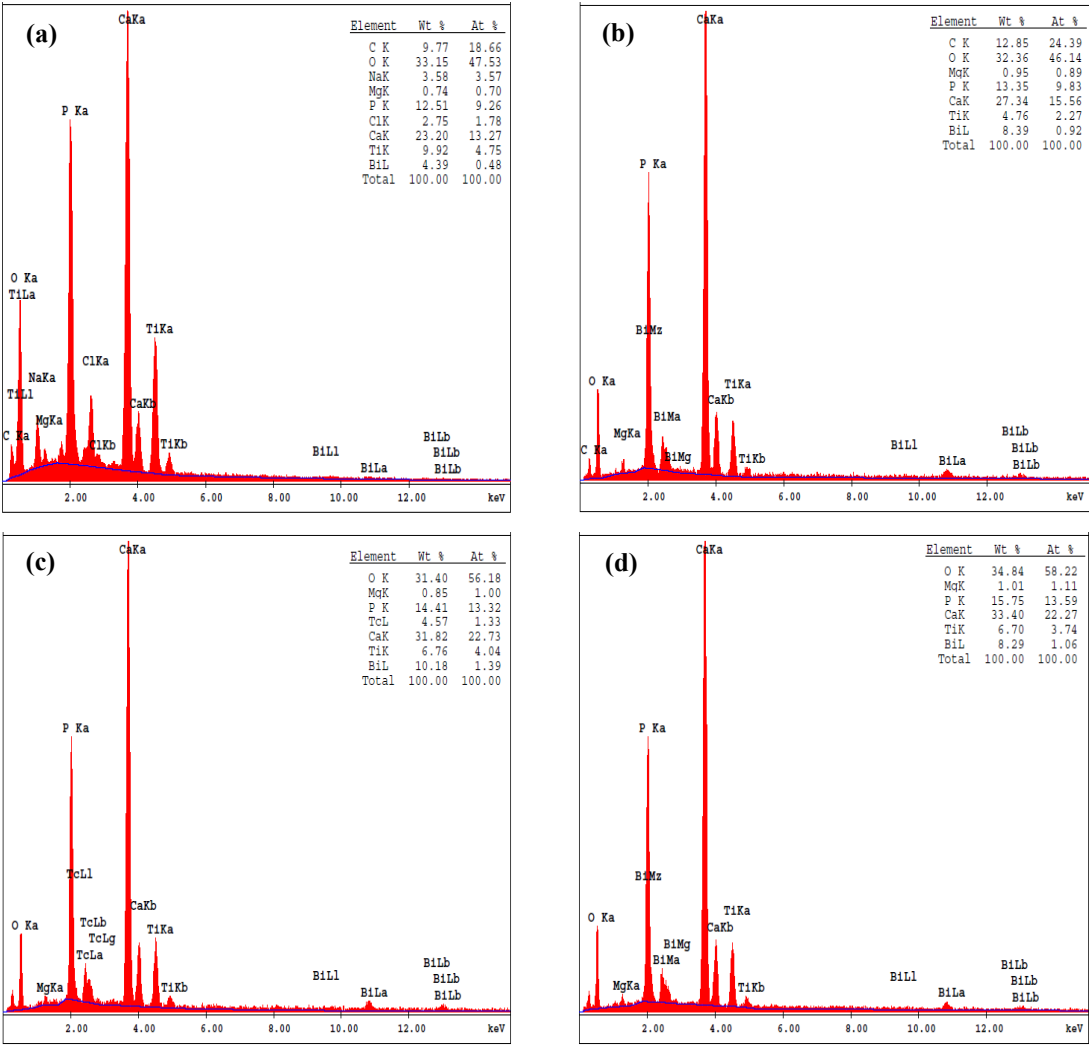
Figure 31 EDS Spectra of a) 0.3-C4, b) 0.3-C7, c) 0.3-C14, d) 0.3-C21.

Figure 32 shows FTIR spectra of Ti-S-A-P plates coated with 0.3 mM Bismuth and Carbonate doped 1.5×SBF for different time periods. The FTIR spectra of 0.3 mM co-doped coatings were found to exhibit no fair distinction than pure HAp, only extra peaks of CO_3^{2-} (co-deposition of carbonate ion) were observed similar to 0.1 mM co-doped coatings.
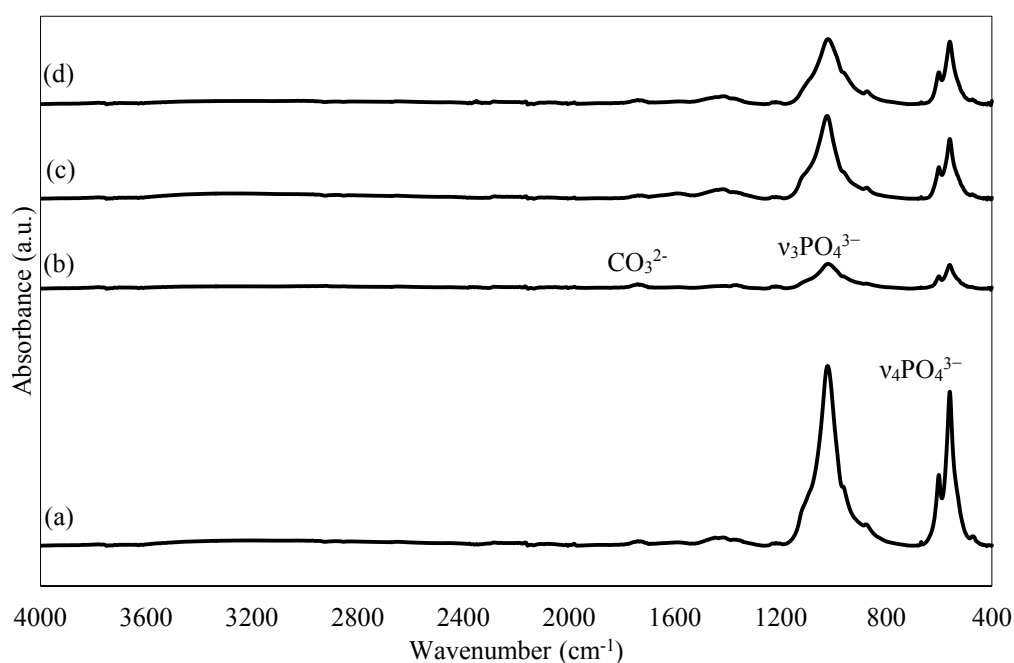
Figure 32 FTIR spectrum of a) 0.3-C4, b) 0.3-C7, c) 0.3-C14, d) 0.3-C21.

The XRD patterns of 0.3 mM Bismuth and Carbonate co-doped 1.5xSBF coated for 4 days, 7 days, 14 days and 21 days plates are represented in Figure 33. All coatings exhibited the standard HAp XRD peaks. Once again, the broad diffraction peaks display that the obtained HAp was not well crystallized or was in nano-scales (Zhang, Zou et al., 2009). It should also be noted that for 4 days coating period the samples surface was not fully covered with HAp homogenously which could be confirmed by Ti6Al4V presence (Teker et al., 2015). The peak shown at (b) at 53 ° belonged to carbonated apatite that came from carbonate doping into SBF (Müller and Müller, 2006).
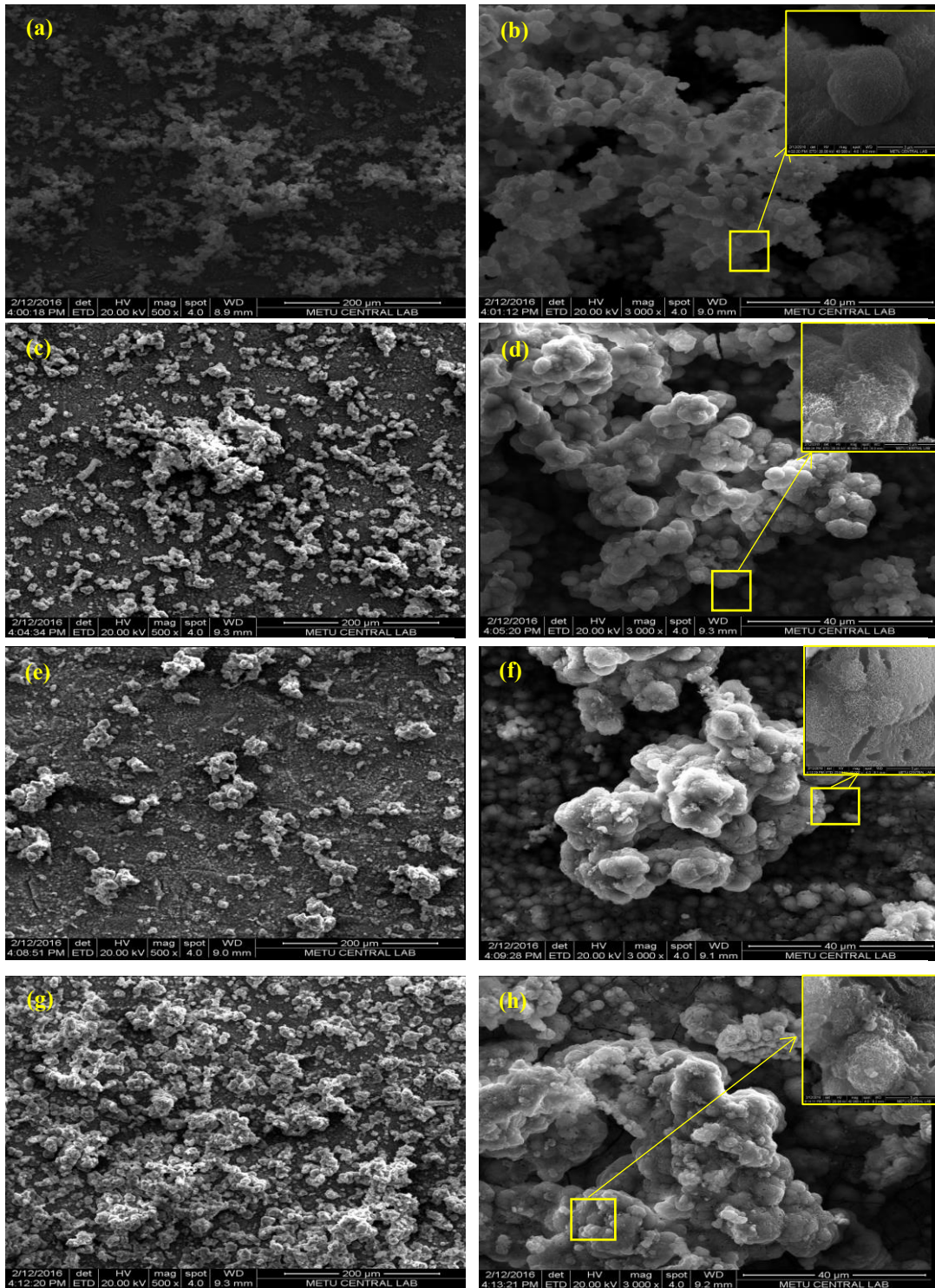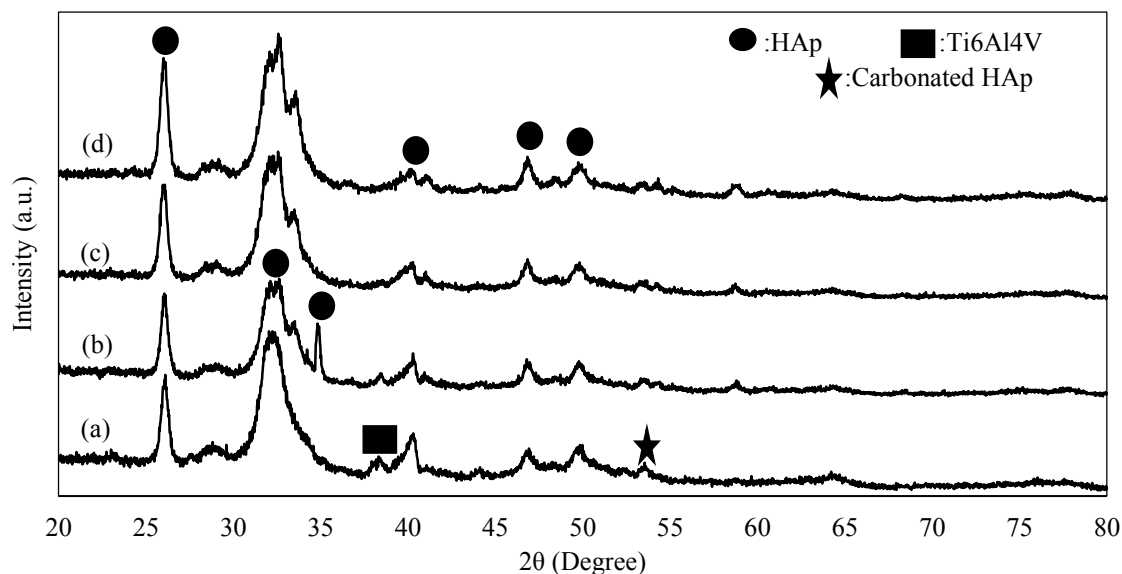
Figure 33 XRD patterns of a) 0.3-C4, b) 0.3-C7, c) 0.3-C14, d) 0.3-C21.

The results of Rietveld analysis obtained from XRD data are shown in Table 14. R_{wp} was appropriate (less than 20.00) for good fitting in all cases. Mainly 'a' parameter decreased while 'c' parameter increased in case of 0.1 mM bismuth and carbonate co-doped coating compare to pure coating. Slight changes in parameters were negligible. Alteration in lattice parameters effected cell volume both positively and negatively.

Table 14 Rietveld analysis results of 0.3 mM Bismuth and Carbonate co-doped 1.5xSBF coated for 4 days, 7 days, 14 days and 21 days plates.

Samples	Lattice parameters				Reference (P4, P7, P14, P21)		
	R_{wp}	a (Å)	c (Å)	V (Å³)	a (Å)	c (Å)	V (Å³)
0.3-C4	11.5141	9.4267	6.8660	610.1311	9.4231	6.8526	608.4753
0.3-C7	16.5932	9.4002	6.8634	606.4758	9.4622	6.8814	616.1139
0.3-C14	15.2525	9.4415	6.8918	614.3483	9.4514	6.8773	614.3421
0.3-C21	16.9696	9.4266	6.9032	613.4238	9.4602	6.8843	616.1131

XPS spectrum of 0.3-C14 is shown in Figure 34. Due to the spectroscopy results, $Ca_{13.1}Bi_{1.4}(HPO_4)_{x-z}(CO_3)_z(PO_4)_{6-x}(OH)_{2-x}$ compound formula was obtained as a coating material.

XPS results proved that bismuth ion substitutes with calcium, on the other hand it is not reliable to predict stoichiometric ratios about anions due to the results.
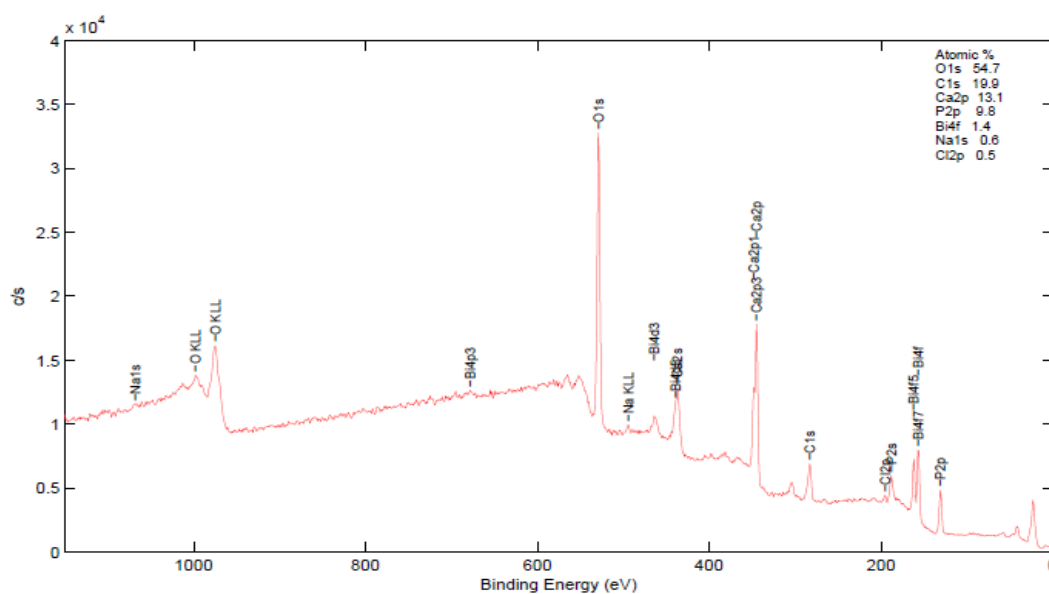
Figure 34 XPS spectrum of 0.3-C14.

0.5 mM Bismuth and Carbonate doped 1.5xSBF:

SEM images of Ti-S-A-P plates after soaking in 0.5 mM Bismuth and Carbonate doped 1.5×SBF for a period of 4 days (0.5-C4), 7 days (0.5-C7), 14 days (0.5-C14) and 21 days (0.5-C21) are shown in Figure 35. As seen from Figure 35, the nucleation started on the surfaces coated in co-doped 1.5×SBF on day 4, just as for the coatings obtained from the 1.5×SBF and 0.1 mM Bismuth and Carbonate doped 1.5×SBF and nucleation continued as the soaking period increased. Brighter areas shown in Figure 35 were assigned for highly doped area due to heavier atomic mass of bismuth. Precipitation started by forming the uniform nano-flake shaped structure of HAp. Furthermore, clusters formed after 4 days of coating.
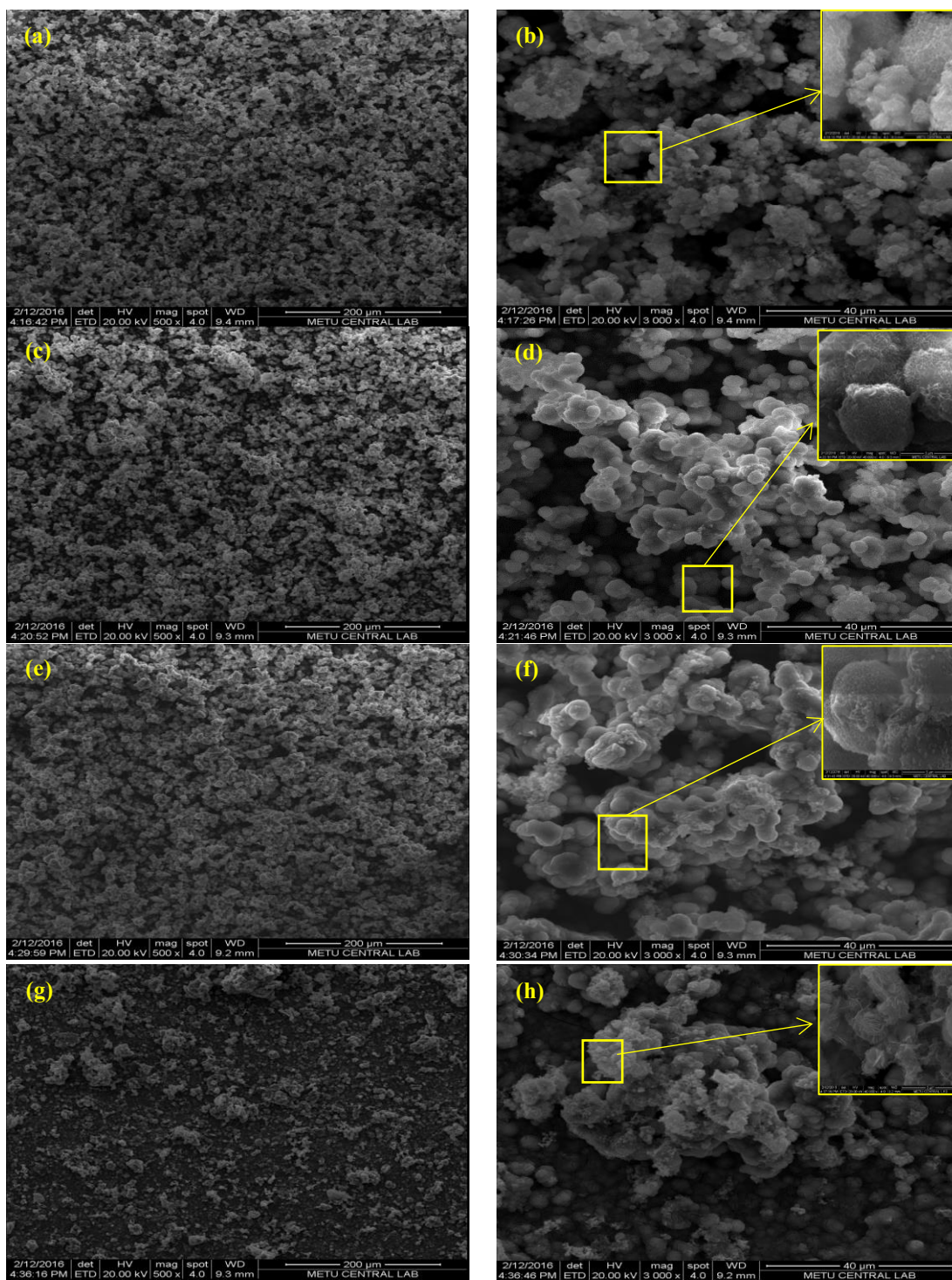
Figure 35 SEM images of a) 0.5-C4 (500x), b) 0.5-C4 (3000x), c) 0.5-C7 (500x), d) 0.5-C7 (3000x), e) 0.5-C14 (500x), f) 0.5-C14 (3000x), g) 0.5-C21 (500x), h) 0.5-C21 (3000x). Insets show particles in high magnification (40 000x).

The EDS analysis results obtained from SEM images, mass and atomic ratios of the elements in the coatings are listed in Figure 36. The Ca/P molar ratios of the coatings obtained from the 0.5 mM Bismuth and Carbonate doped 1.5×SBF was calculated as follows: 1.44 on day 4, 1.44 on day 7, 1.57 on day 14 and 1.38 on day 21. Maximum ratio was obtained on day 14. All EDS results showed the presence of bismuth ion, amount of the ion varied between 1.08-9.37 (at)%.
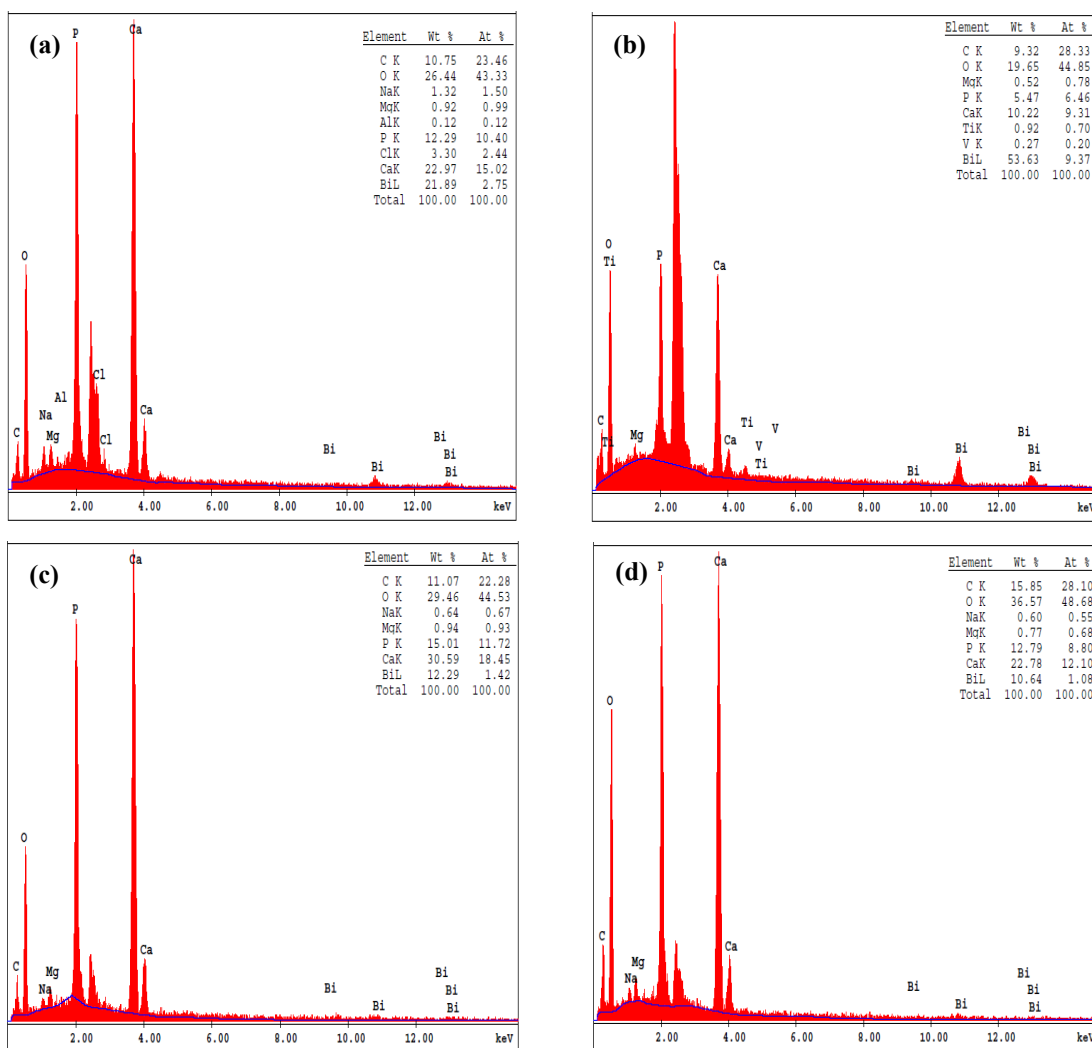
Figure 36 EDS Spectra of a) 0.5-C4, b) 0.5-C7, c) 0.5-C14, d) 0.5-C21.

Figure 37 shows FTIR spectra of Ti-S-A-P plates coated with 0.5 mM Bismuth and Carbonate co-doped 1.5×SBF for different time periods.

FTIR spectra represent similar functional groups with 0.1 mM and 0.3 mM co-doped coatings. All functional groups belonged to HAp structure and extra peaks of CO_3^{2-} (co-deposition of carbonate ion) were observed. The only difference was the intensity of the absorption bands. As expected amounts of HAp were increased by the increment of ionic concentration.
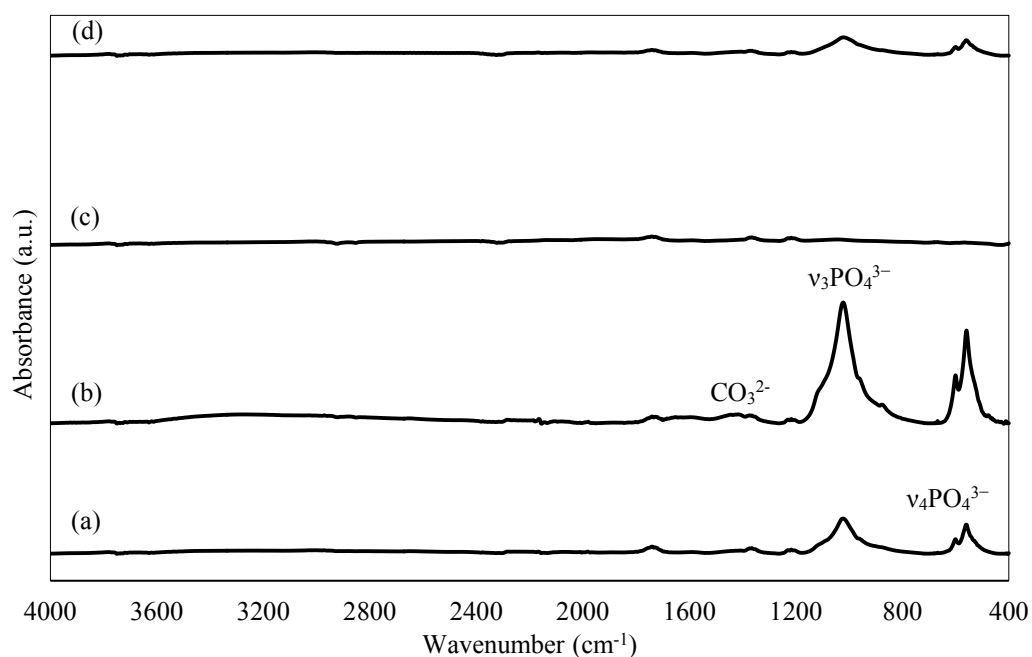
Figure 37 FTIR spectrum of a) 0.5-C4, b) 0.5-C7, c) 0.5-C14, d) 0.5-C21.

The XRD patterns of 0.5 mM Bismuth and Carbonate co-doped 1.5xSBF coated plates are presented in Figure 38. All coatings exhibited the standard HAp XRD peaks. However, the broad diffraction peaks displayed that the obtained HAp was not well crystallized or was in nano-scales (Zhang, Zou et al., 2009). Thus surfaces were not fully covered with HAp homogenously that could be confirmed by Ti6Al4V, TiH$_2$ and carbonated hydroxyapatite presence (Teker et al., 2015; Müller and Müller, 2006).
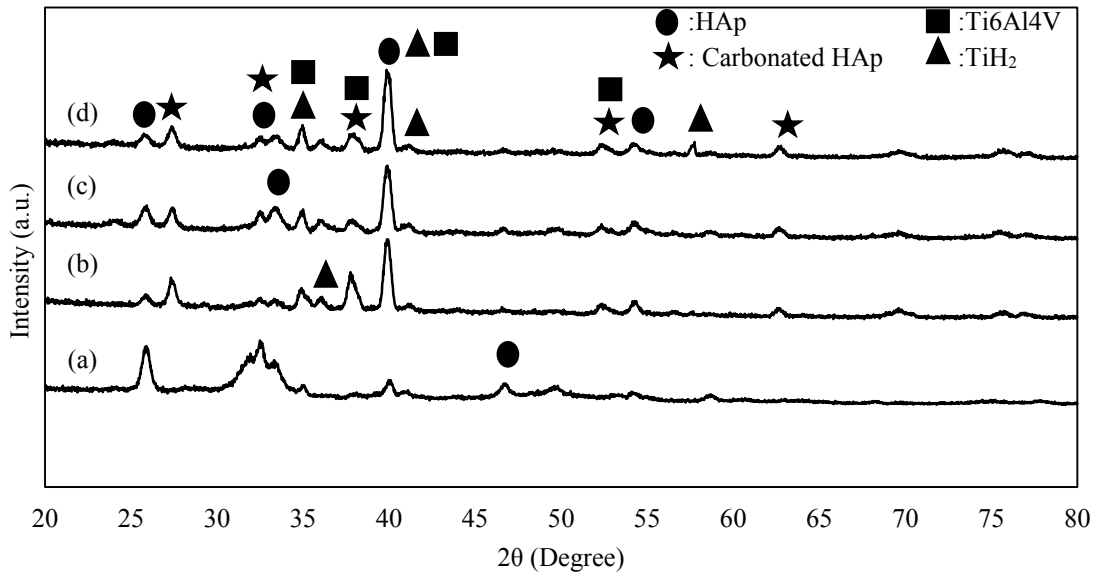
Figure 38 XRD patterns of a) 0.5-C4, b) 0.5-C7, c) 0.5-C14, d) 0.5-C21.

The results of Rietveld analysis obtained from XRD data are shown in Table 15. R_{wp} was appropriate (less than 20.00) for good fitting in all cases. It seems that both 'a' lattice parameter and 'c' were increased greatly. Slight changes in parameters are negligible. As a result of parameter increasing unit cell volumes were also increased. The results were found to be in agreement with literature. According to Sumathi & Buvanesware, the unit cell parameters are: a = 9.412 Å , c= 6.92 Å and the unit cell volume is 530.9 Å^3. Compared to pure HAp (a = 9.42 Å , c= 6.88 Å), substitution of Bi in calcium site results an increase in the 'a' and 'c' lattice parameters except for coating period of 4 days. This is because, Bi^{3+} ion has higher ionic radius (1.60 Å) than Ca^{2+} ionic radius (1.14 Å). Bi ions can push surrounding atoms and cause local distortions. As a result, pure samples have better crystallinity and increasing bismuth content result in crystallinity distortion (Sumathi and Buvaneswari, 2012).

XRD patterns of coated samples proved that for pure, 0.1 mM, 0.3 mM and 0.5 mM coatings the thickness of coatings increased with increasing soaking time.

Table 15 Rietveld analysis results of Ti-S-A-P plates after soaking in 0.5 mM Bismuth and Carbonate doped SBF.

Samples	Lattice parameters				Reference (P4, P7, P14, P21)		
	R_{wp}	a (Å)	c (Å)	V (Å^3)	a (Å)	c (Å)	V (Å^3)
0.5-C4	15.4652	9.4188	6.8682	609.3041	9.4231	6.8526	608.4753
0.5-C7	16.8089	9.7715	6.8911	657.9775	9.4622	6.8814	616.1139
0.5-C14	15.5100	10.0475	7.2167	728.5421	9.4514	6.8773	614.3421
0.5-C21	14.5070	9.8769	7.0175	684.5793	9.4602	6.8843	616.1131

The Ca/Bi atomic ratios of the coatings obtained by soaking the pretreated Ti6Al4V plates into 0.5 mM bismuth and carbonate added 1.5×SBF for different periods are given in Table 16. All of the coatings on the Ti6Al4V plates soaked into the 0.5 mM Bismuth and Carbonate co-doped 1.5×SBF contain bismuth. Since the plates were washed with distilled water after removal from the SBF solutions, the unbound precipitates were removed from the surface and the detected bismuth was only coming from the content of the coatings. Similar to 0.1 mM Bismuth and Carbonate doped 1.5×SBF coating, the Ca/Bi ratio decreased with increasing the soaking time which means the amount of the doped bismuth ion was increasing.

Table 16 Calculated Ca/Bi atomic ratios of 0.5-C4, 05.-C7, 0.5-C14, 0.5-C21.

Sample	Ca/Bi
0.5-C4	6.45±0.03
0.5-C7	6.56±0.08
0.5-C14	5.72±0.03
0.5-C21	1.98±0.02

XPS spectrum of 0.5-C14 is shown in Figure 39. Regarding the spectroscopy results, $Bi_2(HPO_4)_{x-z}(CO_3)_z(PO_4)_{6-x}(OH)_{2-x}$ compound formula was obtained as a coating material. XPS results proved that bismuth ion fully substitutes with calcium while it is not reliable to predict stoichiometric ratios about anions due to the results.
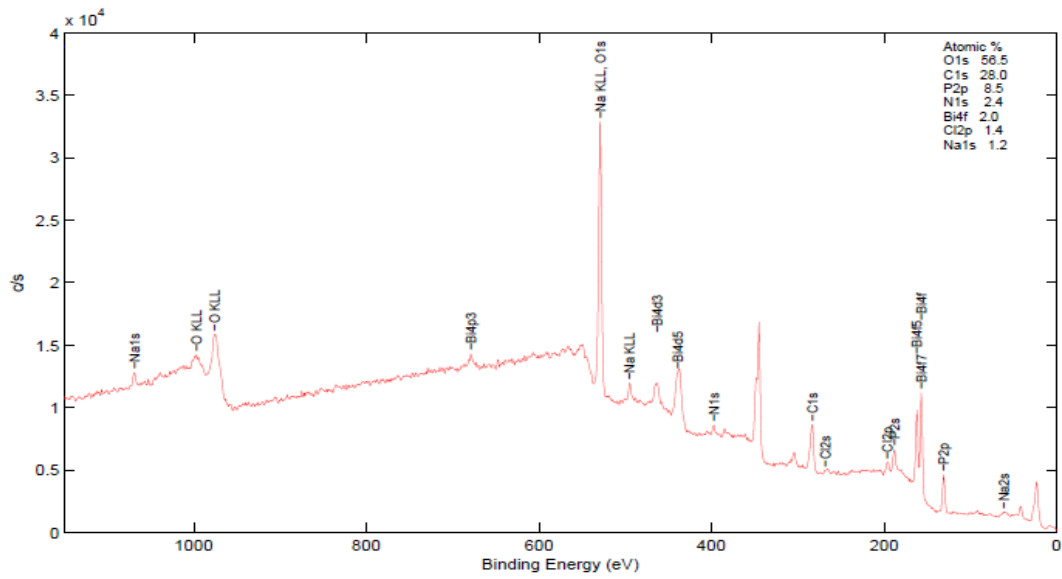
Figure 39 XPS spectrum of 0.5-C14.

3.2. Mechanical properties

Profilometer analysis and scratch tests were performed on coated plates to study mechanical properties of the coatings.

3.2.1. Thickness

Coatings thicknesses were determined by profilometer. Average thickness values are shown in Table 17. The wavy appearance of the coatings was problematic during characterization. In order to quantify geometry changes at each sample, the thickness measurements were performed with stylus profilometer. As seen from Table 17, maximum coating thickness was obtained by soaking in 0.1 mM co-doped 1.5 SBF solution. However, the coatings were not homogenous. It was observed that 0.1 mM co-doped 1.5 SBF coating resulted in coating thickness which were similar to those reported in literature (Lim et al., 2006; Kwaśniak et al., 2015).

Table 17 Thickness values of P21, 0.1-C21, 0.5-C21.

Sample	Thickness (μm)
P21	57.1±0.77
0.1-C21	95.3±0.81
0.5-C21	85.6±0.79

3.2.2. Critical lateral forces

The optical microscope images of the coated samples are shown in Figure 40. The images show the scratched surfaces and approximate critical load levels. Critical load is the load where the coatings are detached from surface. Table 18 shows the critical loads of pure 1.5 SBF, 0.1 mM co-doped 1.5 SBF, 0.3 mM co-doped 1.5 SBF and 0.5 mM co-doped 1.5 SBF coated for 7 days, 14 days and 21 days plates.
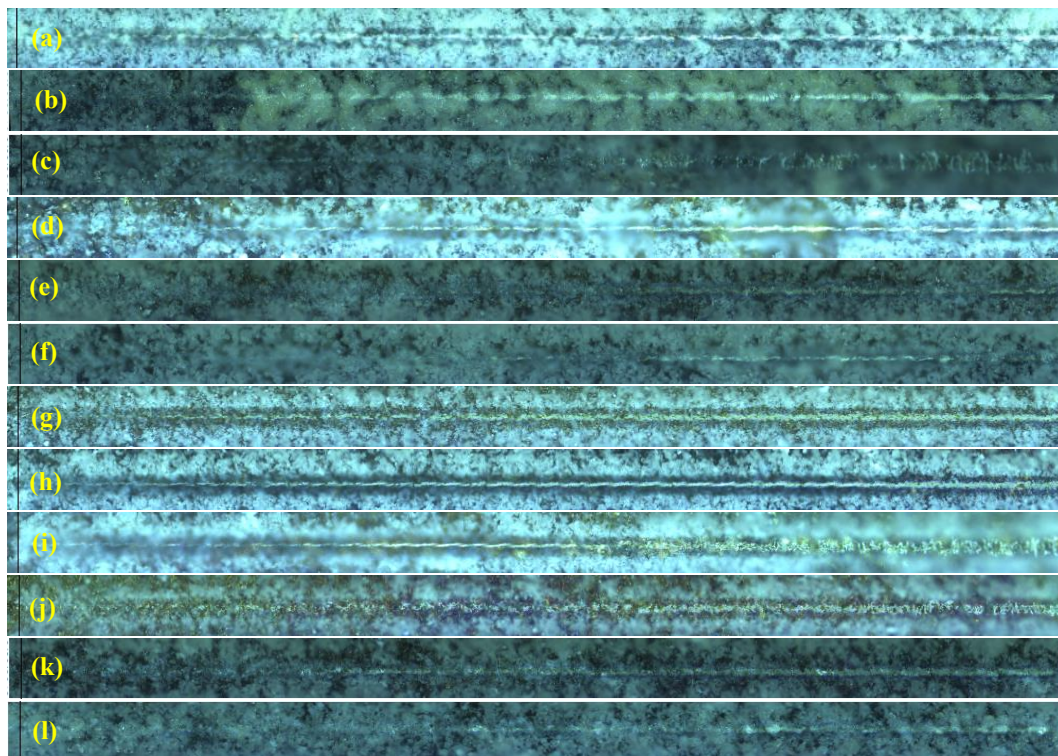
Figure 40 Scratch test optical microscopy images of a) P7, b) P14, c) P21 d) 0.1-C7, e) 0.1-C14, f) 0.1-C21, g) 0.3-C7, h) 0.3-C14, i) 0.3-C21, j) 0.5-C7, k) 0.5-C14, l) 0.5-C21.

Table 18 Critical loads of Ti-S-A-P plates after soaking in pure and co-doped 1.5 SBF for 7 days, 14 days and 21 days.

Sample	Critical Load (mN)
P7	100±1.17
P14	270±3.15
P21	250±3.01
0.1-C7	250±2.87
0.1-C14	330±7.01
0.1-C21	320±6.81
0.3-C7	280±4.77
0.3-C14	390±7.41
0.3-C21	410±7.07
0.5-C7	120±1.07
0.5-C14	330±2.82
0.5-C21	400±6.43

As seen from Table 18, all of the critical loads were above 100 mN. The coating obtained by soaking in 0.3 mM co-doped 1.5 SBF coated for 21 days had the highest critical load value (410 mN). Furthermore, among all co-doped coatings 0.3 mM co-doped coatings exhibited highest critical loads in each coating period.

Addition of Bismuth and Carbonate ion into SBF significantly enhanced adhesion of the coatings. Detaching doped SBF coatings from the Ti-S-A-P surface requires much higher load than detaching the pure SBF coating. When the critical load reached, large pieces of the coating started to detach from the substrate.

The critical load values at the moment of fracture of the coatings were above the expected levels for all types. It is known that pretreatment techniques and dopants can improve mechanical properties (Cochis et al., 2016; Forsgren et al., 2007). The pretreatment routine and dopants had great effect on mechanical properties of coated plates in this study. Such as alkali pretreated and selenium doped SBF coated Ti6Al4V plates exhibited much lower critical loads (about 70 mN) (Yilmaz, 2014). According to Ramesh et al., it was claimed that the undoped sample exhibited intergranular fracture mode. Researchers showed that the grain interior is stronger than the grain boundary. However, the introduction of Bi into HAp matrix has altered the fracture mode from intergranular to transgranular.

This observation suggested that grain boundary exhibited more resistant to fracture than the grain interior. As a result, when crack penetrating into the grain boundary; it would require additional energy to break the triple barrier in the grain boundary as compared to normal transgranular fracture (Ramesh et al., 2011).

3.3. Biological properties

Cytotoxicity and antibacterial properties of the samples were evaluated to designate biological properties.

3.3.1. L929 fibroblast cell line

Fibroblast cells viability percentage of the coated plates are shown in Figure 41.
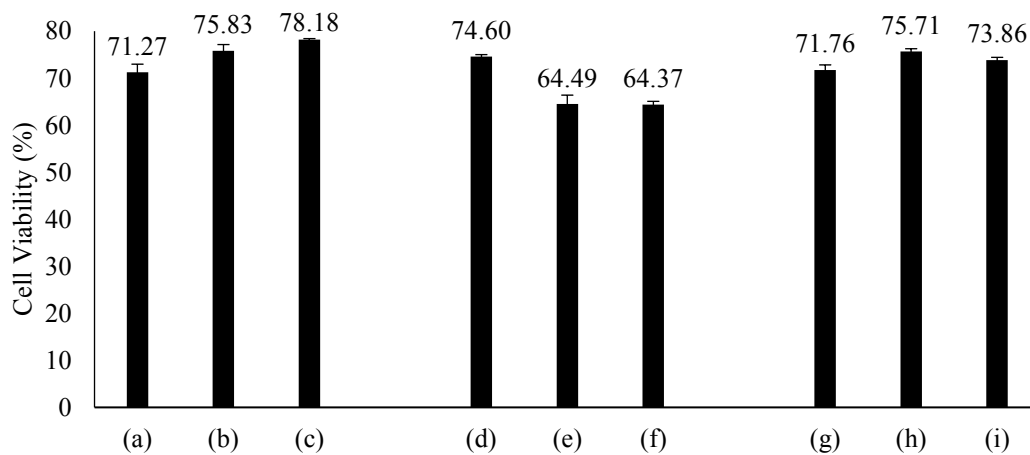
Figure 41 Percentage viability of fibroblast cells seeded on a) 0.1-C7, b) 0.1-C14, c) 0.1-C21, d) 0.5-C7, e) 0.5-C14, f) 0.5-C21, g) P7, h) P14, i) P21.

Fibroblast cells showed slightly higher viability on 0.1 mM co-doped coatings compare to pure coatings. No remarkable toxicity was observed in 0.1 mM co-doped coatings, on the other hand 0.5 mM co-doped coatings seemed to be toxic after 14 day of coating.

72

In this study, higher concentration of bismuth ion resulted in increasing cytotoxicity, though low concentrations (0.1 mM) barely enhanced L929 cell viability similar to literature work (Shanmugam and Gopal, 2014; Qiu et al., 2015).

3.3.2. SaOS-2 cell culture

Human epithelial-like primary osteogenic sarcoma SaOS-2 cell line, used for biological characterization. These cells possess some markers and phenotype typical of primary human osteoblasts cultured on metallic surfaces (Saldaña et al., 2011; Shapira and Halabi, 2009). Figures 42, 43 and 44 show percentage of reduction according to time past after cell seeding for all samples.
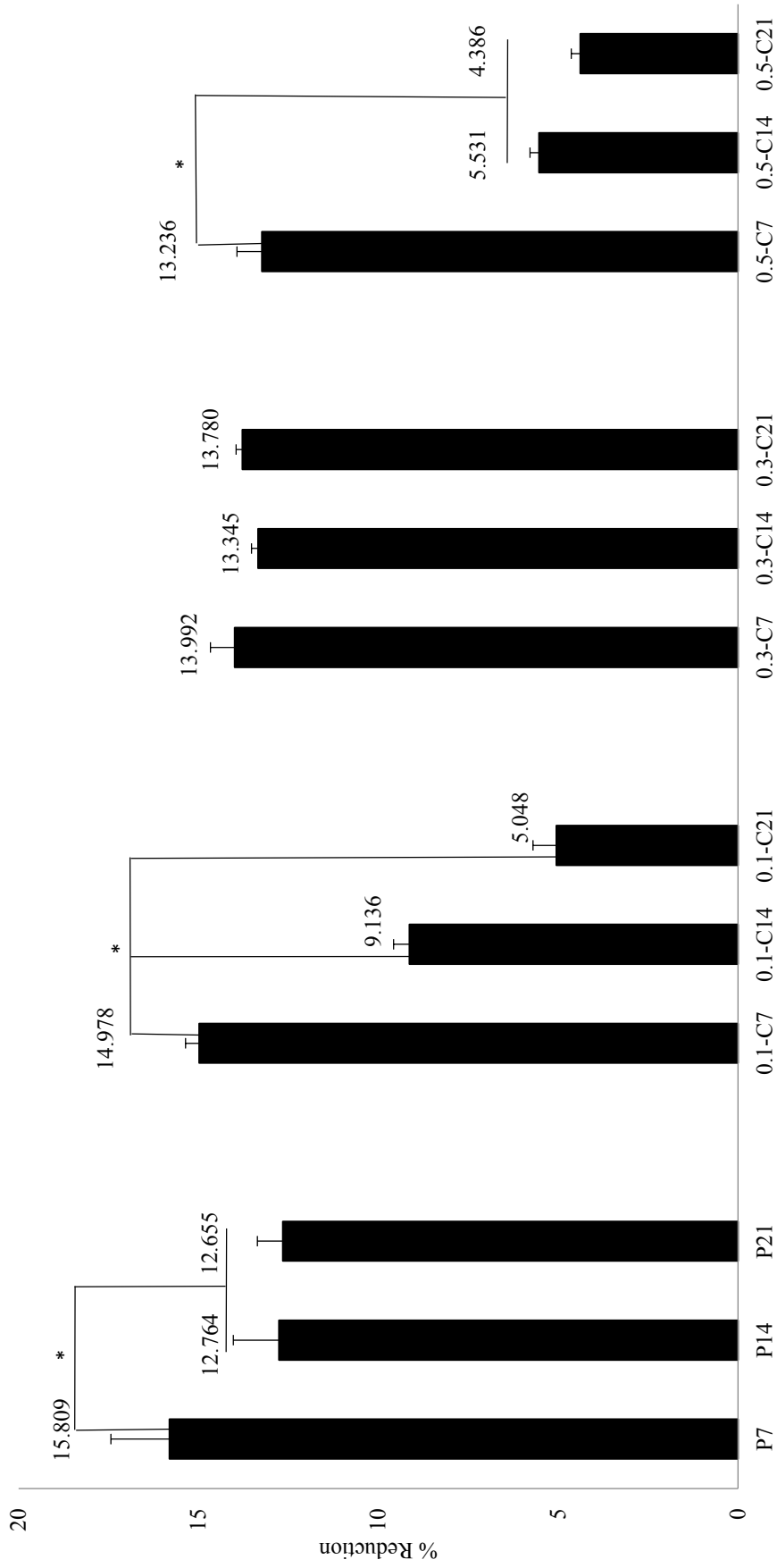
Figure 42 Percentage of reduction 1 day after cell seeding for pure and co-doped SBF coated samples. The error bars represent the standard error. Asterisks indicate differences of statistical significance (*p<0.05) within the groups determined by the ANOVA test.

74
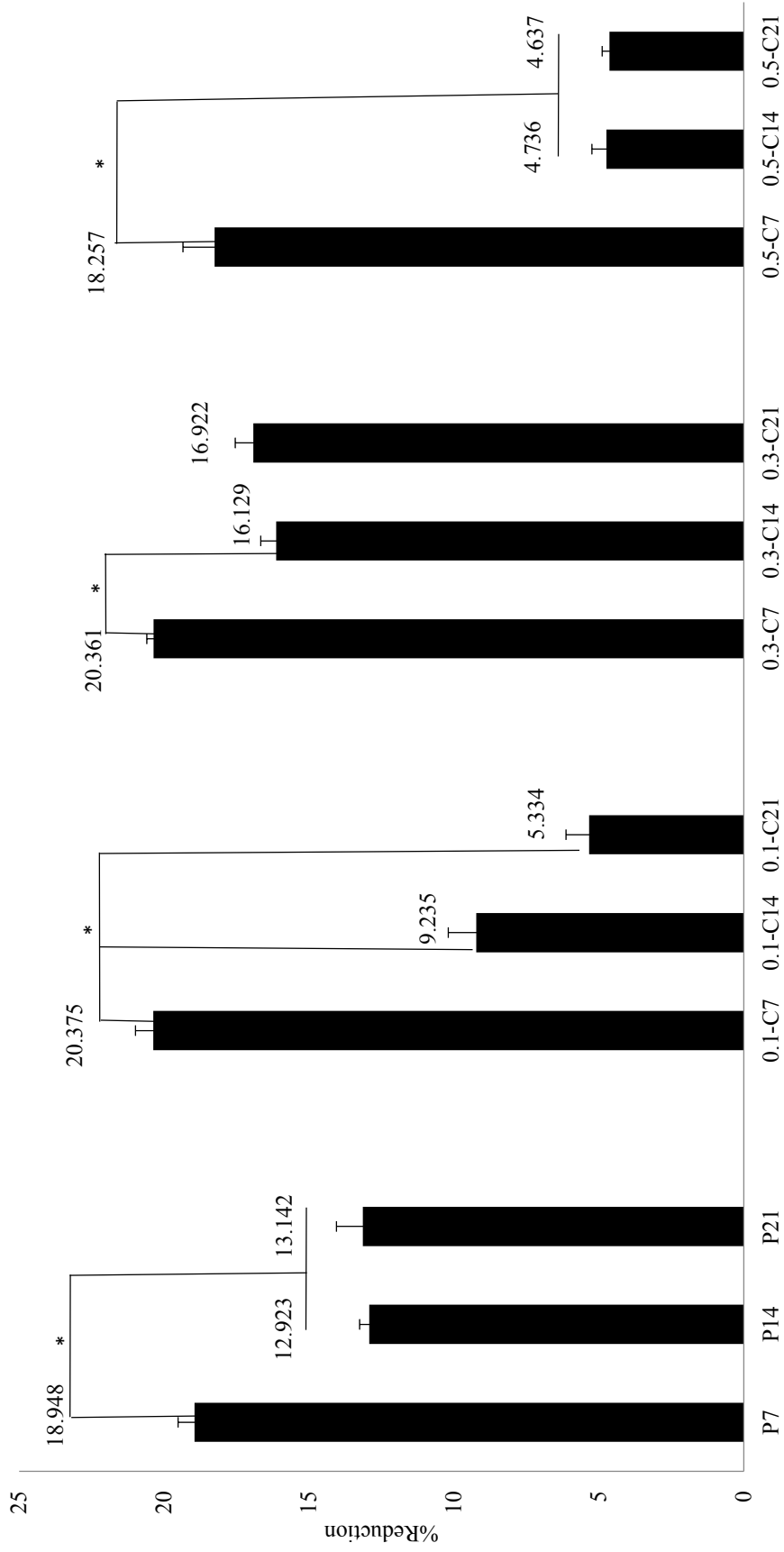
Figure 43 Percentage of reduction 3 day after cell seeding for pure and co-doped SBF coated samples. The error bars represent the standard error. Asterisks indicate differences of statistical significance (*p<0.05) within the groups determined by the ANOVA test.
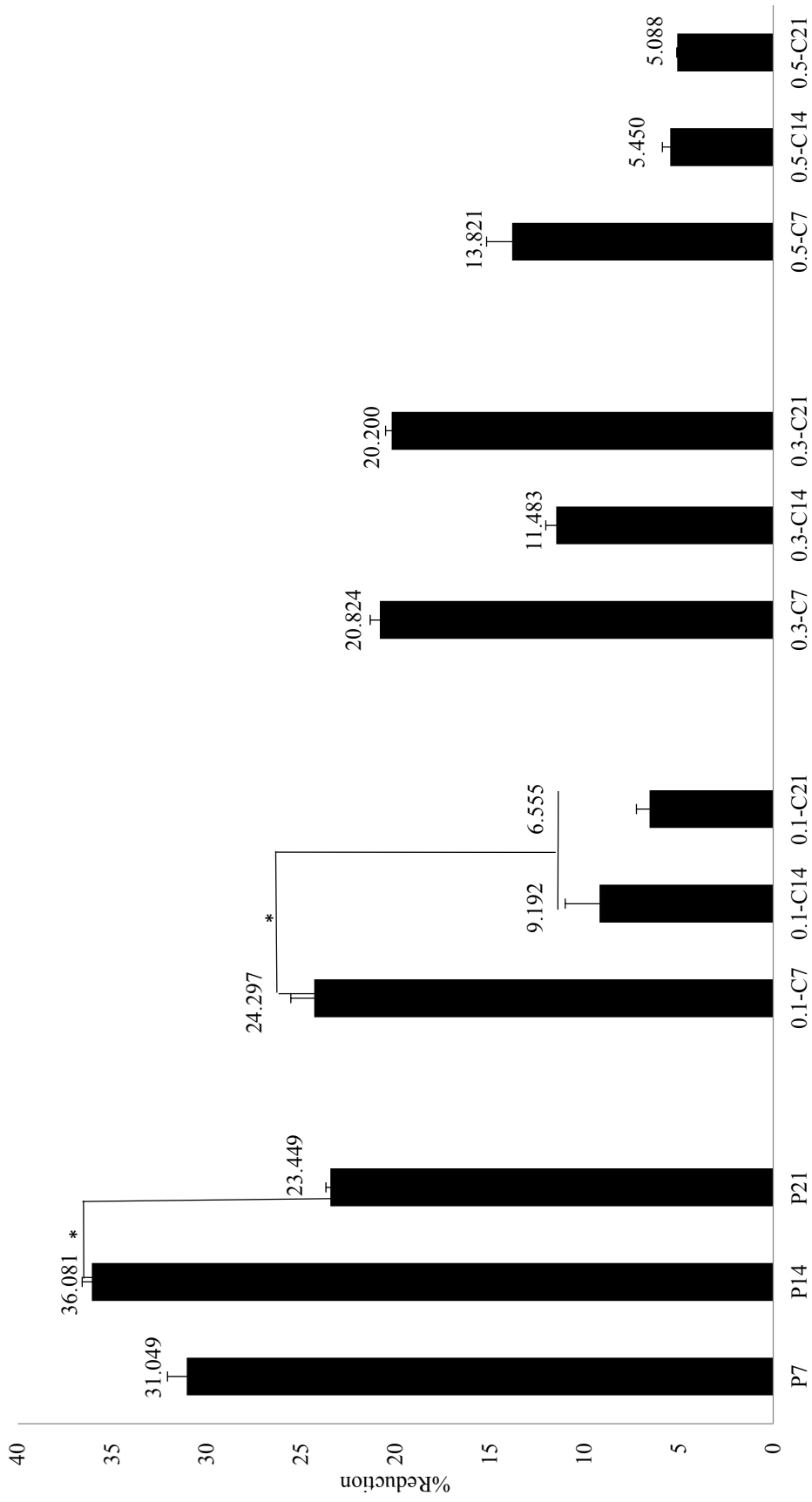
Figure 44 Percentage of reduction 7 day after cell seeding for pure and co-doped SBF coated samples. The error bars represent the standard error. Asterisks indicate differences of statistical significance (*p<0.05) within the groups determined by the ANOVA test.

As it can be seen from Figures 42, 43 and 44, the plates coated with pure and co-doped 1.5xSBF showed different reduction according to coating period. Percentage of reduction increasement is directly related to development of cell proliferation. Percentage of reduction increases as cell mitochondrial activity increase which is related to the number of cells containing mitochondria. Pure SBF coated samples were referred as control group.

Figure 42, indicates percentages of reduction 1 day after cell seeding. For this period of cell seeding, plates that were 0.1 mM co-doped SBF coated for 7 days exhibited the highest reduction percentage among all co-doped samples. Moreover 0.3 mM co-doped SBF coated for all immersion times had significantly high reduction percentages. Each examine group (pure, 0.1 mM co-doped, 0.3 mM co-doped, 0.5 mM co-doped) was in itself showed different reduction according to coating ingredients. For instance in case of pure HAp coating for 7 day immersion time percentage of reduction (15.8% reduction) was significantly high, though it decreased moderately as the immersion time reached to 14 days (12.8% reduction) and 21 days (12.6% reduction). In case of 0.1 mM and 0.5 mM co-doped HAp coatings, reduction of percentage decreased as the immersion period increased due to rise in dissolution of bismuth ion from the coatings. It is important to notify that some cells attached on the surface were also lost during medium renewals. This may also explain sudden drops in cell reduction percentages. Unexpectedly, in case of 0.3 mM co-doped HAp coatings for all immersion periods (7 days, 14 days and 21 days) reduction percentage seemed to be really high and stable almost the same with control group (pure SBF coated samples) which makes it the best concentration of dopant for the period of 1 day after cell seeding.

Figure 43, represents percentages of reduction 3 day after cell seeding. Similar behaviors to the 1 day after cell seeding were observed in each examine group. Generally, in all cases of coatings reduction of percentage increased or remained stable except 0.5 mM co-doped HAp coated for 14 days sample.

Highest rate of reduction percentage change (from 1 day to 3 day after cell seeding) was observed for 0.1 mM co-doped HAp coating and 0.3 mM co-doped HAp coating.

Figure 44, shows percentages of reduction 7 day after cell seeding. Again similar behaviors to the 1 day and 3 day after cell seeding were observed in all cases except 0.3 mM co-doped SBF coated for 14 days and 0.5 mM co-doped SBF coated for 7 days. Stated samples exhibited lower percentage of reduction comparing to the percentage of reductions obtained in 3 days after cell seeding. Meanwhile, 0.1 mM co-doped HAp coating with immersion period 7 days, obtained the highest reduction percentage (24.3% reduction) among all co-doped coating for 7 days after cell seeding. The cell proliferation was inhibited by high release of bismuth ion (as observed from 0.5 mM co-doped HAp coated samples) however low concentrations of bismuth ion enhances the proliferation.

Percentage of reduction data is given in terms of relative viability in Table 19. Table 19 showed percentage of viability due to Alamar Blue test for; pure 1.5 SBF coated plates (control group), 0.1 mM doped, 0.3 mM doped and 0.5 mM doped 1.5 SBF coated plates. Relative viability was calculated according to Equation (13).

$$\text{Relative Viability} = \frac{\text{Absorbance of treated well}}{\text{Mean absorbance of control wells (pure SBF coated samples)}} \text{x}100 \quad (13)$$

Table 19 Relative viabilities of pure and co-doped samples.

Time After Cell Seeding	Sample	% Reduction	Relative Viability
1 day past	P7 (control)	15.809	100.000
	P14 (control)	12.764	100.000
	P21 (control)	12.655	100.000
	0.1-C7	14.978	94.742
	0.1-C14	9.136	71.579
	0.1-C21	5.048	39.885
	0.3-C7	13.992	88.503
	0.3-C14	13.345	104.550
	0.3-C21	13.780	108.886
	0.5-C7	13.236	83.724
	0.5-C14	5.531	43.335
	0.5-C21	4.386	34.658
3 day past	P7 (control)	18.948	100.000
	P14 (control)	12.923	100.000
	P21 (control)	13.142	100.000
	0.1-C7	20.375	107.534
	0.1-C14	9.235	71.459
	0.1-C21	5.334	40.584
	0.3-C7	20.361	107.456
	0.3-C14	16.129	124.807
	0.3-C21	16.922	128.763
	0.5-C7	18.257	96.351
	0.5-C14	4.736	36.646
	0.5-C21	4.637	35.284
7 day past	P7 (control)	31.049	100.000
	P14 (control)	36.081	100.000
	P21 (control)	23.449	100.000
	0.1-C7	24.297	78.255
	0.1-C14	9.192	25.476
	0.1-C21	6.555	27.954
	0.3-C7	20.824	67.069
	0.3-C14	11.483	31.825
	0.3-C21	20.200	86.145
	0.5-C7	13.821	44.514
	0.5-C14	5.450	15.104
	0.5-C21	5.088	21.698

Webster et al. stated that HAp doped with trivalent cations exhibited greater osteoblast adhesion than either pure HAp or HAp doped with divalent cations. It is proved that HAp doped with trivalent cations had smaller grain sizes which contributes to enhance osteoblast adhesion specially bismuth (III) doped HAp resulted excellent results (Webster et al., 2004). According to results of this study:

- 0.1 mM co-doped coatings: In all evaluation periods, 0.1 mM co-doped SBF coated for 7 days sample exhibited highest reduction percentage among all co-doped samples which makes it the best concentration for dopant. Though 0.1 mM co-doped SBF coatings didn't showed the best initial attachment which was related to coating's instability as endorsed with mechanical results. In all 0.1 co-coatings, cell proliferation continued or remained the same after cell seeding. Especially for 0.1 mM co-doped SBF coated for 7 days plates exhibited very high proliferation improvement according to low bismuth ion dissolution rate. It should also be noted that some of the coating was lost during medium renewals.

- 0.3 mM co-doped coatings: 0.3 mM co-doped SBF coated plates showed the best initial attachment and generally the proliferation continued after 7 days of cell seeding. The increments of reduction percentage along seeding period were compatible with mechanical results that prove that the most coherent and stable coating was obtained in 0.3 mM co-doped coatings. Unexpected fall of 14 day coated sample's reduction percentage after 7 days of cell seeding was due to the rise of bismuth ion dissolution rate. Though among other concentrations 0.3 mM co-doped coatings had the lowest bismuth ion dissolution rate.

- 0.5 mM co-doped coatings: 0.5 mM co-doped SBF coated plates resulted in high release of bismuth ion, leading to toxicity increment and suppressing cell proliferation. Generally in all cases, minimum cell proliferation was observed in 0.5 mM co-doped SBF coatings due to bismuth toxic effect.

SEM Microscopy Results

The morphology and attachment of the SaOS-2 cells on the pure and dope SBF coated plates were assessed by using the SEM microscopy, arrows indicate cell extensions in SEM images. The SEM images of the SaOS-2 cells incubated for 1 day and 7 day time period, on P7, P14 and P21 plates are shown in Figure 45 (lower magnification) and Figure 46 (higher magnification).
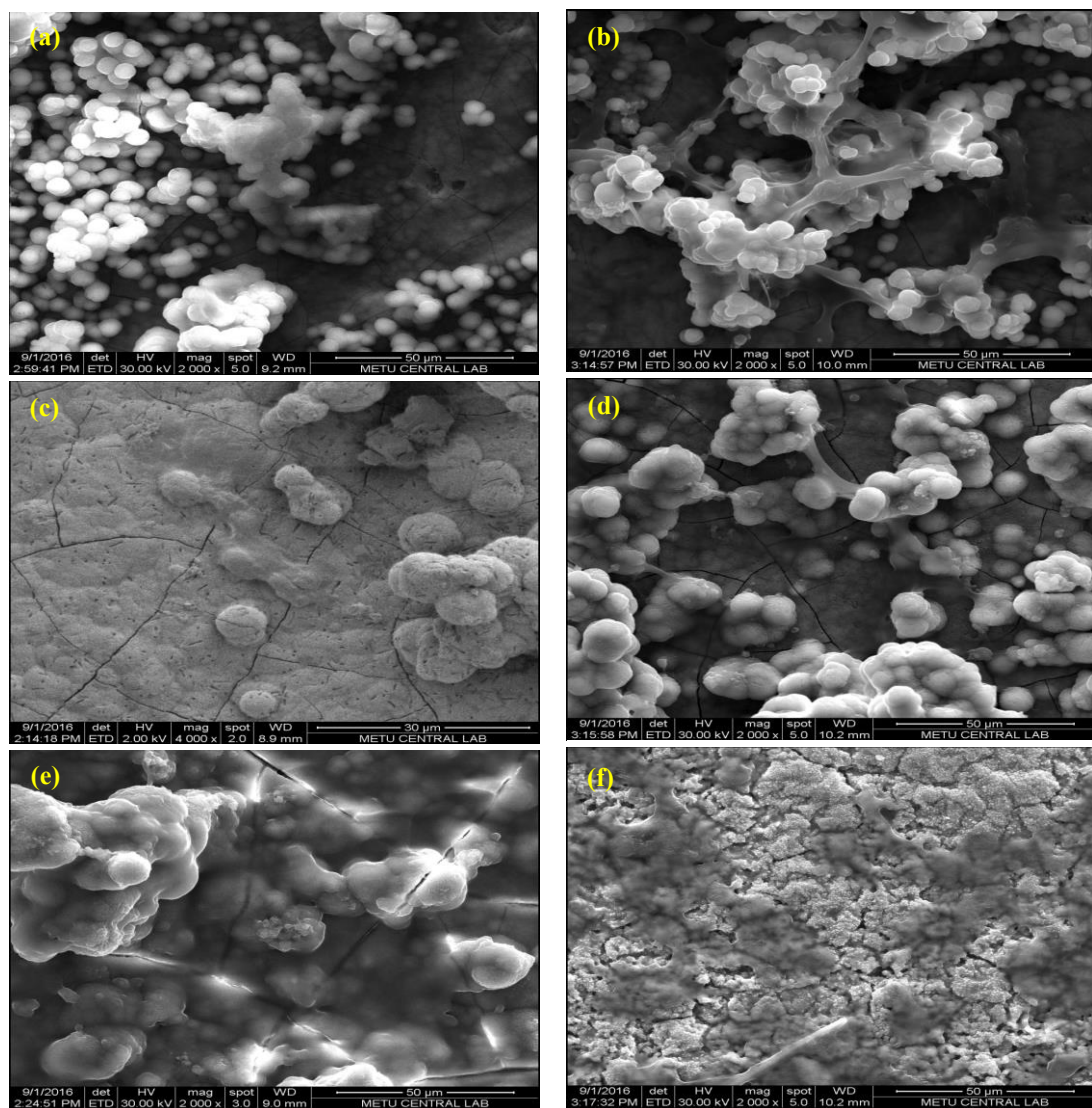
Figure 45 SEM images of the SaOS-2 cells incubated for a) 1 day on P7 (2000x), b) 7 day on P7 (2000x), c) 1 day on P14 (4000x), d) 7 day on P14 (2000x), e) 1 day on P21 (2000x), f) 7 day on P21 (2000x)
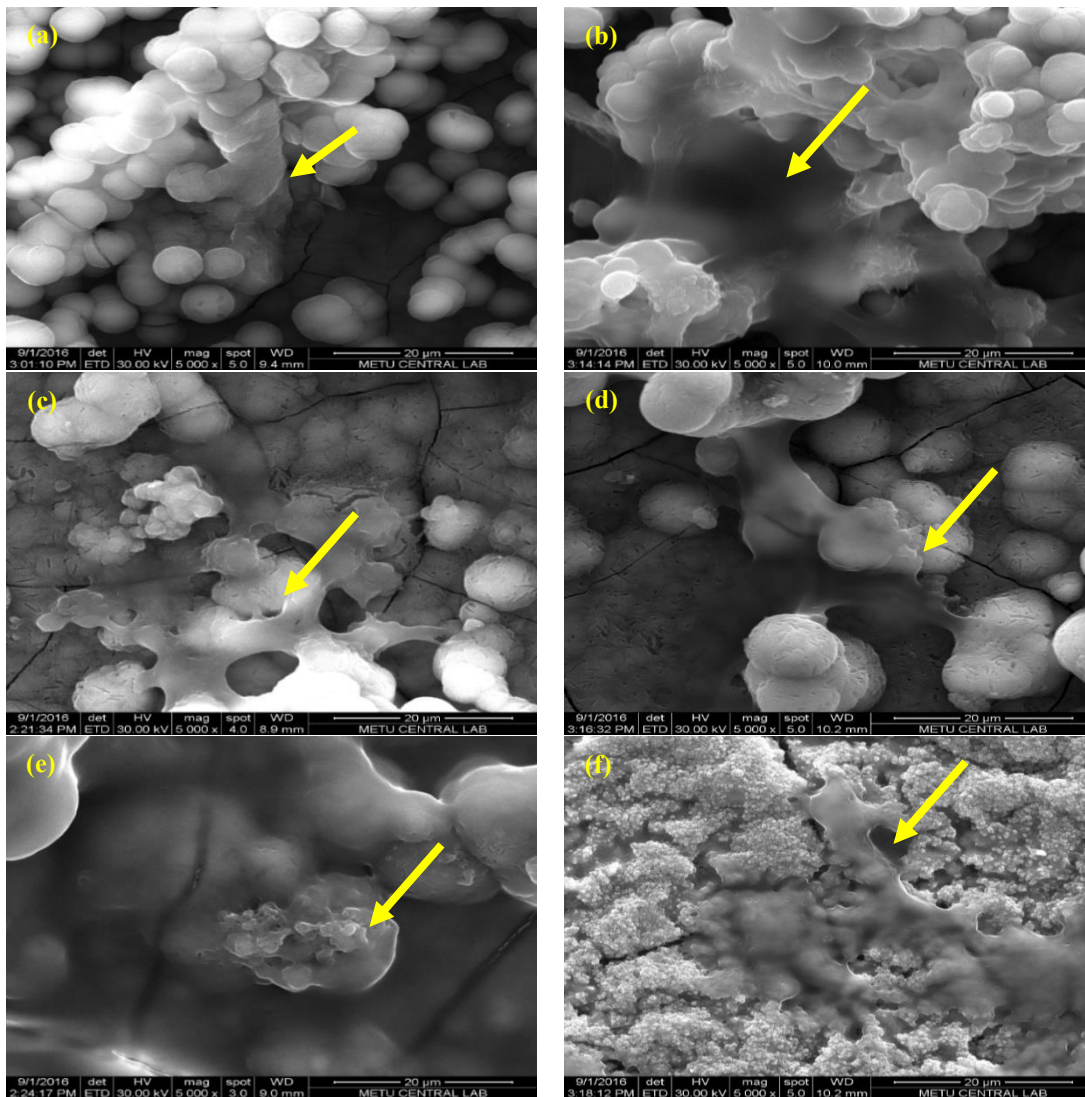
Figure 46 SEM images of the SaOS-2 cells incubated for a) 1 day on P7, b) 7 day on P7, c) 1 day on P14, d) 7 day on P14, e) 1 day on P21, f) 7 day on P21 (5000x).

The SEM images of the SaOS-2 cells incubated for 1 day and 7 day time period, on 0.1-C7, 0.1-C14 and 0.1-C21 plates are represented in Figure 47 (lower magnification) and Figure 48 (higher magnification).
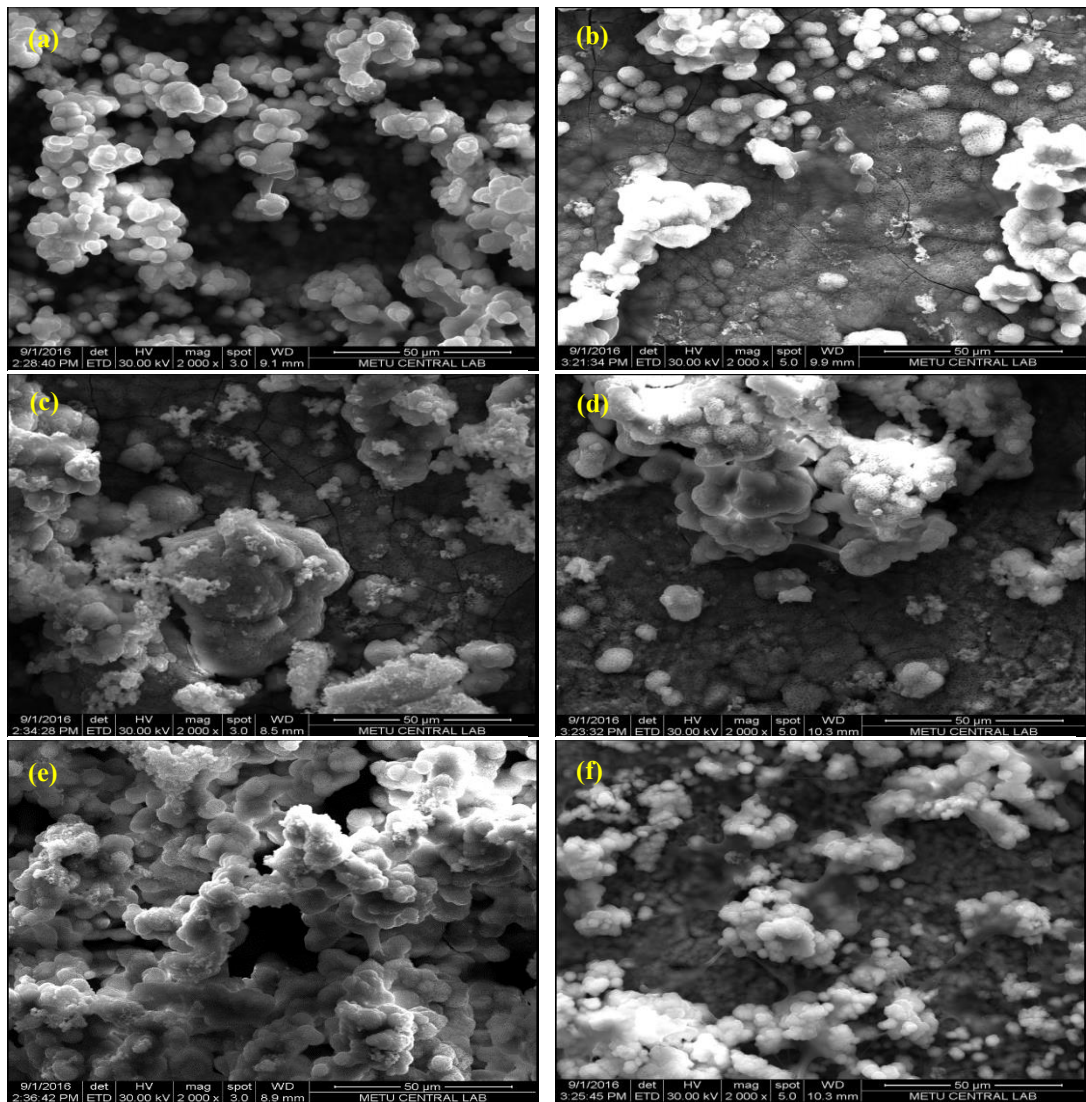
Figure 47 SEM images of the SaOS-2 cells incubated for a) 1 day on 0.1-C7, b) 7 day on 0.1-C7, c) 1 day on 0.1-C14, d) 7 day on 0.1-C14, e) 1 day on 0.1-C21, f) 7 day on 0.1-C21 (2000x).
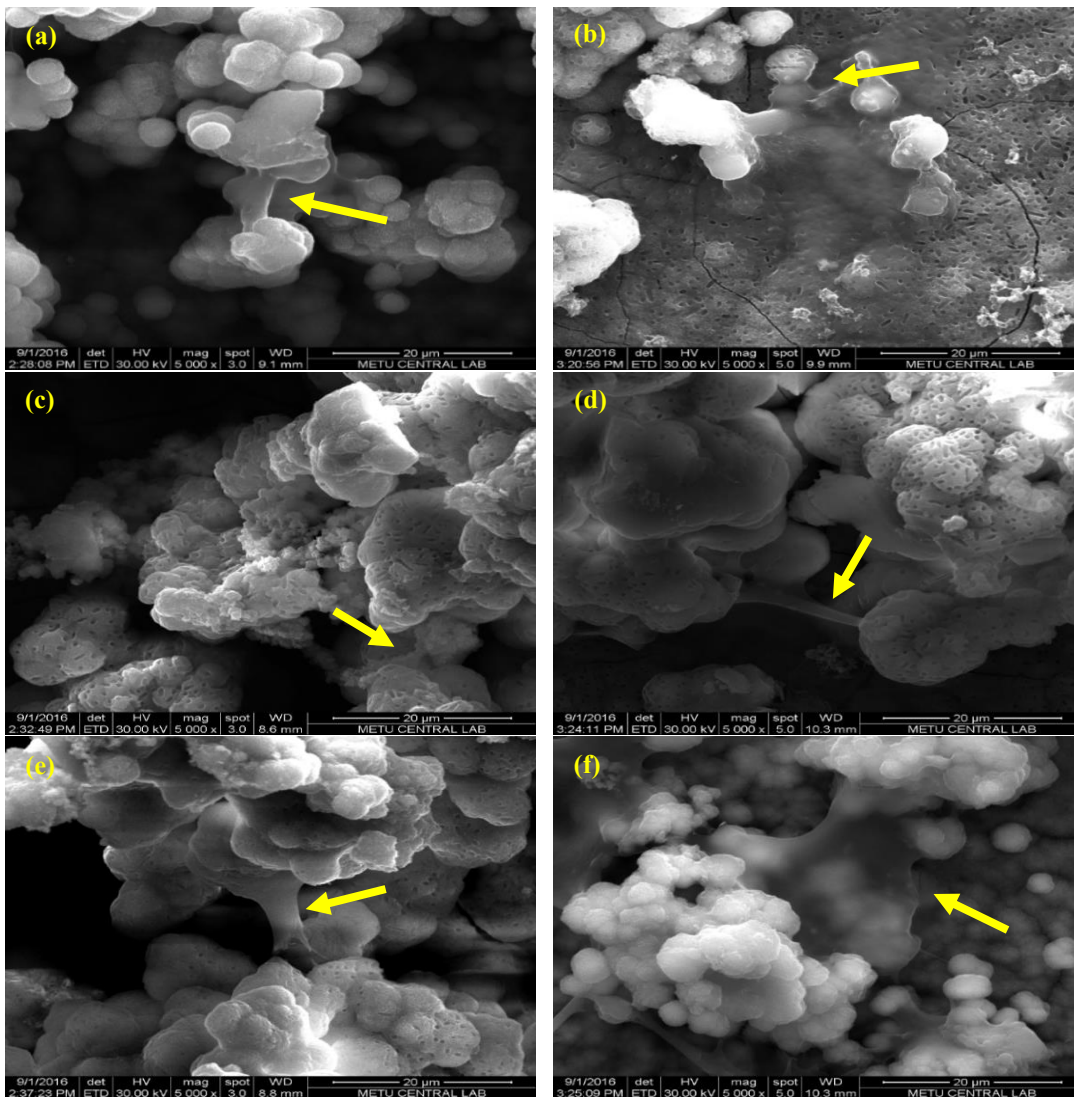
Figure 48 SEM images of the SaOS-2 cells incubated for a) 1 day on 0.1-C7, b) 7 day on 0.1-C7, c) 1 day on 0.1-C14, d) 7 day on 0.1-C14, e) 1 day on 0.1-C21, f) 7 day on 0.1-C21 (5000x).

The SEM images of the SaOS-2 cells incubated for 1 day and 7 day time period, on 0.3-C7, 0.3-C14 and 0.3-C21 plates are represented in Figure 49 (lower magnification) and Figure 50 (higher magnification).
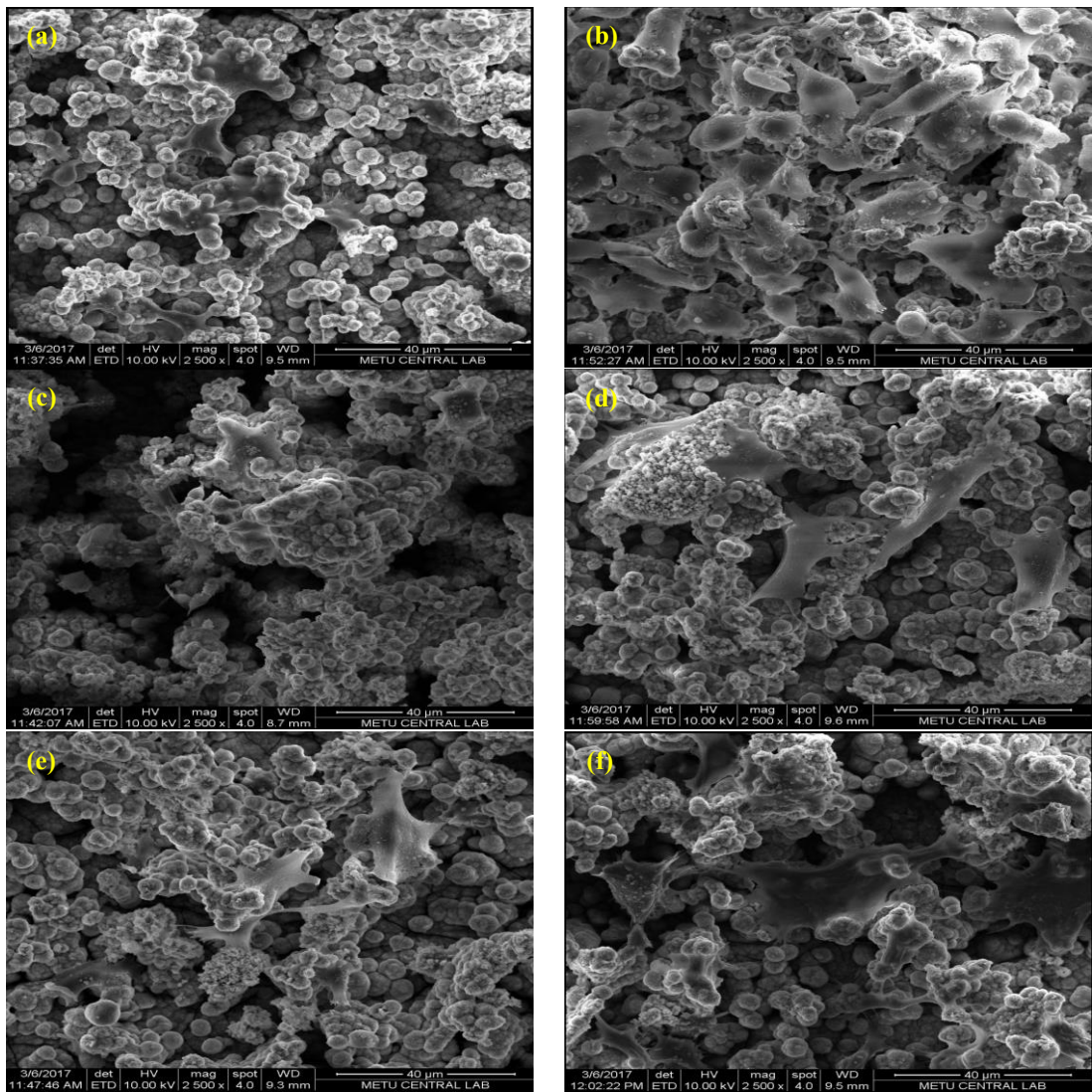
Figure 49 SEM images of the SaOS-2 cells incubated for a) 1 day on 0.3-C7, b) 7 day on 0.3-C7, c) 1 day on 0.3-C14, d) 7 day on 0.3-C14, e) 1 day on 0.3-C21, f) 7 day on 0.3-C21 (2500x).
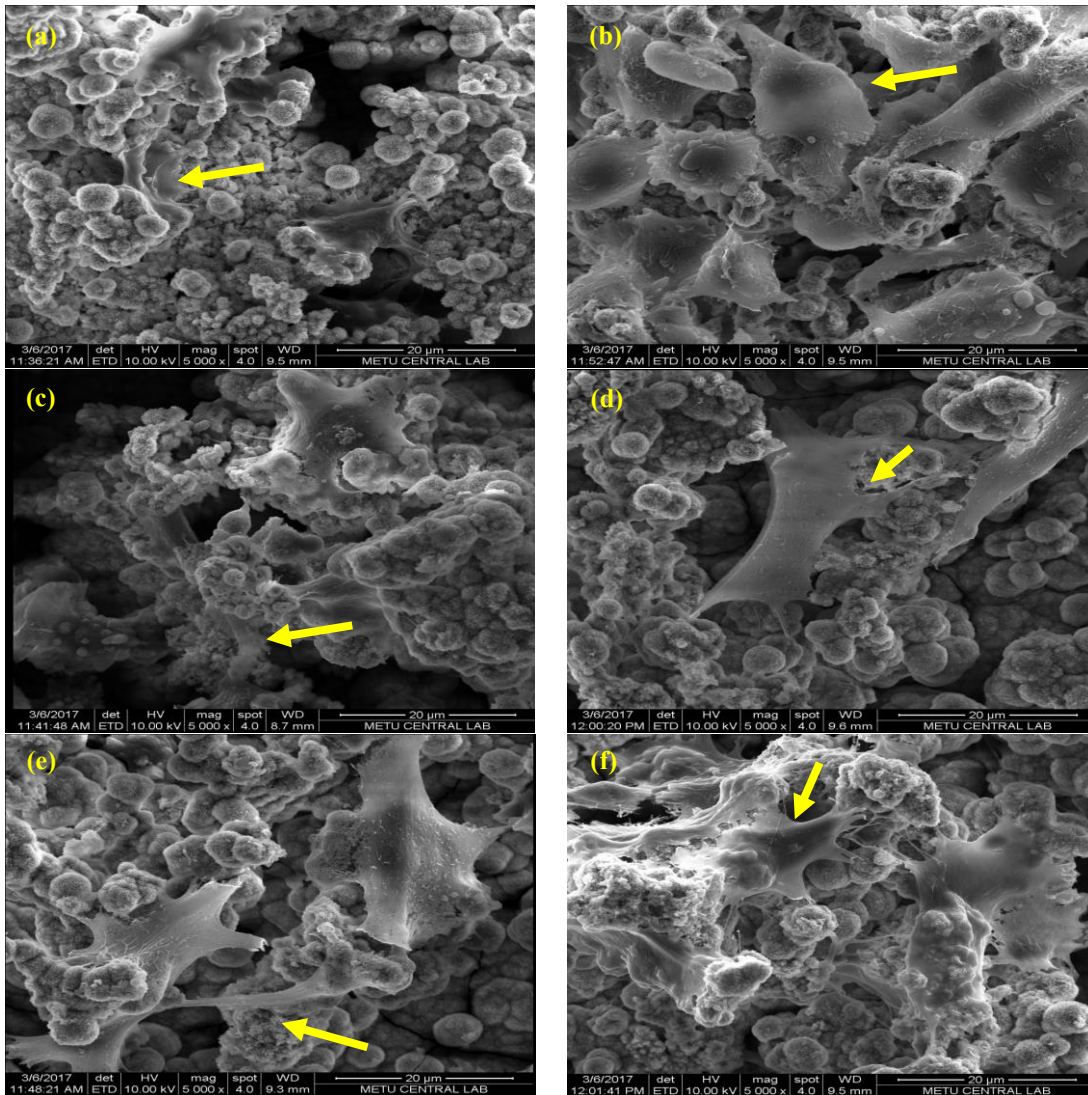
Figure 50 SEM images of the SaOS-2 cells incubated for a) 1 day on 0.3-C7, b) 7 day on 0.3-C7, c) 1 day on 0.3-C14, d) 7 day on 0.3-C14, e) 1 day on 0.3-C21, f) 7 day on 0.3-C21 (5000x).

The SEM images of the SaOS-2 cells incubated for 1 day and 7 day time period, on 0.5-C7, 0.5-C14 and 0.5-C21 plates are indicated in Figure 51 (lower magnification) and Figure 52 (higher magnification).
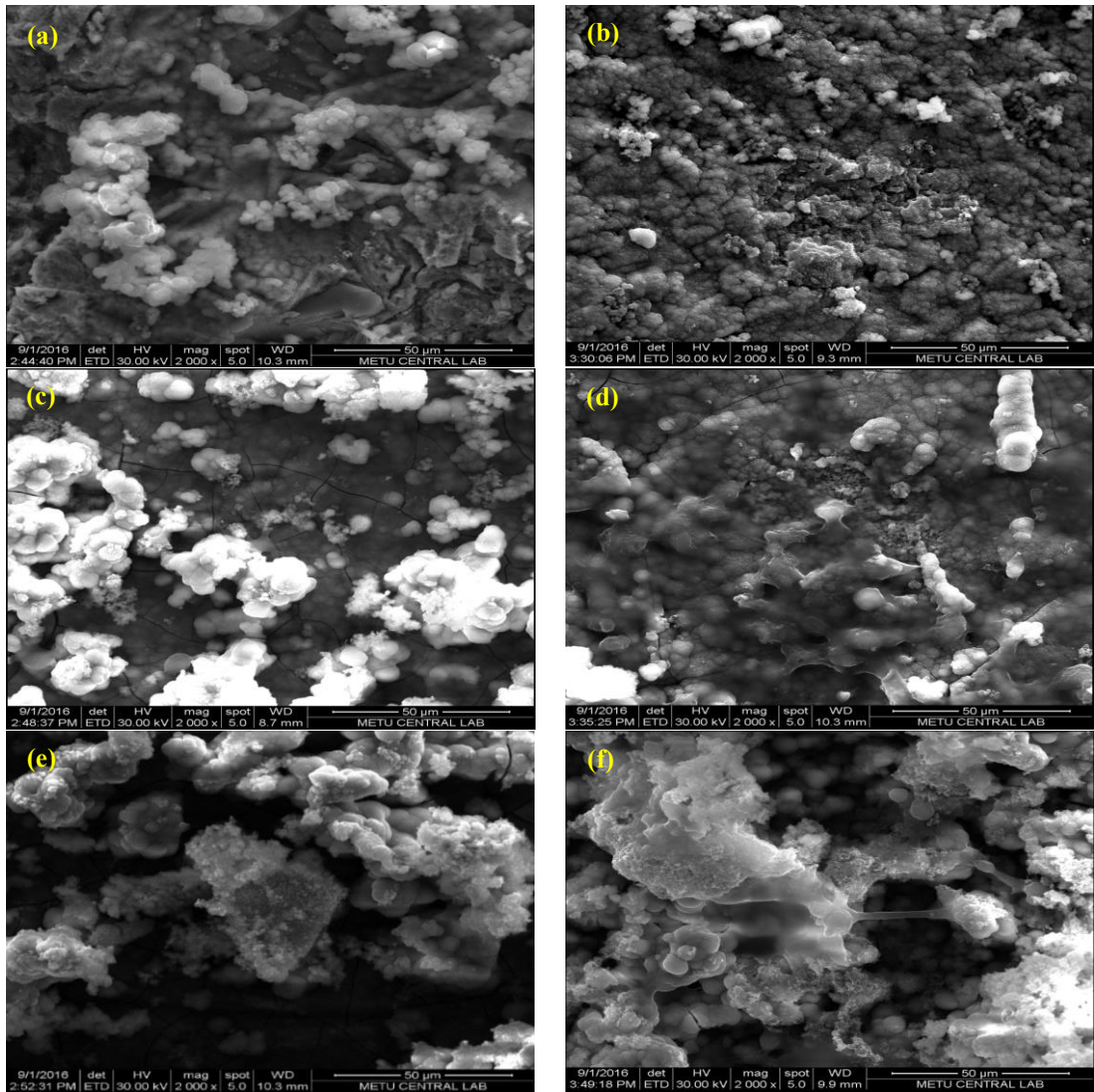
Figure 51 SEM images of the SaOS-2 cells incubated for a) 1 day on 0.5-C7, b) 7 day on 0.5-C7, c) 1 day on 0.5-C14, d) 7 day on 0.5-C14, e) 1 day on 0.5-C21, f) 7 day on 0.5-C21 (2000x).
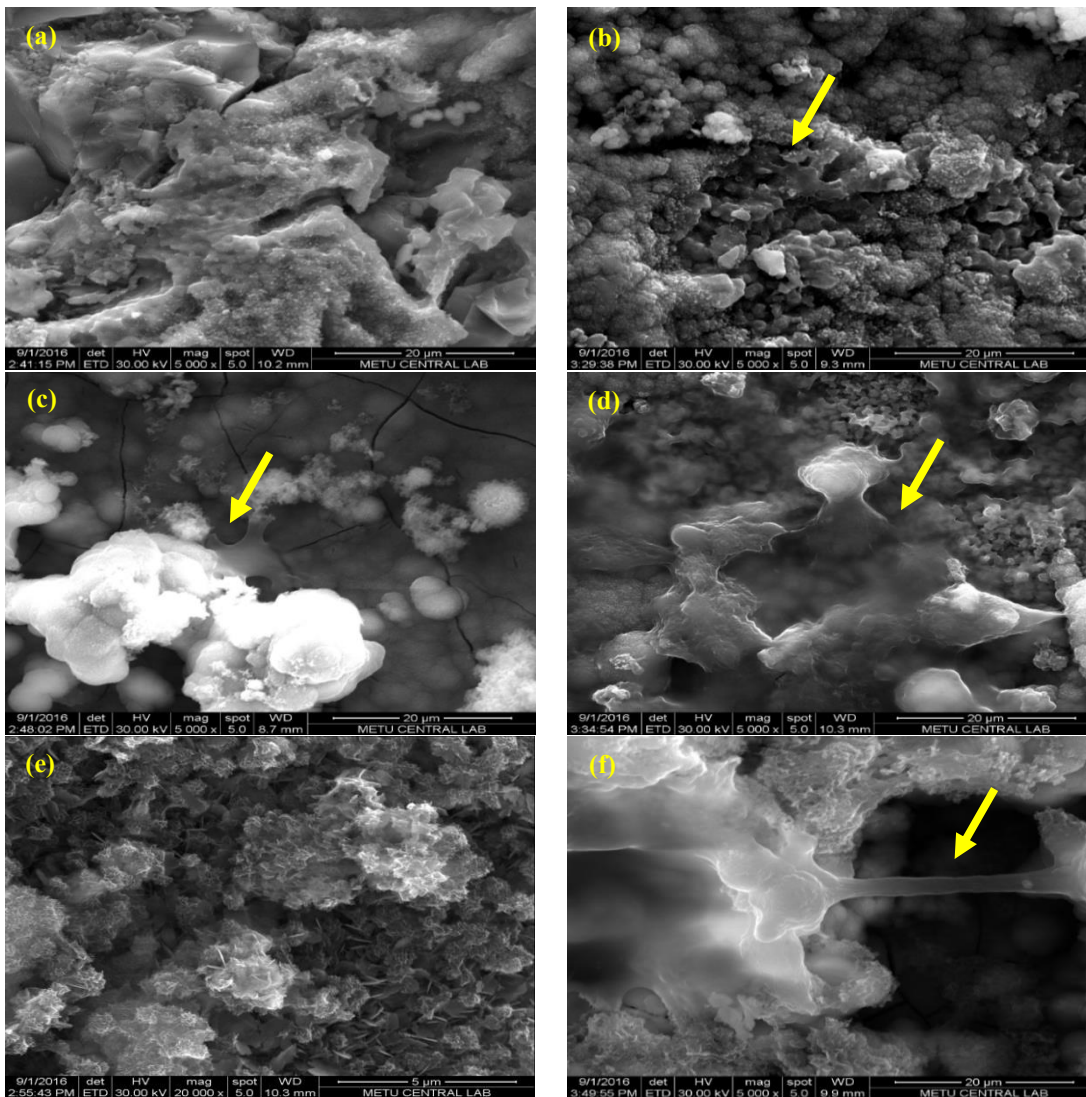
Figure 52 SEM images of the SaOS-2 cells incubated for a) 1 day on 0.5-C7, b) 7 day on 0.5-C7, c) 1 day on 0.5-C14, d) 7 day on 0.5-C14 (5000x), e) 1 day on 0.5-C21 (20 000x), f) 7 day on 0.5-C21 (5000x).

Figures 45-52 indicated that cells attached firmly to the coated plates surfaces in all cases. The globular HAp surface was covered thoroughly by cytoskeleton protrusions of the cells (in nano crater form), indicating that this surface is beneficial for cell anchorage. The migration of the cells on the coated surfaces was proved by the existence of lamellipodia and filopodia that are observed in Figure 46, Figure 47, Figure 49 and Figure 51.

In some cases, cells were not visible due to stratified coating of HAp particles as seen in Figure 46 (a), Figure 47 (c), Figure 51 (a) and Figure 51 (e).

3.3.3. Antibacterial activity

In order to achieve better anti-bacterial activity surface modification of Ti-based medical implants by inclusion of anti-microbial agents into the surface layer is considered relatively simple, cheap and effective. Doping with a bactericide agent is one of popular strategies (Wang et al., 2014). An ideal biomaterial for prosthetic implants should promote cellular adhesion and avoid the bacterial one.

In this study, antibacterial test results were obtained in colony forming unit (CFU) per ml in order to make a good comparison with literature work. Antibacterial tests were carried out for the samples that had the best mechanical tests and cell culture results. Figure 53 presents the photo taken during visual counting of bacterial colonies.
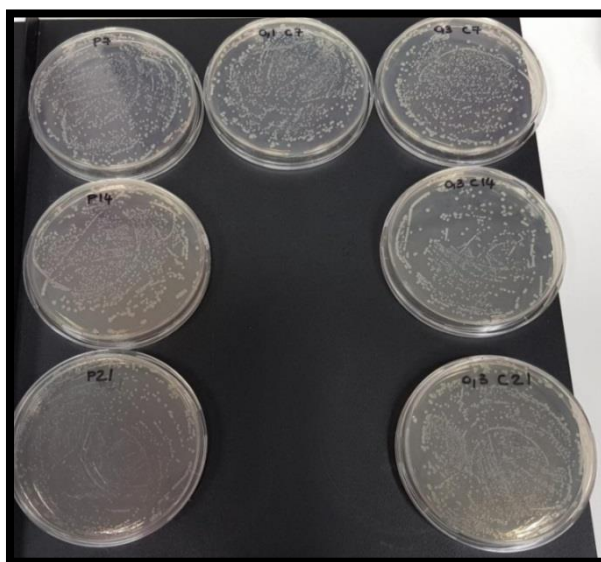
Figure 53 Petri dishes initially supplemented with 10^6 CFU/ml of *S.Epidermidis* during CFU counting.

Antibacterial activity results of Ti-S-A-P plates after soaking in in pure and co -
doped coatings are shown in Figure 54.
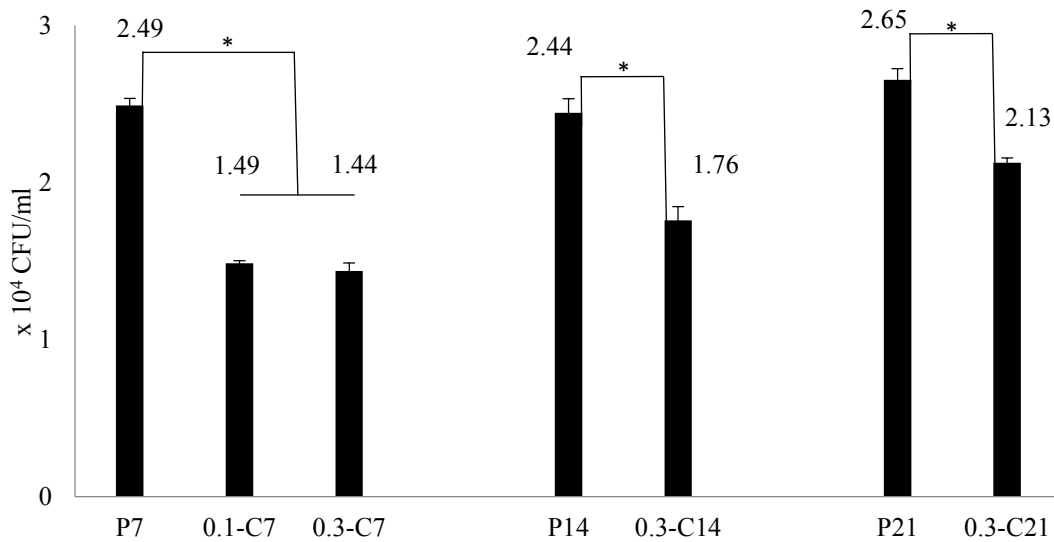
Figure 54 Colony forming units per ml of pure and co-doped coatings. The error
bars represent the standard error. Asterisks indicate differences of statistical
significance (*p<0.05) within the groups determined by the ANOVA test.

Results indicated that statistically fewer bacteria adhered to 0.3 mM co-doped
coating compare to pure coatings. The best antibacterial samples are 0.1-C7 and 0.3-
C7 which had no significant difference between each other. Antibacterial test results
are consistent with cell culture results. Surface chemical composition of the coating
is important for bacterial adhesion. Lugovskoy et al. claimed that the development of
S.epidermidis is depressed by the titanium dioxide on the other hand HAp favors the
growth of the bacteria (Lugovskoy et al., 2016). According to Trujillo et al., doping
HAp with antibacterial ion such as silver results in decrement of bacterial adhesion
(Trujillo et al., 2012). Ohtsu et al. performed a similar technique for antibacterial
tests and as a result they observed that ZnO added HAp had leaded to increase
antibacterial property compare to pure HAp coating (Ohtsu et al., 2017). Similarly in
this study, bacterial adhesion was depressed as the HAp amount decreased and
bismuth + carbonate amount increased.

CHAPTER 4

CONCLUSION

As received Ti substrates were exposed to 3 step (Ti-S, Ti-S-A, Ti-S-A-P) pretreatment routine and structural analysis were performed. It was observed that Ti had the smoothest surface with R_a value 260 nm and as expected EDS and XRD graphs showed no other peak than titanium while FTIR graph confirmed that Ti contains no functional group. As the surface of as received Ti is abraded to Ti-S, Ti-S-A and Ti-S-A-P surface roughness (R_a) increased up to 953 nm. Surface roughness is known to be directly related to enhancement of mechanical interlock between surface and the coating. Structural analysis results of Ti-S revealed the presence of sand particles, meanwhile structural analysis results of Ti-S-A showed the presence of $TiSO_4$ and TiH_2 crystals on the surface. The preheating step was applied for surface stabilization (Ti-S-A-P) by oxidizing step. Ti-S-A-P had the maximum roughness and stabilized surface which makes it optimum substrate for coating process.

The SEM studies indicated that in all types of coatings, HAp nucleation started in 4th days of immersion and increased with the incubation time, yet the shape of the precipitated HAp particles differ (globular or nano flake) according to co-dopants ionic concentration. EDS results revealed that Ca/P molar ratio of pure and co-doped coatings increased by the increased immersion time up to 14 days. FTIR and XRD analysis results showed that pure coatings exhibited characteristic HAp peaks, while co-doped coatings exhibited characteristic HAp peaks plus extra carbonate peak aroused from carbonate doping, however bismuth doping had no peak observed as the deposition was performed at ppm level.

Rietveld method was also employed to XRD data to find out the change in lattice parameters. According to this method, pure coatings had the lattice parameters consistent with literature, R_{wp} value was relevant in all coating types and co-deposition of ions effected the lattice parameters and volume. 0.1 mM co-doped coating had smaller lattice parameters and unit cell volume, while 0.5 mM co-doped coating had larger lattice parameters and unit cell volume compare to pure coating. Besides 0.3 mM co-doped coating had smaller 'a', larger 'c' parameter that leads to enlargement/shrinkage of unit cell volume compare to pure coating. ICP results were consistent with other structural analysis results. According to ICP results, all co-doped coatings contained bismuth ion, furthermore the Ca/Bi ratio decreased with the increment of soaking time. XPS analysis assisted to develop chemical formation for coatings and supported that Ca^{2+} substituted with Bi^{3+}, meanwhile CO_2^{3-} substituted with OH^- in the A sites (A-type substitution) and PO_4^{3-} in the B sites (B-type substitution).

The pretreatment routine and dopants had great effect on mechanical properties of coatings in this study. Coating thicknesses were found to be similar to literature work and maximum thickness (95.3 μm) was obtained from 0.1 mM co-doped coating. Prepared coatings were exposed to scratch test to evaluate their critical load values, in all cases critical loads were above 100 mN. Co-doped coatings specially 0.3 mM co-doped coatings had higher critical loads compare to pure coatings. Highest critical load obtained was 410 mN from 0.3-C21.

The proliferation of fibroblast (L929) and cancerous bone cells (SaOS-2) on pure and co-doped HAp coatings were evaluated by cell viability tests. In the study of L929 fibroblast cell line, higher concentration of bismuth ion resulted in increasing cytotoxicity, though low concentrations (0.1 mM) barely enhanced cell viability.

In the study of SaOS-2, for all evaluation periods 0.1-C7 and 0.3-C7 exhibited highest reduction percentage among all co-doped samples furthermore 0.3 mM co-doped coatings had the best initial attachment, lower dissolution rate and more stability compare to other co-doped coatings. The higher stability and coherence of 0.3 mM co-doped coatings were also confirmed by mechanical test results (highest critical loads). It should also be noted that increasing the amount of bismuth up to 0.5 mM result in cell proliferation inhibition as the dissolution of bismuth increase toxicity is increased and cell proliferation were suppressed. The adherences of SaOS-2 cells onto the coatings were investigated by the SEM analysis. SEM images indicated that cells were attached firmly to the surface of coatings in all cases. The globular HAp surface was covered thoroughly by cytoskeleton protrusions of the cells.

The antibacterial property of pure and co-doped coatings was studying by using *S.epidermidis* bacteria. Results revealed that fewer bacteria adhered to co-doped coatings compare to pure coatings. Antibacterial test results showed the most antibacterial samples were 0.1-C7 and 0.3-C7 and it was found that antibacterial test and cell culture results were consistent.

REFERENCES

Adams, L.A., Essien, E.R., Shaibu, R.O., and Oki, A. 'Sol-Gel Synthesis of SiO_2-CaO-Na_2O-P_2O_5 Bioactive Glass Ceramic From Sodium Metasilicate', *New Journal of Glass and Ceramics*, 3 (2013), 11-15.

Aminian, A., Hashjin, M.S., Samadikuchaksaraei, A., Bakhshi, F., Gorjipour, F., Farzadi, A., Moztarzadeh, F., and Schmücker., M. 'Synthesis of Silicon-Substituted Hydroxyapatite by a Hydrothermal Method With Two Different Phosphorous Sources', *Ceramics International,* 37 (2011), 1219-1229.

Andersson, A.S., Brink, J., Lidberg, U., and Sutherland, D.S. 'Influence of Systematically Varied Nanoscale Topography on the Morphology of Epithelial Cells', *IEEE Transactions on Nanobioscience*, 2 (2003), 49-57.

Anselme, K., and Bigerelle, M. 'Statistical Demonstration of the Relative Effect of Surface Chemistry and Roughness on Human Osteoblast Short-Term Adhesion', *Journal of Materials Science: Materials in Medicine*, 17 (2006), 471-479.

Anselme, K., and Bigerelle, M. 'Topography Effects of Pure Titanium Substrates on Human Osteoblast Long-Term Adhesion', *Acta Biomaterialia*, 1 (2005), 211-222.

Avci, M., Yilmaz, B., Tezcaner, A., and Evis, Z. 'Strontium Doped Hydroxyapatite Biomimetic Coatings on Ti6Al4V Plates', *Ceramics International,* 43 (2017), 9431-9436.

Baek, S.M., Polyakov, A.V., Moon, J.H., Semenova, I.P., Valiev, R.Z., and Kim, H.S. 'Effect of Surface Etching on the Tensile Behavior of Coarse- and Ultrafine-Grained Pure Titanium', *Materials Science and Engineering: A,* 707 (2017), 337-343.

Ban, S., Iwaya, Y., Kono, H., and Sato, H. 'Surface Modification of Titanium by Etching in Concentrated Sulfuric Acid', *Dental Materials*, 22 (2006), 1115-1120.

Ban, S., and Maruno, S. 'Deposition of Calcium Phosphate on Titanium by Electrochemical Process in Simulated Body Fluid', *Japanese Journal of Applied Physics*, 32 (1993), 1577-1580.

Bang, L.T., Ramesh, S., Purbolaksono, J., Ching, Y.C., Long, B.D., Chandran, H., Ramesh, S., and Othman, R. 'Effects of Silicate and Carbonate Substitution on the Properties of Hydroxyapatite Prepared by Aqueous Co-Precipitation Method', *Materials & Design*, 87 (2015), 788-796.

Barrere, F., Blitterswijk, C.A.V., Groot, K.D., and Layrolle, P. 'Influence of Ionic Strength and Carbonate on the Ca-P Coating Formation From SBF×5 Solution', *Biomaterials*, 23 (2002), 1921-1930.

Barrère, F., Valk, C.M.V.D., Dalmeijer, R.A.J., Meijer, G., Blitterswijk, C.A.V., Groot, K.D., and Layrolle, P. 'Osteogenecity of Octacalcium Phosphate Coatings Applied on Porous Metal Implants', *Journal of Biomedical Materials Research*, 66A (2003), 779-788.

Bauer, S., Schmuki, P., Mark, K.V.D., and Park, J. 'Engineering Biocompatible Implant Surfaces: Part I: Materials and Surfaces', *Progress in Materials Science*, 58 (2013), 261-326.

Biesiekierski, A., Wang, J., Gepreel, M.A.H., and Wen, C. 'A New Look at Biomedical Ti-Based Shape Memory Alloys', *Acta Biomaterialia*, 8 (2012), 1661-1669.

Bigi, A., Boanini, E., Bracci, B., Facchini, A., Panzavolta, S., Segatti, F., and Sturba, L. 'Nanocrystalline Hydroxyapatite Coatings on Titanium: A New Fast Biomimetic Method', *Biomaterials*, 26 (2005), 4085-4089.

Boanini, E., Gazzano, M., and Bigi, A. 'Ionic Substitutions In Calcium Phosphates Synthesized At Low Temperature', *Acta Biomaterialia*, 6 (2010), 1882-1894.

Boretos, J.W. 'Advances in Bioceramics', *Advances Ceramic Materials*, 2 (1987), 15-18.

Borsari, V., Giavaresi, G., Fini, M., Torricelli, P., Tschon, M., Chiesa, R., Chiusoli, L., Salito, A., Volpert, A., and Giardino, R. 'Comparative In Vitro Study on a Ultra-High Roughness and Dense Titanium Coating', *Biomaterials,* 26 (2005), 4948-4955.

Boucetta, C., Kacimi, M., Ensuque, A., Piquemal, J.Y., Verduraz, F.B., and Ziyad, M. 'Oxidative Dehydrogenation of Propane Over Chromium-Loaded Calcium-Hydroxyapatite', *Applied Catalysis A: General,* 356 (2009), 201-210.

Bouhaouss, A., Bensaoud, A., Laghzizil, A., and Ferhat, M. 'Effect of Chemical Treatments on the Ionic Conductivity of Carbonate Apatite', *International Journal of Inorganic Materials*, 3 (2001), 437-441.

Brunski, J.B., Puleo, D.A., and Nanci, A. 'Biomaterials and Biomechanics of Oral and Maxillofacial Implants: Current Status and Future Developments', *The International Journal of Oral & Maxillofacial Implants*, 15 (2000), 15-46.

Burnell, J.M., Teubner, E.J., and Miller, A.G. 'Normal Maturational Changes in Bone Matrix, Mineral, and Crystal Size in the Rat', *Calcified Tissue International*, 31 (1980), 13-19.

Cai, Z., Koike, M., Sato, H., Brezner, M., Guo, Q., Komatsu, M., Okuno, O., and Okabe, T. 'Electrochemical Characterization of Cast Ti-Hf Binary Alloys', *Acta Biomaterialia*, 1 (2005), 353-356.

Cassinelli, C., Morra, M., Bruzzone, G., Carpi, A., Santi, G.D., Giardino, R., and Fini, M. 'Surface Chemistry Effects of Topographic Modification of Titanium Dental Implant Surfaces: 2. In Vitro Experiments', *The International Journal of Oral & Maxillofacial Implants*, 18 (2003), 46-52.

Chemistry Libretexts, Infrared Spectroscopy Absorption Table, (2014). <http://chem.libretexts.org/Reference/Reference_Tables/Spectroscopic_Parameters/Infrared_Spectroscopy_Absorption_Table>

Chen, F., Changsheng, L., and Mao, Y. 'Bismuth-Doped Injectable Calcium Phosphate Cement With Improved Radiopacity and Potent Antimicrobial Activity for Root Canal Filling', *Acta Biomaterialia*, 6 (2010), 3199-3207.

Chen, W., Liu, Y., Courtney, H.S., Bettenga, M., Agrawal, C.M. , Bumgardner, J.D. , and Ong, J.L. 'In Vitro Anti-Bacterial and Biological Properties of Magnetron Co-Sputtered Silver-Containing Hydroxyapatite Coating', *Biomaterials*, 27 (2006), 5512-5517.

Cheng, K., Zhang, S., and Weng, W. 'Sol-Gel Prepared β-TCP/FHA Biphasic Coatings', *Thin Solid Films*, 515 (2006), 135-140.

Cho, S.B., Nakanishi, K., Kokubo, T., Soga, N., Ohtsuki, C., Nakamura, T., Kutsigi, T., and Yamamuro, T. 'Dependence of Apatite Formation on Silica Gel on Its Structure: Effect of Heat Treatment', *Journal of the American Ceramic Society*, 78 (1995), 1769-1774.

Cochis, A., Azzimonti, B., Valle, C.D., Giglio, E.D., Bloise, N., Visai, L., Cometa, S., Rimondini, L., and Chiesa, R. 'The Effect of Silver or Gallium Doped Titanium Against the Multidrug Resistant *Acinetobacter Baumannii*', *Biomaterials*, 80 (2016), 80-95.

Dalby, M.J., McCloy, D., Robertson, M., Wilkinson, C.D.W., and Oreffo, R.O.C. 'Osteoprogenitor Response to Defined Topographies with Nanoscale Depths', *Biomaterials*, 27 (2006), 1306-1315.

Das, K., Bose, S., and Bandyopadhyay, A. 'Surface Modifications and Cell-Materials Interactions with Anodized Ti', *Acta Biomaterialia*, 3 (2007), 573-585.

Davis, J.R. 'Handbook of Materials for Medical Devices', *ASM International*, 2003, 205-215.

DeMaio, M., McHale, K., Lenhart, M., Garland, J., McIlvaine, C., and Rhode, M. 'Plaster: Our Orthopaedic Heritage AAOS Exhibit Selection', *The Journal of Bone and Joint Surgery*, 94 (2012), 152-158.

Desoize, B. 'Metals and Metal Compounds in Cancer Treatment', *Anticancer Research*, 24 (2004), 1529-1544.

Dobzyniak, M., Fehring, T.K., and Odum, S. 'Early Failure in Total Hip Arthroplasty', *Clinical Orthopaedics and Related Research*, 447 (2006), 76-78.

Doitpoms, 'University of Cambridge DoITPoMS - TLP Library - Structure of Bone and Implant Materials', *University of Cambridge*, 2011.

Duan, K., and Wang, R. 'Surface Modifications of Bone Implants Through Wet Chemistry', *Journal of Materials Chemistry*, 16 (2006), 2309-2311.

Ducheyne, P., and Qiu, Q. 'Bioactive Ceramics: The Effect of Surface Reactivity on Bone Formation and Bone Cell Function', *Biomaterials*, 20 (1999), 2287-2303.

Eisenbarth, E., Velten, D., Müller, M., Thull, R., and Breme, J. 'Biocompatibility of β-Stabilizing Elements of Titanium Alloys', *Biomaterials*, 25 (2004), 5705-5713.

Elliott, J.C., Holcomb, D.W., and Young, R.A. 'Infrared Determination of the Degree of Substitution of Hydroxyl by Carbonate Ions in Human Dental Enamel', *Calcified Tissue International*, 37 (1985), 372-375.

Ergun, C., Webster, T.J., Bizios, R., and Doremus, R.H. 'Hydroxylapatite With Substituted Magnesium, Zinc, Cadmium, and Yttrium. I. Structure and Microstructure', *Journal of Biomedical Materials Research*, 59 (2002), 305-311.

Farley, J.R., Wergedal, J.E., and Baylink, D.J. 'Fluoride Directly Stimulates Proliferation and Alkaline Phosphatase Activity of Bone-Forming Cells', *Science*, 222 (1983), 330-332.

Fathi, M.H., and Zahrani, E.M. 'Mechanical Alloying Synthesis and Bioactivity Evaluation of Nanocrystalline Fluoridated Hydroxyapatite', *Journal of Crystal Growth*, 311 (2009), 1392-1403.

Feng, B., Weng, J., Yang, B.C., Chen, J.Y., Zhao, J.Z., He, L., Qi, S.K., and Zhang, X.D. 'Surface Characterization of Titanium and Adsorption of Bovine Serum Albumin', *Materials Characterization*, 49 (2002), 129-137.

Feng, B., Weng, J., Yang, B.C., Qu, S.X., and Zhang, X.D. 'Characterization of Surface Oxide Films on Titanium and Adhesion of Osteoblast', *Biomaterials*, 24 (2003), 4663-4670.

Feng, C.F., Khor, K.A., Liu, E.J., and Cheang, P. 'Phase Transformations in Plasma Sprayed Hydroxyapatite Coatings', *Scripta Materialia*, 42 (2000), 103-109.

Filgueiras, M.R., Torre, G.L., and Hench, L.L. 'Solution Effects on the Surface Reactions of a Bioactive Glass', *Journal of Biomedical Materials Research*, 27 (1993), 445-453.

Fleet, M.E., and Liu, X. 'Hydrogen-Carbonate Ion in Synthetic High-Pressure Apatite', *American Mineralogist*, 92 (2007), 1764-1767.

Fleet, M.E., and Liu, X. 'Carbonate Apatite Type A Synthesized at High Pressure: New Space Group (P3̄) and Orientation of Channel Carbonate Ion', *Journal of Solid State Chemistry*, 174 (2003), 412-417.

Forsgren, J., Svahn, F., Jarmar, T., and Engqvist, H. 'Formation and Adhesion of Biomimetic Hydroxyapatite Deposited on Titanium Substrates', *Acta Biomaterialia*, 3 (2007), 980-984.

Frauchiger, V.M., Schlottig, F., Gasser, B., and Textor, M. 'Anodic Plasma-Chemical Treatment of CP Titanium Surfaces for Biomedical Applications', *Biomaterials*, 25 (2004), 593-606.

Fu, Y., and Chen, D. 'Influence of Sr^{2+} on Strontium Substituted Hydroxyapatite's (Sr-HA) Cytotoxicity', *Journal of Oral Tissue Engineering*, 2 (2005), 76-80.

Fujii, E., Ohkubo, M., Tsuru, K., Hayakawa, S., Osaka, A., Kawabata, K., Bonhomme, C., and Babonneau, F. 'Selective Protein Adsorption Property and Characterization of Nano-Crystalline Zinc-Containing Hydroxyapatite', *Acta Biomaterialia*, 2 (2006), 69-74.

Gamble, J. 'Chemical Anatomy, Physiology and Pathology of Exfracellular Fluid', *Harvard University Press*, 6 (1967), 1-17.

Geesink, R.G., Groot, K.D., and Klein, C.P. 'Chemical Implant Fixation Using Hydroxyl-Apatite Coatings. The Development of a Human Total Hip Prosthesis for Chemical Fixation to Bone Using Hydroxyl-Apatite Coating on Titanium Substrates', *Clinical Orthopaedics and Related Research*, 225 (1987), 147-170.

Geetha, M., Singh, A.K., Asokamani, R., and Gogia, A.K. 'Ti Based Biomaterials, the Ultimate Choice for Orthopaedic Implants - A Review', *Progress in Materials Science*, 54 (2009), 397-425.

Gepreel, M.A.H., and Niinomi, M. 'Biocompatibility of Ti-Alloys for Long-Term Implantation', *Journal of the Mechanical Behavior of Biomedical Materials*, 20 (2013), 407-415.

Ginty, F., Flynn, A., and Cashman, K.D. 'The Effect of Dietary Sodium Intake on Biochemical Markers of Bone Metabolism in Young Women', *British Journal of Nutrition*, 79 (1998), 343-350.

Giordano, C., Sandrini, E., Busini, V., Chiesa, R., Fumagalli, G., Giavaresi, G., Fini, M., Giardino, R., and Cigada, A. 'A New Chemical Etching Process to Improve Endosseous Implant Osseointegration: In Vitro Evaluation on Human Osteoblast-like Cell', *The International Journal of Artificial Organs*, 29 (2006), 772-780.

Givan, A., Grothe, H., Loewenschuss, A., and Nielsen, C. J. 'Infrared Spectra and ab Initio Calculations of Matrix Isolated Dimethyl Sulfone and Its Water Complex', *Physical Chemistry Chemical Physics*, 4 (2002), 255-263.

Guizzardi, S., Galli, C., Martini, D., Belletti, S., Tinti, A., Raspanti, M., Taddei, P., Ruggeri, A., and Scandroglio, R. 'Different Titanium Surface Treatment Influences Human Mandibular Osteoblast Response', *Journal of Periodontology*, 75 (2004), 273-282.

Hall, J.E. '*Guyton and Hall Textbook of Medical Physiology*', *WB Saunders Company*, (2011), 150-170.

Hamadanian, M., Vanani, A.R., and Majedi, A. 'Sol-Gel Preparation and Characterization of Co/TiO$_2$ Nanoparticles: Application to the Degradation of Methyl Orange', *Journal of the Iranian Chemical Society*, 7 (2010), 52-58.

Han, Y., Hong, S.H., and Xu, K. 'Structure and In Vitro Bioactivity of Titania-Based Films by Micro-Arc Oxidation', *Surface and Coatings Technology*, 168 (2003), 249-258.

Hazmi, F.E.A. 'Synthesis and Electrical Properties of Bi Doped Hydroxyapatite Ceramics', *Journal of Alloys and Compounds*, 665 (2016), 119-123.

He, Z., Ma, J., and Wang, C. 'Constitutive Modeling of the Densification and the Grain Growth of Hydroxyapatite Ceramics', *Biomaterials*, 26 (2005), 1613-1621.

Heintz, C., Riepe, G., Birken, L., Kaiser, E., Chakfé, N., Morlock, M., Delling, G., and Imig, H. 'Corroded Nitinol Wires in Explanted Aortic Endografts: An Important Mechanism of Failure?', *Journal of Endovascular Therapy*, 8 (2001), 248-253.

Hench, L.L., Splinter, R.J., Allen, W.C., and Greenlee, T.K. 'Bonding Mechanisms at the Interface of Ceramic Prosthetic Materials', *Journal of Biomedical Materials Research*, 5 (1971), 117-141.

Hench, L.L. 'Bioceramics: From Concept to Clinic', *Journal of the American Ceramic Society*, 74 (1991), 1487-1510.

Henriques, B., Sampaio, M., Buciumeanu, M., Souza, J.C.M., Gomes, J.R., Silva, F., Carvalho, O. 'Laser Surface Structuring of Ti6Al4V Substrates for Adhesion Enhancement in Ti6Al4V-PEEK Joints', *Materials Science and Engineering: C,* 79 (2017), 177-184.

Ho, W.F., Ju, C.P., and Lin, J.H.C. 'Structure and Properties of Cast Binary Ti-Mo Alloys', *Biomaterials*, 20 (1999), 2115-2122.

Ho, W.F., Cheng, C.H., Chen, W.K., Wu, S.C., Lin, H.C., and Hsu, H.C. 'Evaluation of Low-Fusing Porcelain Bonded to Dental Cast Ti-Zr Alloys', *Journal of Alloys and Compounds*, 471 (2009), 185-189.

Hsu, H.C., Wu, S.C., Hong, Y.S., and Ho, W.F. 'Mechanical Properties and Deformation Behavior of As-Cast Ti-Sn Alloys', *Journal of Alloys and Compounds*, 479 (2009), 390-394.

Hu, W., Ma, J., Wang, J., and Zhang, S. 'Fine Structure Study on Low Concentration Zinc Substituted Hydroxyapatite Nanoparticles', *Materials Science and Engineering: C,* 32 (2012), 2404-2410.

Ignjatovic, N., Ajdukovic, Z., Rajkovic, J., Najman, S., Mihailovic, D., and Uskokovic, D. 'Enhanced Osteogenesis of Nanosized Cobalt-Substituted Hydroxyapatite', *Journal of Bionic Engineering,* 12 (2015), 604-612.

Ismail, F.S.M., Rohanizadeh, R., Atwa, S., Mason, R.S., Ruys, A.J., Martin, P.J., and Bendavid, A. 'The Influence of Surface Chemistry and Topography on the Contact Guidance of MG63 Osteoblast Cells', *Journal of Materials Science: Materials in Medicine*, 18 (2007), 705-714.

Jonášová, L., Müller, F.A., Helebrant, A., Strnad, J., and Greil, P. 'Biomimetic Apatite Formation on Chemically Treated Titanium', *Biomaterials*, 25 (2004), 1187-1194.

Kaplan, F.S., Hayes, W.C., Keaveny, T.M., Boskey, A., Einhorn, T.A., and Iannotti, J.P. 'Form and Function of Bone', *Orthopaedic Basic Science*, (1994), 127-185.

Kataoka, T., Shiba, K., and Tagaya, M. 'Preparation of Europium(III)-Doped Hydroxyapatite Nanocrystals in the Presence of Cationic Surfactant', *Colloid and Interface Science Communications,* 13 (2016), 1-5.

Kawagoe, K., Saito, M., Shibuya, T., Nakashima, T., Hino, K., and Yoshikawa, H. 'Augmentation of Cancellous Screw Fixation With Hydroxyapatite Composite Resin (CAP) In Vivo', *Journal of Biomedical Materials Research*, 53 (2000), 678-684.

Kawai, T., Ohtsuki, C., Kamitakahara, M., Miyazaki, T., Tanihara, M., Sakaguchi, Y., and Konagaya, S. 'Coating of an Apatite Layer on Polyamide Films Containing Sulfonic Groups by a Biomimetic Process', *Biomaterials*, 25 (2004), 4529-4534.

Kim, H.M., Miyaji, F., Kokubo, T., and Nakamura, T. 'Preparation of Bioactive Ti and Its Alloys via Simple Chemical Surface Treatment', *Journal of Biomedical Materials Research*, 32 (1996), 409-417.

Kim, H.M. 'Ceramic Bioactivity and Related Biomimetic Strategy', *Current Opinion in Solid State and Materials Science*, 7 (2003), 289-299.

Kim, H.M., Himeno, T., Kokubo, T., and Nakamura, T. 'Process and Kinetics of Bonelike Apatite Formation on Sintered Hydroxyapatite in a Simulated Body Fluid', *Biomaterials*, 26 (2005), 4366-4373.

Kim, H.W., Kong, Y.M., Koh, Y.H., Kim, H.E., Kim, H.M., and Ko, J.S. 'Pressureless Sintering and Mechanical and Biological Properties of Fluor-Hydroxyapatite Composites With Zirconia', *Journal of the American Ceramic Society*, 86 (2003), 2019-2026.

Kim, T.N., Feng, Q.L., Kim, J.O., Wu, J., Wang, H., Chen, G.C., and Cui, F.Z. 'Antimicrobial Effects of Metal Ions (Ag^+, Cu^{2+}, Zn^{2+}) in Hydroxyapatite', *Journal of Materials Science: Materials in Medicine*, 9 (1998), 129-134.

Kitsugi, T., Nakamura, T., Yamamura, T., Kokubu, T., Shibuya, T., and Takagi, M. 'SEM-EPMA Observation of Three Types of Apatite-Containing Glass-Ceramics Implanted in Bone: The Variance of a Ca-P-Rich Layer', *Journal of Biomedical Materials Research*, 21 (1987), 1255-1271.

Kokubo, T., Ito, S., Huang, Z.T., Hayashi, T., Sakka, S., Kitsugi, T., and Yamamuro, T. 'Ca, P-Rich Layer Formed on High-Strength Bioactive Glass-Ceramic A-W', *Journal of Biomedical Materials Research*, 24 (1990), 331-343.

Kokubo, T., Kushitani, H., Sakka, S., Kitsugi, T., and Yamamuro, T. 'Solutions Able to Reproduce in Vivo Surface-Structure Changes in Bioactive Glass-Ceramic A-W[3]', *Journal of Biomedical Materials Research*, 24 (1990), 721-734.

Kokubo, T., Kim, H.M., and Kawashita, M. 'Novel Bioactive Materials with Different Mechanical Properties', *Biomaterials*, 24 (2003), 2161-2175.

Kokubo, T., Ohtsuki, C., Kotani, S., Kitsugi, T., and Yamamuro, T. 'Surface Structure of Bioactive Glass-Ceramic A-W Implanted into Sheep and Human Vertebra', *Bioceramics.*, 2 (1990), 113-120.

Kokubo, T., and Takadama, H. 'How Useful is SBF in Predicting In Vivo Bone Bioactivity?', *Biomaterials*, 27 (2006), 2907-2915.

Krupa, D., Baszkiewicz, J., Kozubowski, J.A., Barcz, A., Sobczak, J.W., Biliński, A., Szumieł, M.D.L., and Rajchel, B. 'Effect of Calcium-Ion Implantation on the Corrosion Resistance and Biocompatibility of Titanium', *Biomaterials*, 22 (2001), 2139-2151.

Kwaśniak, P., Pura, J., Zwolińska, M., Wieciński, P., Skarżyński, H., Olszewski, L., Marczak, J., Garbacz, H., and Kurzydłowski, K.J. 'Laser and Chemical Surface Modifications of Titanium Grade 2 for Medical Application', *Applied Surface Science*, 336 (2015), 267-273.

Lakshminarasimhan, N., and Varadaraju, U.V. 'Synthesis and Eu^{3+} Luminescence in New Oxysilicates, $ALa_3Bi(SiO_4)_3O$ and $ALa_2Bi_2(SiO_4)_3O$ [A=Ca, Sr and Ba] with Apatite-Related Structure', *Journal of Solid State Chemistry*, 178 (2005), 3284-3292.

Landsberg, J.P., McDonald, B., and Watt, F. 'Absence of Aluminium in Neuritic Plaque Cores in Alzheimer's Disease', *Nature*, 360 (1992), 65-68.

Lee, C.M., Ju, C.P., and Lin, J.H.C. 'Structure-Property Relationship of Cast Ti-Nb Alloys', *Journal of Oral Rehabilitation*, 29 (2002), 314-322.

Lee, S.M. 'International Encyclopedia of Composites', *VCH Publishers*, 5 (1991), 100-150.

Leeuwenburgh, S.C.G., Wolke, J.G.C., Schoonman, J., and Jansen, J.A. 'Influence of Deposition Parameters on Morphological Properties of Biomedical Calcium Phosphate Coatings Prepared Using Electrostatic Spray Deposition', *Thin Solid Films*, 472 (2005), 105-113.

Li, B., Li, J., Liang, C., Li, H., Guo, L., Liu, S., and Wang, H. 'Surface Roughness and Hydrophilicity of Titanium After Anodic Oxidation', *Rare Metal Materials and Engineering*, 45 (2016), 858-862.

Li, F., Feng, Q.L., Cui, F.Z, Li, H.D., and Schubert, H. 'A Simple Biomimetic Method for Calcium Phosphate Coating', *Surface and Coatings Technology*, 154 (2002), 88-93.

Li, H., and Sun, H. 'Recent Advances in Bioinorganic Chemistry of Bismuth', *Current Opinion in Chemical Biology*, 16 (2012), 74-83.

Li, Q., Feng, X., Zhang, X., Song, H., Zhang, J., Shang, J., Sun, W., Zhu, T., Wakamura, M., Tsukada, M., and Lu, Y. 'Photocatalytic Degradation of Bisphenol A Using Ti-Substituted Hydroxyapatite', *Chinese Journal of Catalysis,* 35 (2014), 90-98.

Lim, P.Y., She, P.L., and Shih, H.C. 'Microstructure Effect on Microtopography of Chemically Etched α+β Ti Alloys', *Applied Surface Science*, 253 (2006), 449-458.

Lin, W.J., Wang, B.L., Qiu, K.J., Zhou, F.Y., Li, L., Lin, J.P., Wang, Y.B., and Zheng, Y.F. 'Ti-Ge Binary Alloy System Developed as Potential Dental Materials', *Journal of Biomedical Materials Research Part B: Applied Biomaterials*, 100B (2012), 2239-2250.

Lin, Y., Yang, Z., and Cheng, J. 'Preparation, Characterization and Antibacterial Property of Cerium Substituted Hydroxyapatite Nanoparticles', *Journal of Rare Earths*, 25 (2007), 452-456.

Linder, L., and Lundskog, J. 'Incorporation of Stainless Steel, Titanium and Vitallium in Bone', *Injury*, 6 (1975), 277-285.

Lintner, F., Zweymüller, K., and Brand, G. 'Tissue Reactions to Titanium Endoprostheses: Autopsy Studies in Four Cases', *The Journal of Arthroplasty*, 1 (1986), 183-195.

Liu, Q., Ding, J., Mante, F.K., Wunder, S.L., and Baran, G.R. 'The Role of Surface Functional Groups in Calcium Phosphate Nucleation on Titanium Foil: A Self-Assembled Monolayer Technique', *Biomaterials*, 23 (2002), 3103-3111.

Liu, X., Chu, P.K., and Ding, C. 'Surface Modification of Titanium, Titanium Alloys, and Related Materials for Biomedical Applications', *Materials Science and Engineering: R: Reports*, 47 (2004), 49-121.

Liu, Y., Layrolle, P., Bruijn, J.D., Blitterswijk, C.V., and Groot, K.D. 'Biomimetic Coprecipitation of Calcium Phosphate and Bovine Serum Albumin on Titanium Alloy', *Journal of Biomedical Materials Research*, 57 (2001), 327-335.

Long, M., and Rack, H.J. 'Titanium Alloys in Total Joint Replacement - A Materials Science Perspective', *Biomaterials*, 19 (1998), 1621-1639.

Losina, E., Barrett, J., Mahomed, N.N., Baron, J.A., and Katz, J.N. 'Early Failures of Total Hip Replacement: Effect of Surgeon Volume', *Arthritis & Rheumatolgy*, 50 (2004), 1338-1343.

Lugovskoy, S., Weiss, D., Tsadok, U., and Lugovskoy, A. 'Morphology and Antimicrobial Properties of Hydroxyapatite-Titanium Oxide Layers on the Surface of Ti-6Al-4V Alloy', *Surface and Coatings Technology*, 301 (2016), 80-84.

Lüthen, F., Lange, R., Becker, P., Rychly, J., Beck, U., and Nebe, J.G.B. 'The Influence of Surface Roughness of Titanium on β1- and β3-Integrin Adhesion and the Organization of Fibronectin in Human Osteoblastic Cells', *Biomaterials*, 26 (2005), 2423-2440.

Maier, P.K., and Klapötke, T. 'Antitumor Activity of Some Organomettalic Bismuth (III) Thiolates', *Inorganica Chimica Acta*, 152 (1988), 49-52.

Mareci, D., Chelariu, R., Gordin, D.M., Ungureanu, G., and Gloriant, T. 'Comparative Corrosion Study of Ti-Ta Alloys for Dental Applications', *Acta Biomaterialia*, 5 (2009), 3625-3639.

Mathijsen, A. 'New Method for Application of Plaster of Paris Bandage 1852', *Clinical Orthopaedics and Related Research*, 458 (2007), 59-62.

Matsumoto, N., Sato, K., Yoshida, K., Hashimoto, K., and Toda, Y. 'Preparation and Characterization of β-Tricalcium Phosphate Co-Doped With Monovalent and Divalent Antibacterial Metal Ions', *Acta Biomaterialia*, 5 (2009), 3157-3164.

Mayer, I., Cuisinier, F.J.G., Gdalya, S., and Popov, I. 'TEM Study of the Morphology of Mn^{2+}-Doped Calcium Hydroxyapatite and β-Tricalcium Phosphate', *Journal of Inorganic Biochemistry,* 102 (2008), 311-317.

Mohammad, N.F., Othman, R., and Yeoh, F.Y. 'Controlling the Pore Characteristics of Mesoporous Apatite Materials: Hydroxyapatite and Carbonate Apatite', *Ceramics International*, 41 (2015), 10624-10633.

Müller, L., Conforto, E., Caillard, D., and Müller, F.A. 'Biomimetic Apatite Coatings-Carbonate Substitution and Preferred Growth Orientation', *Biomolecular Engineering*, 24 (2007), 462-466.

Müller, L., and Müller, F.A. 'Preparation of SBF with Different HCO_3^- Content and Its Influence on the Composition of Biomimetic Apatites', *Acta Biomaterialia*, 2 (2006), 181-189.

Nakagawa, M., Matono, Y., Matsuya, S., Udoh, K., and Ishikawa, K. 'The Effect of Pt and Pd Alloying Additions on the Corrosion Behavior of Titanium in Fluoride-Containing Environments', *Biomaterials*, 26 (2005), 2239-2246.

Nayab, S.N., Jones, F.H., and Olsen, I. 'Human Alveolar Bone Cell Adhesion and Growth on Ion-Implanted Titanium', *Journal of Biomedical Materials Research*, 69A (2004), 651-657.

Nayab, S.N., Jones, F.H., and Olsen, I. 'Effects of Calcium Ion Implantation on Human Bone Cell Interaction with Titanium', *Biomaterials*, 26 (2005), 4717-4727.

Neuman, W.F., and Neuman, M.W. 'The Chemical Dynamics of Bone Mineral', *The University of Chicago Press*, (1958), 200-205.

Nikčević, I., Jokanović, V., Mitrić, M., Nedić, Z., Makovec, D., and Uskoković, D. 'Mechanochemical Synthesis of Nanostructured Fluorapatite / fluorhydroxyapatite and Carbonated Fluorapatite / Fluorhydroxyapatite', *Journal of Solid State Chemistry*, 177 (2004), 2565-2574.

Ogino, M., Ohuchi, F., and Hench, L.L. 'Compositional Dependence of the Formation of Calcium Phosphate Films on Bioglass', *Journal of Biomedical Materials Research*, 14 (1980), 55-64.

Oh, H.J., Lee, J.H., Jeong, Y., Kim, Y.J., and Chi, C.S. 'Microstructural Characterization of Biomedical Titanium Oxide Film Fabricated by Electrochemical Method', *Surface and Coatings Technology*, 198 (2005), 247-252.

Ohkubo, C., Shimura, I., Aoki, T., Hanatani, S., Hosoi, T., Hattori, M., Oda, Y., and Okabe, T. 'Wear Resistance of Experimental Ti-Cu Alloys', *Biomaterials*, 24 (2003), 3377-3381.

Ohtsu, N., Kakuchi, Y., and Ohtsuki, T. 'Antibacterial Effect of Zinc Oxide / Hydroxyapatite Coatings Prepared by Chemical Solution Deposition', *Applied Surface Science*, In Press (2017).

Ohtsuki, C., Kushitani, H., Kokubo, T., Kotani, S., and Yamamuro, T. 'Apatite Formation on the Surface of Ceravital-Type Glass-Ceramic in the Body', *Journal of Biomedical Materials Research*, 25 (1991), 1363-1370.

Okazaki, Y., Rao, S., Ito, Y., and Tateishi, T. 'Corrosion Resistance, Mechanical Properties, Corrosion Fatigue Strength and Cytocompatibility of New Ti Alloys Without Al and V', *Biomaterials*, 19 (1998), 1197-1215.

Oliveira, A.L., Mano, J.F., and Reis, R.L. 'Nature-Inspired Calcium Phosphate Coatings: Present Status and Novel Advances in the Science of Mimicry', *Current Opinion in Solid State and Materials Science*, 7 (2003), 309-318.

Onder, S., Kok, F.N., Kazmanli, K., and Urgen, M. 'Magnesium Substituted Hydroxyapatite Formation on (Ti,Mg)N Coatings Produced by Cathodic Arc PVD Technique', *Materials Science and Engineering: C,* 33 (2013), 4337-4342.

Oyane, A., Kim, H.M., Furuya, T., Kokubo, T., Miyazaki, T., and Nakamura, T. 'Preparation and Assessment of Revised Simulated Body Fluids', *Journal of Biomedical Materials Research*, 65A (2003), 188-195.

Ödman, J., Lekholm, U., Jemt, T., Brånemark, P.I., and Thilander, B. 'Osseointegrated Titanium Implants - A New Approach in Orthodontic Treatment', *The European Journal of Orthodontics*, 10 (1988), 98-105.

Park, J.B. 'Biomaterials Science and Engineering', *Plenum Press,* 1 (1984), 11-38.

Park, J., and Lakes, R.S. 'Biomaterials: An Introduction', *Springer*, 3 (2007), 41-81.

Pazarçeviren, A.E., Tahmasebifar, A., Tezcaner, A., Keskin, D., and Evis, Z. 'Investigation of Bismuth Doped Bioglass/Graphene Oxide Nanocomposites for Bone Tissue Engineering', *Ceramics International*, 44 (2018), 3791-3799.

Perl, D.P., and Brody, A.R. 'Alzheimer's Disease: X-Ray Spectrometric Evidence of Aluminum Accumulation in Neurofibrillary Tangle-Bearing Neurons', *Science*, 208 (1980), 297-299.

Peroos, S., Du, Z., and Leeuw, N.H.D. 'A Computer Modelling Study of the Uptake, Structure and Distribution of Carbonate Defects in Hydroxy-Apatite', *Biomaterials*, 27 (2006), 2150-2161.

Porter, A.E., Taak, P., Hobbs, L.W., Coathup, M.J., Blunn, G.W., and Spector, M. 'Bone Bonding to Hydroxyapatite and Titanium Surfaces on Femoral Stems Retrieved from Human Subjects at Autopsy', *Biomaterials*, 25 (2004), 5199-5208.

Pylypchuk, I.V., Gorbyk, P.P., Petranovska, A.L., Korduban, O.M., Markovsky, P.E., and Ivasyshyn, O.M. 'Chapter 7-Formation of Biomimetic Hydroxyapatite Coatings on the Surface of Titanium and Ti-Containing Alloys: Ti-6Al-4V and Ti-Zr-Nb', *Surface Chemistry of Nanobiomaterials,* 3 (2016), 193-229.

Qiu, K.J., Lin, W.J., Zhou, F.Y., Nan, H.Q., Wang, B.L., Li, L., Lin, J.P., Zheng, Y.F., and Liu, Y.H. 'Ti-Ga Binary Alloys Developed as Potential Dental Materials', *Materials Science and Engineering: C*, 34 (2014), 474-483.

Qiu, K.J., Liu, Y., Zhou, F.Y., Wang, B.L., Li, L., Zheng, Y.F., and Liu, Y.H. 'Microstructure, Mechanical Properties, Castability and In Vitro Biocompatibility of Ti-Bi Alloys Developed for Dental Applications', *Acta Biomaterialia*, 15 (2015), 254-265.

Ramesh, S., Tan, C.Y., Yeo, W.H., Tolouei, R., Amiriyan, M., Sopyan, I., and Teng, W.D. 'Effects of Bismuth Oxide on the Sinterability of Hydroxyapatite', *Ceramics International*, 37 (2011), 599-606.

Refai, A.K., Textor, M., Brunette, D.M., and Waterfield, J.D. 'Effect of Titanium Surface Topography on Macrophage Activation and Secretion of Proinflammatory Cytokines and Chemokines', *Journal of Biomedical Materials Research*, 70A (2004), 194-205.

Rey, C., Renugopalakrishman, V., Collins, B., and Glimcher, M.J. 'Fourier Transform Infrared Spectroscopic Study of the Carbonate Ions in Bone Mineral During Aging', *Calcified Tissue International*, 49 (1991), 251-258.

Rho, J.Y., Spearing, L.K., and Zioupos, P. 'Mechanical Properties and the Hierarchical Structure of Bone', *Medical Engineering & Physics*, 20 (1998), 92-102.

Rønold, H.J., Lyngstadaas, S.P., and Ellingsen, J.E. 'Analysing the Optimal Value for Titanium Implant Roughness in Bone Attachment Using a Tensile Test', *Biomaterials*, 24 (2003), 4559-4564.

Saldaña, L., Bensiamar, F., Boré, A., and Vilaboa, N. 'In Search of Representative Models of Human Bone-Forming Cells for Cytocompatibility Studies', *Acta Biomaterialia*, 7 (2011), 4210-4221.

Samanipour, F., Bayati, M.R., Fard, F.G., Zargar, H.R., Mirhabibi, A.R., Rad, V.S., and Abbasi, S. 'Innovative Fabrication of ZrO_2-Hap-TiO_2 Nano/Micro-Structured Composites through MAO/EPD Combined Method', *Materials Letters*, 65 (2011), 926-928.

Sandrini, E., Giordano, C., Busini, V., Signorelli, E., and Cigada, A. 'Apatite Formation and Cellular Response of a Novel Bioactive Titanium', *Journal of Materials Science: Materials in Medicine*, 18 (2007), 1225-1237.

Schreckenbach, J.P., Marx, G., Schlottig, F., Textor, M., and Spencer, N.D. 'Characterization of Anodic Spark-Converted Titanium Surfaces for Biomedical Applications', *Journal of Materials Science: Materials in Medicine*, 10 (1999), 453-457.

Sebti, S., Tahir, R., Nazih, R., and Boulaajaj, S. 'Comparison of Different Lewis Acid Supported on Hydroxyapatite as New Catalysts of Friedel-Crafts Alkylation', *Applied Catalysis A: General*, 218 (2001), 25-30.

Semlitsch, M.F., Weber, H., Streicher, R.M., and Schön, R. 'Joint Replacement Components Made of Hot-Forged and Surface-Treated Ti-6Al-7Nb Alloy', *Biomaterials*, 13 (1992), 781-788.

Shanmugam, S., and Gopal, B. 'Antimicrobial and Cytotoxicity Evaluation of Aliovalent Substituted Hydroxyapatite', *Applied Surface Science*, 303 (2014), 277-281.

Shapira, L., and Halabi, A. 'Behavior of Two Osteoblast-Like Cell Lines Cultured on Machined or Rough Titanium Surfaces', *Clinical Oral Implants Research*, 20 (2009), 50-55.

Shokri, B., Firouzjah, M.A., and Hosseini, S.I. 'FTIR Analysis of Silicon Dioxide Thin Film Deposited by Metal Organic-Based PECVD', *Proceedings of 19th International Symposium on Plasma Chemistry Society*, 2631 (2009), 1-4.

Silva, C.C., Pinheiro, A.G., Miranda, M.A.R., Góes, J.C., and Sombra, A.S.B. 'Structural Properties of Hydroxyapatite Obtained by Mechanosynthesis', *Solid State Sciences*, 5 (2003), 553-558.

Sittig, C., Textor, M., Spencer, N.D.,Wieland, M., and Vallotton, P.H. 'Surface Characterization of Implant Materials c.p. Ti, Ti-6Al-7Nb and Ti-6Al-4V with Different Pretreatments', *Journal of Materials Science: Materials in Medicine*, 10 (1999), 35-46.

Song, W.H., Jun, Y.K., Han, Y., and Hong, S.H. 'Biomimetic Apatite Coatings on Micro-Arc Oxidized Titania', *Biomaterials*, 25 (2004), 3341-3349.

Song, W.H., Ryu, H.S., and Hong, S.H. 'Apatite Induction on Ca-Containing Titania Formed by Micro-Arc Oxidation', *Journal of the American Ceramic Society*, 88 (2005), 2642-2644.

Stoeckel, D., Pelton, A., and Duerig, T. 'Self - Expanding Nitinol Stents: Material and Design Considerations', *European Radiology*, 14 (2004), 292-301.

Suchanek, W., and Yoshimura, M. 'Processing and Properties of Hydroxyapatite-Based Biomaterials for Use as Hard Tissue Replacement Implants', *Journal of Materials Research*, 13 (1998), 94-117.

Sumathi, S., and Buvaneswari, G. 'Synthesis of Apatite Structure Based $BiNaCa_3(PO_4)_3OH$ and Its Application for Condensation Reaction', *Ceramics International*, 38 (2012), 3547-3552.

Šupová, M. 'Substituted Hydroxyapatites For Biomedical Applications: A Review', *Ceramics International*, 41 (2015), 9203-9231.

Suska, F., Gretzer, C., Esposito, M., Emanuelsson, L., Wennerberg, A., Tengvall, P., and Thomsen, P. 'In Vivo Cytokine Secretion and NF-κB Activation Around Titanium and Copper Implants', *Biomaterials*, 26 (2005), 519-527.

Suzuki, T., Hatsushika, T., and Hayakawa, Y. 'Synthetic Hydroxyapatites Employed as Inorganic Cation-Exchangers', *Journal of the Chemical Society, Faraday Transactions 1: Physical Chemistry in Condensed Phases,* 77 (1981), 1059-1062.

Takadama, H., Hashimoto, M., Mizuno, M., and Kokubo, T. 'Round-Robin Test of SBF for In Vitro Measurement of Apatite-Forming Ability of Synthetic Materials', *Phosphorus Research Bulletin*, 17 (2004), 119-125.

Takahashi, M., Kikuchi, M., and Okuno, O. 'Mechanical Properties and Grindability of Experimental Ti-Au Alloys', *Dental Materials Journal*, 23 (2004), 203-210.

Tas, A.C. 'Synthesis of Biomimetic Ca-Hydroxyapatite Powders at 37°C in Synthetic Body Fluids', *Biomaterials*, 21 (2000), 1429-1438.

Teker, D., Muhaffel, F., Menekse, M., Karaguler, N.G., Baydogan, M., and Cimenoglu, H. 'Characteristics of Multi-Layer Coating Formed on Commercially Pure Titanium for Biomedical Applications', *Materials Science and Engineering: C*, 48 (2015), 579-585.

Thian, E.S., Khor, K.A., Loh, N.H., and Tor, S.B. 'Processing of HA-Coated Ti-6Al-4V by a Ceramic Slurry Approach: an In Vitro Study', *Biomaterials*, 22 (2001), 1225-1232.

Thomas, M.B., Doremus, R.H., Jarcho, M., and Salsbury, R.L. 'Dense Hydroxylapatite: Fatigue and Fracture Strength After Various Treatments, From Diametral Tests', *Journal of Materials Science*, 15 (1980), 891-894.

Thompson, S.A. 'An Overview of Nickel-Titanium Alloys Used in Dentistry', *International Endodontic Journal*, 33 (2000), 297-310.

Tiekink, E.R.T. 'Antimony and Bismuth Compounds in Oncology', *Critical Reviews in Oncology/Hematology*, 42 (2002), 217-224.

Tolchard, J.R., Islam, M.S., and Slater, P.R. 'Defect Chemistry and Oxygen Ion Migration in the Apatite-Type Materials $La_{9.33}Si_6O_{26}$ and $La_8Sr_2Si_6O_{26}$', *Journal of Materials Chemistry*, 13 (2003), 1956-1961.

Tolchard, J.R., Sansom, J.E.H., Islam, M.S., and Slater, P.R. 'Structural Studies of Apatite-Type Oxide Ion Conductors Doped With Cobalt', *Dalton Transactions*, 7 (2005), 1273-1280.

Tônsuaadu, K., Peld, M., Leskelä, T., Mannonen, R., Niinistö, L., and Veiderma, M. 'A Thermoanalytical Study of Synthetic Carbonate-Containing Apatites', *Thermochimica Acta*, 256 (1995), 55-65.

Toworfe, G.K., Composto, R.J., Shapiro, I.M., and Ducheyne, P. 'Nucleation and Growth of Calcium Phosphate on Amine-, Carboxyl- and Hydroxyl-Silane Self-Assembled Monolayers', *Biomaterials*, 27 (2006), 631-642.

Trujillo, N.A., Oldinski, R.A., Ma, H., Bryers, J.D., Williams, J.D., and Popat, K.C. 'Antibacterial Effects of Silver-Doped Hydroxyapatite Thin Films Sputter Deposited on Titanium', *Materials Science and Engineering: C*, 32 (2012), 2135-2144.

Vignoles, M., Bonel, G., Holcomb, D.W., and Young, R.A. 'Influence of Preparation Conditions on the Composition of Type B Carbonated Hydroxyapatite and on the Localization of the Carbonate Ions', *Calcified Tissue International*, 43 (1988), 33-40.

Walker, P.R, LeBlanc, J., and Sikorska, M. 'Effects of Aluminum and Other Cations on the Structure of Brain and Liver Chromatin', *Biochemistry*, 28 (1989), 3911-3915.

Wang, Q.Y., Wang, Y.B., Lin, J.P., and Zheng, Y.F. 'Development and Properties of Ti-In Binary Alloys as Dental Biomaterials', *Materials Science and Engineering: C*, 33 (2013), 1601-1606.

Wang, X., Xu, S., Zhou, S., Xu, W., Leary, M., Choong, P., Qian, M., Brandt, M., and Xie, Y.M. 'Topological Design and Additive Manufacturing of Porous Metals for Bone Scaffolds and Orthopaedic Implants: A Review', *Biomaterials*, 83 (2016), 127-141.

Wang, X.X., Hayakawa, S., Tsuru, K., and Osaka, A. 'Improvement of Bioactivity of $H_2O_2/TaCl_5$-Treated Titanium After Subsequent Heat Treatments', *Journal of Biomedical Materials Research*, 52 (2000), 171-176.

Wang, X.X., Hayakawa, S., Tsuru, K., and Osaka, A. 'Bioactive Titania Gel Layers Formed by Chemical Treatment of Ti Substrate with a H_2O_2/HCl Solution', *Biomaterials*, 23 (2002), 1353-1357.

Wang, Z., Shen, Y., and Haapasalo, M. 'Dental Materials With Antibiofilm Properties', *Dental Materials*, 30 (2014), 1-16.

Wapner, K.L. 'Implications of Metallic Corrosion in Total Knee Arthroplasty', *Clinical Orthopaedics and Related Research*, 271 (1991), 12-20.

Webster, T.J., Schlueter, E.A.M., Smith, J.L., and Slamovich, E.B. 'Osteoblast Response to Hydroxyapatite Doped With Divalent and Trivalent Cations', *Biomaterials*, 25 (2004), 2111-2121.

Wiesmann, H.P., Plate, U., Zierold, K., and Höhling, H.J. 'Potassium is Involved in Apatite Biomineralization', *Journal of Dental Research*, 77 (1998), 1654-1657.

With, G.D., Dijk, H.J.A.V., Hattu, N., and Prijs, K. 'Preparation, Microstructure and Mechanical Properties of Dense Polycrystalline Hydroxy Apatite', *Journal of Materials Science*, 16 (1981), 1592-1598.

Wong, W.Y., and Noor, A.F.M. 'Synthesis and Sintering-Wet Carbonation of Nano-Sized Carbonated Hydroxyapatite', *Procedia Chemistry*, 19 (2016), 98-105.

Xavier, S.P., Carvalho, P.S.P., Beloti, M.M., and Rosa, A.L. 'Response of Rat Bone Marrow Cells to Commercially Pure Titanium Submitted to Different Surface Treatments', *Journal of Dentistry*, 31 (2003), 173-180.

Xiao, F., Tsuru, K., Hayakawa, S., and Osaka, A. 'In Vitro Apatite Deposition on Titania Film Derived from Chemical Treatment of Ti Substrates with an Oxysulfate Solution Containing Hydrogen Peroxide at Low Temperature', *Thin Solid Films*, 441 (2003), 271-276.

Xie, Y., Liu, X., Zheng, X., Ding, C., and Chu, P.K. 'Improved Stability of Plasma-Sprayed Dicalcium Silicate/Zirconia Composite Coating', *Thin Solid Films*, 515 (2006), 1214-1218.

Yang, A., Han, Y., Pan, Y., Xing, H., and Li, J. 'Optimum Surface Roughness Prediction for Titanium Alloy by Adopting Response Surface Methodology', *Results in Physics,* 7 (2017), 1046-1050.

Yang, B., Uchida, M., Kim, H.M., Zhang, X., and Kokubo, T. 'Preparation of Bioactive Titanium Metal via Anodic Oxidation Treatment', *Biomaterials*, 25 (2004), 1003-1010.

Yang, Y.C., and Chang, E. 'Influence of Residual Stress on Bonding Strength and Fracture of Plasma-Sprayed Hydroxyapatite Coatings on Ti-6Al-4V Substrate', *Biomaterials*, 22 (2001), 1827-1836.

Yilmaz, B., Evis, Z., and Güldiken, M. 'Titanyum Alaşımının Biyomimetik Yöntemle Kalsiyum Fosfat Kaplanması', *Journal of the Faculty of Engineering and Architecture of Gazi University*, 29 (2014), 105-109.

Yilmaz, B. 'Selenium Doped Calcium Phosphate Biomimetic Coating on Ti6Al4V Orthopedic Implant Material for Anti-Cancer and Anti-Bacterial Purposes', Middle East Technical University PhD Thesis, (2014), 30-41.

Yoder, C.H., Pasteris, J.D., Krol, K.A., Weidner, V.L., and Schaeffer, R.W. 'Synthesis, Structure, and Solubility of Carbonated Barium Chlor- and Hydroxylapatites', *Polyhedron*, 44 (2012), 143-149.

Zeng, S., Yang, Z., Ling, P., Xu, G., and Cao, W. 'Hydroxyapatite/Al_2O_3 Composite Biomaterial Implant', *Materials Research Society Symposium Proceedings*, 292 (1993), 271-275.

Zhang, B.B., Zheng, Y.F., and Liu, Y. 'Effect of Ag on the Corrosion Behavior of Ti-Ag Alloys in Artificial Saliva Solutions', *Dental Materials*, 25 (2009), 672-677.

Zhang, E.L., and Yang, K. 'Coating of Calcium Phosphate on Biometallic Materials by Electrophoretic Deposition', *Transactions of Nonferrous Metals Society of China* , 15 (2005), 957-964.

Zhang, E., Zou, C., and Yu, G. 'Surface Microstructure and Cell Biocompatibility of Silicon-Substituted Hydroxyapatite Coating on Titanium Substrate Prepared by a Biomimetic Process', *Materials Science and Engineering: C*, 29 (2009), 298-305.

Zhang, Q., Chen, J., Feng, J., Cao, Y., Deng, C., and Zhang, X. 'Dissolution and Mineralization Behaviors of HA Coatings', *Biomaterials*, 24 (2003), 4741-4748.

Zhao, G., Zinger, O., Schwartz, Z., Wieland, M., Landolt, D., and Boyan, B.D. 'Osteoblast-like Cells are Sensitive to Submicron-Scale Surface Structure', *Clinical Oral Implants Research*, 17 (2006), 258-264.

Zhu, K., Qiu, J., Ji, H., Yanagisawa, K., Shimanouchi, R., Onda, A., and Kajiyoshi, K. 'Crystallographic Study of Lead-Substituted Hydroxyapatite Synthesized by High-Temperature Mixing Method Under Hydrothermal Conditions', *Inorganica Chimica Acta,* 363 (2010), 1785-1790.

Zhu, X., Kim, K.H., and Jeong, Y. 'Anodic Oxide Films Containing Ca and P of Titanium Biomaterial', *Biomaterials*, 22 (2001), 2199-2206.

Zhu, X., Chen, J., Scheideler, L., Reichl, R., and Gerstorfer, J.G. 'Effects of Topography and Composition of Titanium Surface Oxides on Osteoblast Responses', *Biomaterials*, 25 (2004), 4087-4103.

Zhu, X., Ong, J.L., Kim, S., and Kim, K. 'Surface Characteristics and Structure of Anodic Oxide Films Containing Ca and P on a Titanium Implant Material', *Journal of Biomedical Materials Research*, 60 (2002), 333-338.

SPSS OUTPUT DATA RELATIVE TO CELL CULTURE STUDIES

Table A1 Experimental data obtained 1 day after cell seeding.

Group	Variable	Variable	Variable	Label
1	14,624	15,143	17,661	P7
2	12,251	14,206	11,834	P14
3	11,863	13,217	12,887	P21
4	15,162	14,541	15,230	0.1-C7
5	9,355	8,632	9,422	0.1-C14
6	5,798	4,634	4,711	0.1-C21
7	14,726	13,848	13,401	0.3-C7
8	13,475	13,139	13,419	0.3-C14
9	13,587	13,923	13,830	0.3-C21
10	12,489	13,857	13,362	0.5-C7
11	5,298	5,497	5,798	0.5-C14
12	4,507	4,551	4,100	0.5-C21

Table A2 SPSS output of 1 day after cell seeding samples.

Multiple Comparisons						
Dependent Variable: Variable						
Tukey HSD						
(I) Groups	(J) Groups	Mean Difference (I-J)	Std. Error	Sig.	95% Confidence Interval	
					Lower Bound	Upper Bound
P7	P14	3,045667*	,606569	,002	,85861	5,23273
	P21	3,153667*	,606569	,001	,96661	5,34073
	0.1-C7	,831667	,606569	,959	-1,35539	3,01873
	0.1-C14	6,673000*	,606569	,000	4,48594	8,86006
	0.1-C21	10,761667*	,606569	,000	8,57461	12,94873
	0.3-C7	1,817667	,606569	,170	-,36939	4,00473
	0.3-C14	2,465000*	,606569	,018	,27794	4,65206
	0.3-C21	2,029333	,606569	,086	-,15773	4,21639
	0.5-C7	2,573333*	,606569	,012	,38627	4,76039
	0.5-C14	10,278333*	,606569	,000	8,09127	12,46539
	0.5-C21	11,423333*	,606569	,000	9,23627	13,61039

Table A2 Cont'd.

	P7	-3,045667*	,606569	,002	-5,23273	-,85861
	P21	,108000	,606569	1,000	-2,07906	2,29506
	0.1-C7	-2,214000*	,606569	,045	-4,40106	-,02694
	0.1-C14	3,627333*	,606569	,000	1,44027	5,81439
	0.1-C21	7,716000*	,606569	,000	5,52894	9,90306
P14	0.3-C7	-1,228000	,606569	,674	-3,41506	,95906
	0.3-C14	-,580667	,606569	,997	-2,76773	1,60639
	0.3-C21	-1,016333	,606569	,862	-3,20339	1,17073
	0.5-C7	-,472333	,606569	1,000	-2,65939	1,71473
	0.5-C14	7,232667*	,606569	,000	5,04561	9,41973
	0.5-C21	8,377667*	,606569	,000	6,19061	10,56473
	P7	-3,153667*	,606569	,001	-5,34073	-,96661
	P14	-,108000	,606569	1,000	-2,29506	2,07906
	0.1-C7	-2,322000*	,606569	,031	-4,50906	-,13494
	0.1-C14	3,519333*	,606569	,000	1,33227	5,70639
	0.1-C21	7,608000*	,606569	,000	5,42094	9,79506
P21	0.3-C7	-1,336000	,606569	,563	-3,52306	,85106
	0.3-C14	-,688667	,606569	,989	-2,87573	1,49839
	0.3-C21	-1,124333	,606569	,774	-3,31139	1,06273
	0.5-C7	-,580333	,606569	,997	-2,76739	1,60673
	0.5-C14	7,124667*	,606569	,000	4,93761	9,31173
	0.5-C21	8,269667*	,606569	,000	6,08261	10,45673
	P7	-,831667	,606569	,959	-3,01873	1,35539
	P14	2,214000*	,606569	,045	,02694	4,40106
	P21	2,322000*	,606569	,031	,13494	4,50906
	0.1-C14	5,841333*	,606569	,000	3,65427	8,02839
	0.1-C21	9,930000*	,606569	,000	7,74294	12,11706
0.1-C7	0.3-C7	,986000	,606569	,883	-1,20106	3,17306
	0.3-C14	1,633333	,606569	,287	-,55373	3,82039
	0.3-C21	1,197667	,606569	,705	-,98939	3,38473
	0.5-C7	1,741667	,606569	,213	-,44539	3,92873
	0.5-C14	9,446667*	,606569	,000	7,25961	11,63373
	0.5-C21	10,591667*	,606569	,000	8,40461	12,77873
	P7	-6,673000*	,606569	,000	-8,86006	-4,48594
	P14	-3,627333*	,606569	,000	-5,81439	-1,44027
	P21	-3,519333*	,606569	,000	-5,70639	-1,33227
	0.1-C7	-5,841333*	,606569	,000	-8,02839	-3,65427
	0.1-C21	4,088667*	,606569	,000	1,90161	6,27573
0.1-C14	0.3-C7	-4,855333*	,606569	,000	-7,04239	-2,66827
	0.3-C14	-4,208000*	,606569	,000	-6,39506	-2,02094
	0.3-C21	-4,643667*	,606569	,000	-6,83073	-2,45661
	0.5-C7	-4,099667*	,606569	,000	-6,28673	-1,91261
	0.5-C14	3,605333*	,606569	,000	1,41827	5,79239
	0.5-C21	4,750333*	,606569	,000	2,56327	6,93739

Table A2 Cont'd.

	P7	-10,761667*	,606569	,000	-12,94873	-8,57461
	P14	-7,716000*	,606569	,000	-9,90306	-5,52894
	P21	-7,608000*	,606569	,000	-9,79506	-5,42094
	0.1-C7	-9,930000*	,606569	,000	-12,11706	-7,74294
	0.1-C14	-4,088667*	,606569	,000	-6,27573	-1,90161
0.1-C21	0.3-C7	-8,944000*	,606569	,000	-11,13106	-6,75694
	0.3-C14	-8,296667*	,606569	,000	-10,48373	-6,10961
	0.3-C21	-8,732333*	,606569	,000	-10,91939	-6,54527
	0.5-C7	-8,188333*	,606569	,000	-10,37539	-6,00127
	0.5-C14	-,483333	,606569	,999	-2,67039	1,70373
	0.5-C21	,661667	,606569	,992	-1,52539	2,84873
	P7	-1,817667	,606569	,170	-4,00473	,36939
	P14	1,228000	,606569	,674	-,95906	3,41506
	P21	1,336000	,606569	,563	-,85106	3,52306
	0.1-C7	-,986000	,606569	,883	-3,17306	1,20106
	0.1-C14	4,855333*	,606569	,000	2,66827	7,04239
0.3-C7	0.1-C21	8,944000*	,606569	,000	6,75694	11,13106
	0.3-C14	,647333	,606569	,994	-1,53973	2,83439
	0.3-C21	,211667	,606569	1,000	-1,97539	2,39873
	0.5-C7	,755667	,606569	,979	-1,43139	2,94273
	0.5-C14	8,460667*	,606569	,000	6,27361	10,64773
	0.5-C21	9,605667*	,606569	,000	7,41861	11,79273
	P7	-2,465000*	,606569	,018	-4,65206	-,27794
	P14	,580667	,606569	,997	-1,60639	2,76773
	P21	,688667	,606569	,989	-1,49839	2,87573
	0.1-C7	-1,633333	,606569	,287	-3,82039	,55373
	0.1-C14	4,208000*	,606569	,000	2,02094	6,39506
0.3-C14	0.1-C21	8,296667*	,606569	,000	6,10961	10,48373
	0.3-C7	-,647333	,606569	,994	-2,83439	1,53973
	0.3-C21	-,435667	,606569	1,000	-2,62273	1,75139
	0.5-C7	,108333	,606569	1,000	-2,07873	2,29539
	0.5-C14	7,813333*	,606569	,000	5,62627	10,00039
	0.5-C21	8,958333*	,606569	,000	6,77127	11,14539
	P7	-2,029333	,606569	,086	-4,21639	,15773
	P14	1,016333	,606569	,862	-1,17073	3,20339
	P21	1,124333	,606569	,774	-1,06273	3,31139
	0.1-C7	-1,197667	,606569	,705	-3,38473	,98939
	0.1-C14	4,643667*	,606569	,000	2,45661	6,83073
0.3-C21	0.1-C21	8,732333*	,606569	,000	6,54527	10,91939
	0.3-C7	-,211667	,606569	1,000	-2,39873	1,97539
	0.3-C14	,435667	,606569	1,000	-1,75139	2,62273
	0.5-C7	,544000	,606569	,999	-1,64306	2,73106
	0.5-C14	8,249000*	,606569	,000	6,06194	10,43606
	0.5-C21	9,394000*	,606569	,000	7,20694	11,58106

Table A2 Cont'd.

	P7	-2,573333*	,606569	,012	-4,76039	-,38627
	P14	,472333	,606569	1,000	-1,71473	2,65939
	P21	,580333	,606569	,997	-1,60673	2,76739
	0.1-C7	-1,741667	,606569	,213	-3,92873	,44539
	0.1-C14	4,099667*	,606569	,000	1,91261	6,28673
0.5-C7	0.1-C21	8,188333*	,606569	,000	6,00127	10,37539
	0.3-C7	-,755667	,606569	,979	-2,94273	1,43139
	0.3-C14	-,108333	,606569	1,000	-2,29539	2,07873
	0.3-C21	-,544000	,606569	,999	-2,73106	1,64306
	0.5-C14	7,705000*	,606569	,000	5,51794	9,89206
	0.5-C21	8,850000*	,606569	,000	6,66294	11,03706
	P7	-10,278333*	,606569	,000	-12,46539	-8,09127
	P14	-7,232667*	,606569	,000	-9,41973	-5,04561
	P21	-7,124667*	,606569	,000	-9,31173	-4,93761
	0.1-C7	-9,446667*	,606569	,000	-11,63373	-7,25961
	0.1-C14	-3,605333*	,606569	,000	-5,79239	-1,41827
0.5-C14	0.1-C21	,483333	,606569	,999	-1,70373	2,67039
	0.3-C7	-8,460667*	,606569	,000	-10,64773	-6,27361
	0.3-C14	-7,813333*	,606569	,000	-10,00039	-5,62627
	0.3-C21	-8,249000*	,606569	,000	-10,43606	-6,06194
	0.5-C7	-7,705000*	,606569	,000	-9,89206	-5,51794
	0.5-C21	1,145000	,606569	,755	-1,04206	3,33206
	P7	-11,423333*	,606569	,000	-13,61039	-9,23627
	P14	-8,377667*	,606569	,000	-10,56473	-6,19061
	P21	-8,269667*	,606569	,000	-10,45673	-6,08261
	0.1-C7	-10,591667*	,606569	,000	-12,77873	-8,40461
	0.1-C14	-4,750333*	,606569	,000	-6,93739	-2,56327
0.5-C21	0.1-C21	-,661667	,606569	,992	-2,84873	1,52539
	0.3-C7	-9,605667*	,606569	,000	-11,79273	-7,41861
	0.3-C14	-8,958333*	,606569	,000	-11,14539	-6,77127
	0.3-C21	-9,394000*	,606569	,000	-11,58106	-7,20694
	0.5-C7	-8,850000*	,606569	,000	-11,03706	-6,66294
	0.5-C14	-1,145000	,606569	,755	-3,33206	1,04206
*. The mean difference is significant at the 0.05 level.						

Table A3 Experimental data obtained 3 day after cell seeding.

Group	Variable	Variable	Variable	Label
1	16,255	19,216	21,373	P7
2	11,153	15,565	12,050	P14
3	13,326	13,948	12,154	P21
4	21,010	19,791	20,325	0.1-C7
5	10,075	8,187	9,442	0.1-C14
6	4,713	6,238	5,050	0.1-C21
7	20,208	20,245	20,629	0.3-C7
8	15,774	15,866	16,745	0.3-C14
9	16,287	16,947	17,533	0.3-C21
10	17,411	17,868	19,491	0.5-C7
11	4,158	4,967	5,081	0.5-C14
12	4,568	4,418	4,926	0.5-C21

Table A4 SPSS output of 3 day after cell seeding samples.

					95% Confidence Interval	
(I) Groups	(J) Groups	Mean Difference (I-J)	Std. Error	Sig.	Lower Bound	Upper Bound
Multiple Comparisons						
Dependent Variable: Variable						
Tukey HSD						
P7	P14	6,025333*	,973390	,000	2,51565	9,53502
	P21	5,805333*	,973390	,000	2,29565	9,31502
	0.1-C7	-1,427333	,973390	,936	-4,93702	2,08235
	0.1-C14	9,713333*	,973390	,000	6,20365	13,22302
	0.1-C21	13,614333*	,973390	,000	10,10465	17,12402
	0.3-C7	-1,412667	,973390	,940	-4,92235	2,09702
	0.3-C14	2,819667	,973390	,204	-,69002	6,32935
	0.3-C21	2,025667	,973390	,639	-1,48402	5,53535
	0.5-C7	,691333	,973390	1,000	-2,81835	4,20102
	0.5-C14	14,212667*	,973390	,000	10,70298	17,72235
	0.5-C21	14,310667*	,973390	,000	10,80098	17,82035
P14	P7	-6,025333*	,973390	,000	-9,53502	-2,51565
	P21	-,220000	,973390	1,000	-3,72968	3,28968
	0.1-C7	-7,452667*	,973390	,000	-10,96235	-3,94298
	0.1-C14	3,688000*	,973390	,033	,17832	7,19768
	0.1-C21	7,589000*	,973390	,000	4,07932	11,09868
	0.3-C7	-7,438000*	,973390	,000	-10,94768	-3,92832
	0.3-C14	-3,205667	,973390	,096	-6,71535	,30402
	0.3-C21	-3,999667*	,973390	,016	-7,50935	-,48998
	0.5-C7	-5,334000*	,973390	,001	-8,84368	-1,82432
	0.5-C14	8,187333*	,973390	,000	4,67765	11,69702
	0.5-C21	8,285333*	,973390	,000	4,77565	11,79502

Table A4 Cont'd.

P21	P7	-5,805333*	,973390	,000	-9,31502	-2,29565
	P14	,220000	,973390	1,000	-3,28968	3,72968
	0.1-C7	-7,232667*	,973390	,000	-10,74235	-3,72298
	0.1-C14	3,908000*	,973390	,020	,39832	7,41768
	0.1-C21	7,809000*	,973390	,000	4,29932	11,31868
	0.3-C7	-7,218000*	,973390	,000	-10,72768	-3,70832
	0.3-C14	-2,985667	,973390	,149	-6,49535	,52402
	0.3-C21	-3,779667*	,973390	,027	-7,28935	-,26998
	0.5-C7	-5,114000*	,973390	,001	-8,62368	-1,60432
	0.5-C14	8,407333*	,973390	,000	4,89765	11,91702
	0.5-C21	8,505333*	,973390	,000	4,99565	12,01502
0.1-C7	P7	1,427333	,973390	,936	-2,08235	4,93702
	P14	7,452667*	,973390	,000	3,94298	10,96235
	P21	7,232667*	,973390	,000	3,72298	10,74235
	0.1-C14	11,140667*	,973390	,000	7,63098	14,65035
	0.1-C21	15,041667*	,973390	,000	11,53198	18,55135
	0.3-C7	,014667	,973390	1,000	-3,49502	3,52435
	0.3-C14	4,247000*	,973390	,009	,73732	7,75668
	0.3-C21	3,453000	,973390	,057	-,05668	6,96268
	0.5-C7	2,118667	,973390	,579	-1,39102	5,62835
	0.5-C14	15,640000*	,973390	,000	12,13032	19,14968
	0.5-C21	15,738000*	,973390	,000	12,22832	19,24768
0.1-C14	P7	-9,713333*	,973390	,000	-13,22302	-6,20365
	P14	-3,688000*	,973390	,033	-7,19768	-,17832
	P21	-3,908000*	,973390	,020	-7,41768	-,39832
	0.1-C7	-11,140667*	,973390	,000	-14,65035	-7,63098
	0.1-C21	3,901000*	,973390	,020	,39132	7,41068
	0.3-C7	-11,126000*	,973390	,000	-14,63568	-7,61632
	0.3-C14	-6,893667*	,973390	,000	-10,40335	-3,38398
	0.3-C21	-7,687667*	,973390	,000	-11,19735	-4,17798
	0.5-C7	-9,022000*	,973390	,000	-12,53168	-5,51232
	0.5-C14	4,499333*	,973390	,005	,98965	8,00902
	0.5-C21	4,597333*	,973390	,004	1,08765	8,10702
0.1-C21	P7	-13,614333*	,973390	,000	-17,12402	-10,10465
	P14	-7,589000*	,973390	,000	-11,09868	-4,07932
	P21	-7,809000*	,973390	,000	-11,31868	-4,29932
	0.1-C7	-15,041667*	,973390	,000	-18,55135	-11,53198
	0.1-C14	-3,901000*	,973390	,020	-7,41068	-,39132
	0.3-C7	-15,027000*	,973390	,000	-18,53668	-11,51732
	0.3-C14	-10,794667*	,973390	,000	-14,30435	-7,28498
	0.3-C21	-11,588667*	,973390	,000	-15,09835	-8,07898
	0.5-C7	-12,923000*	,973390	,000	-16,43268	-9,41332
	0.5-C14	,598333	,973390	1,000	-2,91135	4,10802
	0.5-C21	,696333	,973390	1,000	-2,81335	4,20602

124

Table A4 Cont'd.

	P7	1,412667	,973390	,940	-2,09702	4,92235
	P14	7,438000*	,973390	,000	3,92832	10,94768
	P21	7,218000*	,973390	,000	3,70832	10,72768
	0.1-C7	-,014667	,973390	1,000	-3,52435	3,49502
	0.1-C14	11,126000*	,973390	,000	7,61632	14,63568
0.3-C7	0.1-C21	15,027000*	,973390	,000	11,51732	18,53668
	0.3-C14	4,232333*	,973390	,009	,72265	7,74202
	0.3-C21	3,438333	,973390	,058	-,07135	6,94802
	0.5-C7	2,104000	,973390	,589	-1,40568	5,61368
	0.5-C14	15,625333*	,973390	,000	12,11565	19,13502
	0.5-C21	15,723333*	,973390	,000	12,21365	19,23302
	P7	-2,819667	,973390	,204	-6,32935	,69002
	P14	3,205667	,973390	,096	-,30402	6,71535
	P21	2,985667	,973390	,149	-,52402	6,49535
	0.1-C7	-4,247000*	,973390	,009	-7,75668	-,73732
	0.1-C14	6,893667*	,973390	,000	3,38398	10,40335
0.3-C14	0.1-C21	10,794667*	,973390	,000	7,28498	14,30435
	0.3-C7	-4,232333*	,973390	,009	-7,74202	-,72265
	0.3-C21	-,794000	,973390	,999	-4,30368	2,71568
	0.5-C7	-2,128333	,973390	,573	-5,63802	1,38135
	0.5-C14	11,393000*	,973390	,000	7,88332	14,90268
	0.5-C21	11,491000*	,973390	,000	7,98132	15,00068
	P7	-2,025667	,973390	,639	-5,53535	1,48402
	P14	3,999667*	,973390	,016	,48998	7,50935
	P21	3,779667*	,973390	,027	,26998	7,28935
	0.1-C7	-3,453000	,973390	,057	-6,96268	,05668
	0.1-C14	7,687667*	,973390	,000	4,17798	11,19735
0.3-C21	0.1-C21	11,588667*	,973390	,000	8,07898	15,09835
	0.3-C7	-3,438333	,973390	,058	-6,94802	,07135
	0.3-C14	,794000	,973390	,999	-2,71568	4,30368
	0.5-C7	-1,334333	,973390	,959	-4,84402	2,17535
	0.5-C14	12,187000*	,973390	,000	8,67732	15,69668
	0.5-C21	12,285000*	,973390	,000	8,77532	15,79468
	P7	-,691333	,973390	1,000	-4,20102	2,81835
	P14	5,334000*	,973390	,001	1,82432	8,84368
	P21	5,114000*	,973390	,001	1,60432	8,62368
	0.1-C7	-2,118667	,973390	,579	-5,62835	1,39102
	0.1-C14	9,022000*	,973390	,000	5,51232	12,53168
0.5-C7	0.1-C21	12,923000*	,973390	,000	9,41332	16,43268
	0.3-C7	-2,104000	,973390	,589	-5,61368	1,40568
	0.3-C14	2,128333	,973390	,573	-1,38135	5,63802
	0.3-C21	1,334333	,973390	,959	-2,17535	4,84402
	0.5-C14	13,521333*	,973390	,000	10,01165	17,03102
	0.5-C21	13,619333*	,973390	,000	10,10965	17,12902

Table A4 Cont'd.

	P7	-14,212667*	,973390	,000	-17,72235	-10,70298
	P14	-8,187333*	,973390	,000	-11,69702	-4,67765
	P21	-8,407333*	,973390	,000	-11,91702	-4,89765
	0.1-C7	-15,640000*	,973390	,000	-19,14968	-12,13032
	0.1-C14	-4,499333*	,973390	,005	-8,00902	-,98965
0.5-C14	0.1-C21	-,598333	,973390	1,000	-4,10802	2,91135
	0.3-C7	-15,625333*	,973390	,000	-19,13502	-12,11565
	0.3-C14	-11,393000*	,973390	,000	-14,90268	-7,88332
	0.3-C21	-12,187000*	,973390	,000	-15,69668	-8,67732
	0.5-C7	-13,521333*	,973390	,000	-17,03102	-10,01165
	0.5-C21	,098000	,973390	1,000	-3,41168	3,60768
	P7	-14,310667*	,973390	,000	-17,82035	-10,80098
	P14	-8,285333*	,973390	,000	-11,79502	-4,77565
	P21	-8,505333*	,973390	,000	-12,01502	-4,99565
	0.1-C7	-15,738000*	,973390	,000	-19,24768	-12,22832
	0.1-C14	-4,597333*	,973390	,004	-8,10702	-1,08765
0.5-C21	0.1-C21	-,696333	,973390	1,000	-4,20602	2,81335
	0.3-C7	-15,723333*	,973390	,000	-19,23302	-12,21365
	0.3-C14	-11,491000*	,973390	,000	-15,00068	-7,98132
	0.3-C21	-12,285000*	,973390	,000	-15,79468	-8,77532
	0.5-C7	-13,619333*	,973390	,000	-17,12902	-10,10965
	0.5-C14	-,098000	,973390	1,000	-3,60768	3,41168
*. The mean difference is significant at the 0.05 level.						

Table A5 Experimental data obtained 7 day after cell seeding.

Group	Variable	Variable	Variable	Label
1	31,692	27,755	33,700	P7
2	42,692	40,367	25,183	P14
3	19,891	26,216	24,239	P21
4	24,413	23,001	25,478	0.1-C7
5	9,250	10,984	7,342	0.1-C14
6	7,284	5,914	6,467	0.1-C21
7	12,468	27,023	22,982	0.3-C7
8	12,123	11,236	11,088	0.3-C14
9	20,550	20,140	19,910	0.3-C21
10	13,935	12,412	15,116	0.5-C7
11	5,044	5,423	5,882	0.5-C14
12	5,091	5,070	5,102	0.5-C21

Table A6 SPSS output of 7 day after cell seeding samples.

(I) Groups	(J) Groups	Mean Difference (I-J)	Std. Error	Sig.	95% Confidence Interval	
					Lower Bound	Upper Bound
P7	P14	-5,031667	3,111449	,886	-16,25040	6,18707
	P21	7,600333	3,111449	,417	-3,61840	18,81907
	0.1-C7	6,751667	3,111449	,583	-4,46707	17,97040
	0.1-C14	21,857000*	3,111449	,000	10,63827	33,07573
	0.1-C21	24,494000*	3,111449	,000	13,27527	35,71273
	0.3-C7	10,224667	3,111449	,097	-,99407	21,44340
	0.3-C14	19,566667*	3,111449	,000	8,34793	30,78540
	0.3-C21	10,849000	3,111449	,064	-,36973	22,06773
	0.5-C7	17,228000*	3,111449	,001	6,00927	28,44673
	0.5-C14	25,599333*	3,111449	,000	14,38060	36,81807
	0.5-C21	25,961333*	3,111449	,000	14,74260	37,18007
P14	P7	5,031667	3,111449	,886	-6,18707	16,25040
	P21	12,632000*	3,111449	,018	1,41327	23,85073
	0.1-C7	11,783333*	3,111449	,034	,56460	23,00207
	0.1-C14	26,888667*	3,111449	,000	15,66993	38,10740
	0.1-C21	29,525667*	3,111449	,000	18,30693	40,74440
	0.3-C7	15,256333*	3,111449	,002	4,03760	26,47507
	0.3-C14	24,598333*	3,111449	,000	13,37960	35,81707
	0.3-C21	15,880667*	3,111449	,002	4,66193	27,09940
	0.5-C7	22,259667*	3,111449	,000	11,04093	33,47840
	0.5-C14	30,631000*	3,111449	,000	19,41227	41,84973
	0.5-C21	30,993000*	3,111449	,000	19,77427	42,21173
P21	P7	-7,600333	3,111449	,417	-18,81907	3,61840
	P14	-12,632000*	3,111449	,018	-23,85073	-1,41327
	0.1-C7	-,848667	3,111449	1,000	-12,06740	10,37007
	0.1-C14	14,256667*	3,111449	,005	3,03793	25,47540
	0.1-C21	16,893667*	3,111449	,001	5,67493	28,11240
	0.3-C7	2,624333	3,111449	,999	-8,59440	13,84307
	0.3-C14	11,966333*	3,111449	,029	,74760	23,18507
	0.3-C21	3,248667	3,111449	,995	-7,97007	14,46740
	0.5-C7	9,627667	3,111449	,142	-1,59107	20,84640
	0.5-C14	17,999000*	3,111449	,000	6,78027	29,21773
	0.5-C21	18,361000*	3,111449	,000	7,14227	29,57973
0.1-C7	P7	-6,751667	3,111449	,583	-17,97040	4,46707
	P14	-11,783333*	3,111449	,034	-23,00207	-,56460
	P21	,848667	3,111449	1,000	-10,37007	12,06740
	0.1-C14	15,105333*	3,111449	,003	3,88660	26,32407
	0.1-C21	17,742333*	3,111449	,000	6,52360	28,96107
	0.3-C7	3,473000	3,111449	,991	-7,74573	14,69173
	0.3-C14	12,815000*	3,111449	,016	1,59627	24,03373
	0.3-C21	4,097333	3,111449	,968	-7,12140	15,31607
	0.5-C7	10,476333	3,111449	,083	-,74240	21,69507
	0.5-C14	18,847667*	3,111449	,000	7,62893	30,06640
	0.5-C21	19,209667*	3,111449	,000	7,99093	30,42840

Note: Table header spans — Multiple Comparisons; Dependent Variable: Variable; Tukey HSD

Table A6 Cont'd.

	P7	-21,857000*	3,111449	,000	-33,07573	-10,63827
	P14	-26,888667*	3,111449	,000	-38,10740	-15,66993
	P21	-14,256667*	3,111449	,005	-25,47540	-3,03793
	0.1-C7	-15,105333*	3,111449	,003	-26,32407	-3,88660
	0.1-C21	2,637000	3,111449	,999	-8,58173	13,85573
0.1-C14	0.3-C7	-11,632333*	3,111449	,037	-22,85107	-,41360
	0.3-C14	-2,290333	3,111449	1,000	-13,50907	8,92840
	0.3-C21	-11,008000	3,111449	,058	-22,22673	,21073
	0.5-C7	-4,629000	3,111449	,930	-15,84773	6,58973
	0.5-C14	3,742333	3,111449	,984	-7,47640	14,96107
	0.5-C21	4,104333	3,111449	,968	-7,11440	15,32307
	P7	-24,494000*	3,111449	,000	-35,71273	-13,27527
	P14	-29,525667*	3,111449	,000	-40,74440	-18,30693
	P21	-16,893667*	3,111449	,001	-28,11240	-5,67493
	0.1-C7	-17,742333*	3,111449	,000	-28,96107	-6,52360
	0.1-C14	-2,637000	3,111449	,999	-13,85573	8,58173
0.1-C21	0.3-C7	-14,269333*	3,111449	,005	-25,48807	-3,05060
	0.3-C14	-4,927333	3,111449	,899	-16,14607	6,29140
	0.3-C21	-13,645000*	3,111449	,009	-24,86373	-2,42627
	0.5-C7	-7,266000	3,111449	,481	-18,48473	3,95273
	0.5-C14	1,105333	3,111449	1,000	-10,11340	12,32407
	0.5-C21	1,467333	3,111449	1,000	-9,75140	12,68607
	P7	-10,224667	3,111449	,097	-21,44340	,99407
	P14	-15,256333*	3,111449	,002	-26,47507	-4,03760
	P21	-2,624333	3,111449	,999	-13,84307	8,59440
	0.1-C7	-3,473000	3,111449	,991	-14,69173	7,74573
	0.1-C14	11,632333*	3,111449	,037	,41360	22,85107
0.3-C7	0.1-C21	14,269333*	3,111449	,005	3,05060	25,48807
	0.3-C14	9,342000	3,111449	,168	-1,87673	20,56073
	0.3-C21	,624333	3,111449	1,000	-10,59440	11,84307
	0.5-C7	7,003333	3,111449	,533	-4,21540	18,22207
	0.5-C14	15,374667*	3,111449	,002	4,15593	26,59340
	0.5-C21	15,736667*	3,111449	,002	4,51793	26,95540
	P7	-19,566667*	3,111449	,000	-30,78540	-8,34793
	P14	-24,598333*	3,111449	,000	-35,81707	-13,37960
	P21	-11,966333*	3,111449	,029	-23,18507	-,74760
	0.1-C7	-12,815000*	3,111449	,016	-24,03373	-1,59627
	0.1-C14	2,290333	3,111449	1,000	-8,92840	13,50907
0.3-C14	0.1-C21	4,927333	3,111449	,899	-6,29140	16,14607
	0.3-C7	-9,342000	3,111449	,168	-20,56073	1,87673
	0.3-C21	-8,717667	3,111449	,240	-19,93640	2,50107
	0.5-C7	-2,338667	3,111449	1,000	-13,55740	8,88007
	0.5-C14	6,032667	3,111449	,726	-5,18607	17,25140
	0.5-C21	6,394667	3,111449	,655	-4,82407	17,61340

128

Table A6 Cont'd.

	P7	-10,849000	3,111449	,064	-22,06773	,36973
	P14	-15,880667*	3,111449	,002	-27,09940	-4,66193
	P21	-3,248667	3,111449	,995	-14,46740	7,97007
	0.1-C7	-4,097333	3,111449	,968	-15,31607	7,12140
	0.1-C14	11,008000	3,111449	,058	-,21073	22,22673
0.3-C21	0.1-C21	13,645000*	3,111449	,009	2,42627	24,86373
	0.3-C7	-,624333	3,111449	1,000	-11,84307	10,59440
	0.3-C14	8,717667	3,111449	,240	-2,50107	19,93640
	0.5-C7	6,379000	3,111449	,659	-4,83973	17,59773
	0.5-C14	14,750333*	3,111449	,004	3,53160	25,96907
	0.5-C21	15,112333*	3,111449	,003	3,89360	26,33107
	P7	-17,228000*	3,111449	,001	-28,44673	-6,00927
	P14	-22,259667*	3,111449	,000	-33,47840	-11,04093
	P21	-9,627667	3,111449	,142	-20,84640	1,59107
	0.1-C7	-10,476333	3,111449	,083	-21,69507	,74240
	0.1-C14	4,629000	3,111449	,930	-6,58973	15,84773
0.5-C7	0.1-C21	7,266000	3,111449	,481	-3,95273	18,48473
	0.3-C7	-7,003333	3,111449	,533	-18,22207	4,21540
	0.3-C14	2,338667	3,111449	1,000	-8,88007	13,55740
	0.3-C21	-6,379000	3,111449	,659	-17,59773	4,83973
	0.5-C14	8,371333	3,111449	,288	-2,84740	19,59007
	0.5-C21	8,733333	3,111449	,238	-2,48540	19,95207
	P7	-25,599333*	3,111449	,000	-36,81807	-14,38060
	P14	-30,631000*	3,111449	,000	-41,84973	-19,41227
	P21	-17,999000*	3,111449	,000	-29,21773	-6,78027
	0.1-C7	-18,847667*	3,111449	,000	-30,06640	-7,62893
	0.1-C14	-3,742333	3,111449	,984	-14,96107	7,47640
0.5-C14	0.1-C21	-1,105333	3,111449	1,000	-12,32407	10,11340
	0.3-C7	-15,374667*	3,111449	,002	-26,59340	-4,15593
	0.3-C14	-6,032667	3,111449	,726	-17,25140	5,18607
	0.3-C21	-14,750333*	3,111449	,004	-25,96907	-3,53160
	0.5-C7	-8,371333	3,111449	,288	-19,59007	2,84740
	0.5-C21	,362000	3,111449	1,000	-10,85673	11,58073
	P7	-25,961333*	3,111449	,000	-37,18007	-14,74260
	P14	-30,993000*	3,111449	,000	-42,21173	-19,77427
	P21	-18,361000*	3,111449	,000	-29,57973	-7,14227
	0.1-C7	-19,209667*	3,111449	,000	-30,42840	-7,99093
	0.1-C14	-4,104333	3,111449	,968	-15,32307	7,11440
0.5-C21	0.1-C21	-1,467333	3,111449	1,000	-12,68607	9,75140
	0.3-C7	-15,736667*	3,111449	,002	-26,95540	-4,51793
	0.3-C14	-6,394667	3,111449	,655	-17,61340	4,82407
	0.3-C21	-15,112333*	3,111449	,003	-26,33107	-3,89360
	0.5-C7	-8,733333	3,111449	,238	-19,95207	2,48540
	0.5-C14	-,362000	3,111449	1,000	-11,58073	10,85673
*. The mean difference is significant at the 0.05 level.						

APPENDIX B

SPSS OUTPUT DATA RELATIVE TO ANTIBACTERIAL STUDIES

Table B1 Experimental data obtained from antibacterial tests.

Group	Variable	Variable	Variable	Label
1	2,53	2,44	2,50	P7
2	2,34	2,48	2,51	P14
3	2,73	2,64	2,59	P21
4	1,49	1,50	1,47	0.1-C7
5	1,38	1,45	1,48	0.3-C7
6	1,66	1,82	1,80	0.3-C14
7	2,16	2,10	2,12	0.3-C21

Table B2 SPSS output of antibacterial tests.

Multiple Comparisons						
Dependent Variable: Variable						
Tukey HSD						
(I) Groups	(J) Groups	Mean Difference (I-J)	Std. Error	Sig.	95% Confidence Interval	
					Lower Bound	Upper Bound
P7	P14	,046667	,050490	,962	-,12573	,21907
	P21	-,163333	,050490	,069	-,33573	,00907
	0.1-C7	1,003333*	,050490	,000	,83093	1,17573
	0.3-C7	1,053333*	,050490	,000	,88093	1,22573
	0.3-C14	,730000*	,050490	,000	,55760	,90240
	0.3-C21	,363333*	,050490	,000	,19093	,53573
P14	P7	-,046667	,050490	,962	-,21907	,12573
	P21	-,210000*	,050490	,013	-,38240	-,03760
	0.1-C7	,956667*	,050490	,000	,78427	1,12907
	0.3-C7	1,006667*	,050490	,000	,83427	1,17907
	0.3-C14	,683333*	,050490	,000	,51093	,85573
	0.3-C21	,316667*	,050490	,000	,14427	,48907
P21	P7	,163333	,050490	,069	-,00907	,33573
	P14	,210000*	,050490	,013	,03760	,38240
	0.1-C7	1,166667*	,050490	,000	,99427	1,33907
	0.3-C7	1,216667*	,050490	,000	1,04427	1,38907
	0.3-C14	,893333*	,050490	,000	,72093	1,06573
	0.3-C21	,526667*	,050490	,000	,35427	,69907

Table B2 Cont'd.

0.1-C7	P7	-1,003333*	,050490	,000	-1,17573	-,83093
	P14	-,956667*	,050490	,000	-1,12907	-,78427
	P21	-1,166667*	,050490	,000	-1,33907	-,99427
	0.3-C7	,050000	,050490	,948	-,12240	,22240
	0.3-C14	-,273333*	,050490	,001	-,44573	-,10093
	0.3-C21	-,640000*	,050490	,000	-,81240	-,46760
0.3-C7	P7	-1,053333*	,050490	,000	-1,22573	-,88093
	P14	-1,006667*	,050490	,000	-1,17907	-,83427
	P21	-1,216667*	,050490	,000	-1,38907	-1,04427
	0.1-C7	-,050000	,050490	,948	-,22240	,12240
	0.3-C14	-,323333*	,050490	,000	-,49573	-,15093
	0.3-C21	-,690000*	,050490	,000	-,86240	-,51760
0.3-C14	P7	-,730000*	,050490	,000	-,90240	-,55760
	P14	-,683333*	,050490	,000	-,85573	-,51093
	P21	-,893333*	,050490	,000	-1,06573	-,72093
	0.1-C7	,273333*	,050490	,001	,10093	,44573
	0.3-C7	,323333*	,050490	,000	,15093	,49573
	0.3-C21	-,366667*	,050490	,000	-,53907	-,19427
0.3-C21	P7	-,363333*	,050490	,000	-,53573	-,19093
	P14	-,316667*	,050490	,000	-,48907	-,14427
	P21	-,526667*	,050490	,000	-,69907	-,35427
	0.1-C7	,640000*	,050490	,000	,46760	,81240
	0.3-C7	,690000*	,050490	,000	,51760	,86240
	0.3-C14	,366667*	,050490	,000	,19427	,53907
*. The mean difference is significant at the 0.05 level.						

CURRICULUM VITAE

PERSONAL INFORMATION

Surname, Name: Hacıoğlu, Tuğçe
Nationality: Turkish (TC)
Date of Birth: 28.07.1987
Marital Status: Married
E-mail: tugce.aktar@metu.edu.tr

EDUCATION

Degree	Institution	Year of Graduation
M.S.	Ankara University, Chemical Engineering	2011
B.S.	Ankara University, Chemical Engineering	2009

WORK EXPERIENCE

Year	Place	Enrollment
12.2012-Now	Ministry of Labor and Social Security, Directorate General of Occupational Health and Safety	Occupational Health Safety Expert
07.2011-12.2012	Kortek Engineering and Consultancy Co. Ltd.	Project Coordinator
02.2010-08.2011	TÜBİTAK Project No 109M400 (Bilateral Cooperation Turkey-Ukraine)	Project Assistant
06.2008-07.2008	ÇİMSA Cement Industry and Trade Inc.	Engineering Intern
07.2007-08.2007	Eczacıbaşı Baxter Hospital Supply Inc.	Engineering Intern

PUBLICATIONS AND CONFERENCES PARTICIPATED

T. Aktar, Z. Evis, A. Tezcaner, "Enhancement of Mechanical Properties Of Co-Doped Hydroxyapatite Coatings on Pre-Treated Ti6Al4V", 1st International Conference of Advanced Materials and Manufacturing Technologies, Karabük, Turkey, 25-27 October 2017.

Z. Evis, A. Tezcaner, **T. Aktar**, "Preparation of orthopedic implant by coating bismuth and carbonate doped hydroxyapatite onto acid etched Ti6Al4V via biomimetic method", International Participated 8th National Biomechanics Conference, Ankara, Turkey, 19-23 October 2016.

T. Aktar, Z. Evis, "Coating of hydroxyapatite onto surface modified Ti6Al5V plates via biomimetic method and structural analysis", IXth International Participation Ceramic Conference, Afyonkarahisar, Turkey, 26-28 November 2015.

T. Aktar, I.I.G. Inal, E. Yagmur, N. Sych, V.V. Strelko, Z. Aktas, ''Preparation and characterisation of activated carbon from dogwood stone with microwave pre-treatment'', 9th International Symposium on Characterisation of Porous Solids (IX COPS 2011), 5-8 June 2011Dresden/ Germany,1, 205, 2011.

E.Geyik, **T.Aktar**, E.Yagmur, Z.Aktas, "Preparation of activated carbons from various biomasses with H_3PO_4 activation using microwave radiation", 10th International Conference on Materials Chemistry (MC10), AT_P35 pp., Manchester, UK, July 4-7, 2011.

E.Yağmur, **T.Aktar**, S.Koçum, A.Şahin, Z.Aktas, "Ön İşlem Görmüş Çay Atığı ve Domates Bitkisinden Aktif Karbon Üretimi", 25th National Chemistry Conference, 100 pp., Erzurum, Turkey, 27 June-02 July 2011.

T. Aktar, E. Yağmur, Z. Aktaş, "Biyokütle ve Bileşenlerinin TGA-FTIR Birleşik Sisteminde İncelenmesi", 25th National Chemistry Conference, Erzurum, Turkey, 27 June-02 July 2011.

RESEARCH INTERESTS

Biomaterials: Orthopedic and dental implants and their coatings
High Porous Active Carbons: Preparation from agricultural by-products

LABORATORY SKILLS

Synthesis of Bioceramics: Biomimetic Methods
Synthesis of Active Carbons: Chemical Methods
Material Characterization Experience: SEM, EDS, AFM, FTIR, XRD, ICP, XPS, Mechanical Tests (Scratch test, profilometer), TGA, TGA/FTIR, Elemental Analysis, Surface Area and Pore Size Analyzer, Laser Particle Size Analyzer, GC, GC/MS, Density Analyzer
Cell Culture: SaOS-2 cell subculturing, proliferation, viability tests, fixation and SEM observations

LANGUAGE SKILLS

English-Advanced
German-Intermediate

COMPUTER SKILLS

Working knowledge of MS office Applications (Word, Excel, Powerpoint), SPSS, Matlab, Autocad, Chemcad

HOBBIES

Travelling, food tasting